An Investigation of Molecular Properties Using Magnetic Shielding Calculations

Kate Elizabeth Horner *MChem(hons)*

PhD Thesis

University of York

Chemistry

September, 2014

For my grandparents, Cliff and Irene,

for constant inspiration, support and love,

just to see me in a funny hat.

Abstract

Isotropic shielding calculations were performed across finely spaced two- and three-dimensional grids positioned through and around a wide range of molecules. These magnetic shielding calculations were used to investigate aromaticity, antiaromaticity and a variety of chemical bonding features.

This technique was found to be incredibly sensitive and able to distinguish between bonds of different order as well as bonds of the same order but in different environments. The shielding along the whole bonding region, as well as 1 Å above the bond and cross-sections through the bond, can be used to provide detailed information about the nature of the chemical bonding and the conjugation with the rest of the system.

Regions of deshielding have been found around unsaturated nuclei and these areas can be used to determine relative aromaticities as well as degrees of conjugation. The same is true of shielding features found at 1 Å above the molecular plane. Unsaturated heavy atoms also display these deshielded surroundings, but they can be harder to observe.

Antiaromatic systems exhibit a dumbbell shaped region of deshielding at the ring centre as well as significantly bent bonding regions which have been found to be a result, primarily, of the antiaromaticity rather than ring strain.

H-bonding can also be studied with this technique and it has been found that the shielding on the atoms involved is most informative. In the case of substituted malonaldehydes, the oxygen shieldings were used to determine relative aromaticities in the pseudo rings and, therefore, H-bond strength.

The sensitivity and information-rich nature of this technique has proven far superior to existing methods, such as the commonly used nucleus-independent chemical shift (NICS) technique, and therefore has great scope for future applications.

Contents

List of Figures

List of Tables

Preface

When I was about 8 years old, my brother bought me a GCSE Physics textbook. Fast forward 17 years and I'm just finishing this thesis. How did that happen? As a child I told my mother that I had two goals for my life, firstly, to get a PhD and secondly, to own a pygmy goat. Now where do you buy a goat. . .

But more seriously, this door-stop of a document is the culmination of 3 years of research, including almost 600 hours of teaching undergraduates, what feels like the same length of time spent fighting with the typesetting in LaTeX to get it just right and also a few buckets of blood, sweat and tears (though luckily not too much blood). There were times of excitement, disappointment and frustration, perhaps with a few splashes of apathy and laughter along the way.

Obtaining a PhD is supposedly one of the most stressful milestones in one's life, and perhaps that's true, but it also makes you the only person in the world who is an expert in your exact research. So now that I have finished, I can safely claim that I am the world-leading authority on the application and interpretation of finely-spaced isotropic shielding calculations performed in two-dimensions in and around the molecules discussed here for the purposes of exploring molecular properties such as aromaticity, antiaromaticity and bonding. Though that's quite long for a door plaque. But I think the thought that sums this up nicely comes from a famous scientist in the field of quantum mechanics:

"An expert is someone who knows some of the worst mistakes that can be made in his subject, and how to avoid them." Werner Heisenberg

On that note, here is my thesis. For the non-chemist readers (and the chemists who aren't keen on quantum chemistry) I recommend the acknowledgements and the pictures. For the rest of you, I hope you're sitting comfortably.

Acknowledgements

I would like to thank my supervisor Peter Karadakov for all his support, guidance and tolerance over the years. His tales of bagel-hunting in Sofia and discussions of Skyrim have kept me sane during my PhD and his feedback on my written work has been completely invaluable. Thanks also go the Chemistry Department at the University of York for granting me a teaching scholarship which allowed me to carry out my PhD.

I am incredibly grateful to many members of the same department, in particular, the D block, 2nd floor organic chemists for their inclusion of me (nicknamed *Computer Girl*, or CG for short) in their festivities, the Inorganic Group for including me in their group meetings and the various teaching lab staff for being generally amazing during my many hours in teaching labs. A special mention should go to Joseph Atkin, Julia Sarju and David Pugh for their daily interactions, without whom my PhD would have been much harder and far less enjoyable. I am also thankful for the members of the Karadakov group, both current and previous. They made each day different and have tolerated my ramblings on many occasions. Some of them also helped check this for typos, which I really appreciate.

I must also thank Stephen Bromfield for tremendous amounts of advice and support as well as the many favours I have asked of him. He has been a mentor, confidante and shoulder-to-cry-on throughout my whole PhD for which I am eternally grateful. There are many other supportive friends and relatives who also deserve thanks. In particular, my grandparents who are a constant source of inspiration and motivation- I love you both very much. A mention should also be made of Sarah Hayes, a beautiful young lady and wonderful housemate, who, on the precipice of starting her own PhD, tragically lost her life.

Finally, a huge thank you goes to my lovely rats, Hector and Socrates. They have been excellent at listening to my problems and comforting me, for which they deserve an endless supply of Rice Krispies.

Declaration

The research contained within this thesis was carried out between October, 2011 and October, 2014 in the Department of Chemistry at the University of York. To the best of my knowledge, except where reference is made to other authors within, this research is original and my own.

The work on benzene and cyclobutadiene has been published in the Journal of Physical Chemistry A and the work on furan, thiophene and pyrrole has been published in the Journal of Organic Chemistry.

Kate Elizabeth Horner

Introduction 1

"It starts..."
Timon from The Lion King

1.1   Investigation of Chemical Bonding

The nature of chemical bonding is one of the most fundamental concepts in chemistry, and yet it is sometimes poorly understood. There has long been debate over the correct description of bonding in increasingly complex systems, and as a result, a lot of work has gone into improving the understanding of such things.

The concept of the chemical bond has been greatly influenced by Pauling,[1] Slater[2] and Mulliken.[3] Consequently, the general understanding is that bond strength is affected by covalent effects, i.e. the degree of overlap between atomic orbitals, and ionic effects, meaning the bond polarity. If either of these effects is increased, the bond strength also increases. But the question of how best to investigate, measure and characterise varying bond strengths remains a matter of debate.

Chemical bonds can be treated as rudimentary springs by using Hooke's law, which relates the restoring force of a molecule undergoing harmonic motion, F, to the force constant of the bond, k, and the displacement from the equilibrium position, x.

$$F = -kx \tag{1}$$

The stronger a bond is, the stiffer the spring will be and therefore the larger the force constant that is required to displace the atoms. This force constant can be obtained by experiment, using vibrational spectroscopy, but this assumes that molecules behave only as harmonic oscillators and that each vibrational mode is independent of the others. Force constants can also be calculated with computational methods, some of which allow the isolation of vibrations in vibrational modes in order to examine one bond specifically.[4]

Energetic measurements/calculations, such as bond dissociation enthalpies, are also popular bond descriptors. Bond dissociation enthalpies can be measured experimentally in several ways, three of the most common being radical kinetics, photoionisation mass spectrometry and acidity/electron affinity cycles.[5] However, each of these is fairly tricky to perform and all require specialised equipment. Moreover, care must be taken when using bond dissociation enthalpies as a measure of bond strength. For example, once you break one bond in a molecule, the bond dissociation energies for the remaining bonds change. Furthermore, these values also depend upon the relative stabilities of the fragments formed and therefore are not necessarily comparable between molecules.

Detailed coupled cluster calculations of local force constants, performed on a range of some of the strongest known bonds, have also shown that bond dissociation energies can be misleading when used as a bond strength indicator.[6] The work carried out correlated relative bond strength orders with local mode force constants. Relative bond strength orders are used instead of bond orders since the latter is simply the number of bonding interactions between two nuclei. This is related to molecular orbitals and their populations. Consequently, bond orders do not necessarily quantify bond strength. This analysis concluded that the strongest bond in chemistry is the N–N bond found in the doubly protonated dinitrogen dication. The authors were also able to compare a range of triple bonds, but the relative bond strength order concept still requires suitable reference bonds.

Recently, an attempt to directly image covalent bonds was published in *Science*.[7] This work used non-contact atomic force microscopy which was supported by density functional theory calculations. The images obtained were remarkable and allowed insight into complicated mechanisms of single-molecule reactions, in this case, thermally induced cyclisations. Being able to observe the internal bonding structure of important molecules and processes is key in gaining a better understanding of complicated mechanisms.

But understanding more unusual bonding is also important. Hydrogen bonding has featured in chemical research for decades, but the proper definition of a hydrogen bond is still debated today. In 2011, an updated definition was released which emphasised the requirement for evidence of a hydrogen bond.[8] In this definition, six criteria were suggested as suitable evidence of hydrogen bond formation. These include the tendency towards linearity of the three atoms involved in the interaction as well as physical and spectroscopic criteria. The partial covalent nature of the hydrogen bond has been explored extensively,[9] with experimental evidence available from NMR spin-spin coupling[10] and Compton scattering experiments.[11] More recently, a study of the quantum nature of the H-bond was also carried out finding that quantum nuclear effects weaken already weak H-bonds but strengthen strong ones.[12] Hydrogen bonds are key interactions throughout biology, materials science and supramolecular chemistry, amongst other fields, making a sound understanding of their nature a vital area for research.

Multicentre bonding is also unconventional and often debated. Some take a topological approach as opposed to considering multi-centre bonding in terms

of molecular orbitals.[13] Bader's popular Atoms in Molecules theory has also proposed a formalism for multicentre bonding.[14] In 2004, a variety of computational calculations were performed by Cooper *et al.* to scrutinise the concept and it was found that the bonding description is very dependent upon the quality of the wavefunction being used.[15]

There are many different ways to characterise and describe the types and strengths of chemical bonds. But it is clear that with the evolving definitions of more complicated bonding interactions, the methods with which these are analysed must also evolve.

1.2 Aromaticity & Antiaromaticity

In 1825, Michael Faraday isolated benzene,[16] and from that point, the concept of aromaticity developed from initially referring to pungent aromas, to something far more complex. In 1931, Hückel proposed the $(4n + 2)$ π electron rule for defining aromaticity in planar, cyclic systems,[17,18] which became very popular. Since then, this definition has been extended to include antiaromaticity, which involves $(4n)$ π electrons and results in the opposite properties to aromaticity. Where aromatic systems benefit from increased stabilisation, lowered reactivity and bond equalisation, antiaromatic systems suffer from decreased stabilisation, increased reactivity and bond alternation. Both of these properties have an important role across many fields of chemistry.

1.2.1 Aromaticity- More Than Just Benzene

In the beginning, aromaticity was a concept that was restricted to benzene and benzenoid relatives. However, gradually this widened and began to include an increasing number of systems. For example, heterocycle aromaticity was described in 1925 by Armit and Robinson[19] and metal involvement in aromaticity was found in 1945.[20]

In 1959, the term 'homoaromaticity' was introduced to describe systems that exhibit aromatic properties despite at least one saturated linkage, something which should disrupt cyclic conjugation.[21,22] Homoaromatic systems require some form of homoconjugation which could exist as through-space homoconjugation i.e. conjugation that does not require a bond between two π systems, or as σ homo-

conjugation which exists along a bond. The presence of this kind of conjugation, along with typical aromatic properties, are some of the requirements for a system to be termed homoaromatic.

Another very interesting addition to the concept of aromaticity is Möbius aromaticity introduced by Heilbronner.[23] Möbius systems are rings which contain an odd number of twists, and therefore only possess one side. These types of system can be considered as Möbius aromatics if they also have (4n) π electrons which gives them increased stability. Conversely, Möbius systems with (4n + 2) π electrons are destabilised which is a complete reversal of the Hückel aromaticity rules. Since their definition, there has been increasing amounts of interest in these types of molecule and some have even been synthesised, though with some difficulty.[24,25]

In 1978, Aihara published a paper on three-dimensional aromaticity in polyhedral boranes, as observed by their positive resonance energies and general chemistry.[26] Shortly after this, Dewar and co-workers introduced the concept of σ aromaticity and conjugation.[27–29] This idea was used to try to explain the unusual properties of cyclopropane, a system which Dewar describes as 'isoconjugate with benzene' and therefore σ aromatic.[29] These unexplained properties included a calculated conventional strain energy for cyclopropane being almost identical to that calculated for the larger, less strained cyclobutane. Yet, despite the similar strain energies, cyclopropane is far more reactive than cyclobutane, including undergoing ring opening reactions, something which the four-membered ring does not do. Regardless of the ring strain, the C–C bonds in cyclopropane are shorter and therefore stronger than those in cyclobutane. Dewar proposes that all of these observations can be explained by the presence of σ aromaticity in cyclopropane.

Whilst the extensions to the term aromaticity are vast and seemingly innumerable, one more definition worth a mention is that of 'superaromaticity'.[30,31] This is the idea that extra stabilisation can be achieved by conjugating multiple aromatic rings, usually benzene rings, together into chains, sheets or spheres (see C_{60}). However, different methods and authors can produce different findings, for example, the superaromaticity of C_{60}, or lack thereof will be discussed here later.

1.2.2 The Addition of Antiaromaticity

Long after aromaticity had become popular, Breslow proposed the definition of an opposite property- antiaromaticity.[32,33] This is defined as a cyclic, conjugated system which contains (4n) π electrons leading to a significant destabilisation. An antiaromatic system will have a π electron energy which is higher than a non-cyclically delocalised reference compound. Unfortunately, just as for similar comparisons used in aromaticity determination, the selection of a suitable reference system is not trivial.[33] In magnetic terms, it was proposed that the ring currents induced in (4n) π electron systems should cause the opposite trend in NMR chemical shifts, something which has been observed experimentally.[34]

Just like with aromaticity, the concept of antiaromaticity has also been extended. For example, it has been suggested by Schleyer and collaborators that cyclobutane and related structures, like cubane, exhibit σ antiaromaticity.[35] The Al_4^{4-} all-metal cluster was predicted as possessing conflicting aromaticity i.e. being both σ aromatic and π antiaromatic at the same time, or *vice versa*.[36,37] However, the overall resultant property is difficult to predict since it is hard to know which will overpower the other.

It is clear that the concept of antiaromaticity is gradually becoming as popular and complex as its predecessor.

1.2.3 The Importance of Aromaticity & Antiaromaticity

Approximately two thirds of the *ca* 20 million chemical compounds that had been identified by the year 2000 are considered either partially or fully aromatic, with half of them containing heteroaromatic moieties.[38] It is clear from this statistic alone that aromaticity has a key part to play in modern chemistry.

Biochemistry, for example, is full of aromatic systems. Both DNA and RNA, each essential to life, are based on two well-known heteroaromatic rings- purine and pyrimidine (see Figure 1.1). The aromatic properties of these nucleobases play an important part in their function and structure. Two of the amino acids that make up proteins, histidine and tryptophan, also contain aromatic moieties. Histidine, for example, breaks down into a vasodilator released in allergic reactions. It also stimulates stomach acid production which can cause heartburn. This latter role has made histidine receptor antagonists very popular for pharmaceuti-

cal targets.[38] Nitrogen-containing heteroaromatics are also commonly found in coenzymes which perform biologically important reactions within organisms.
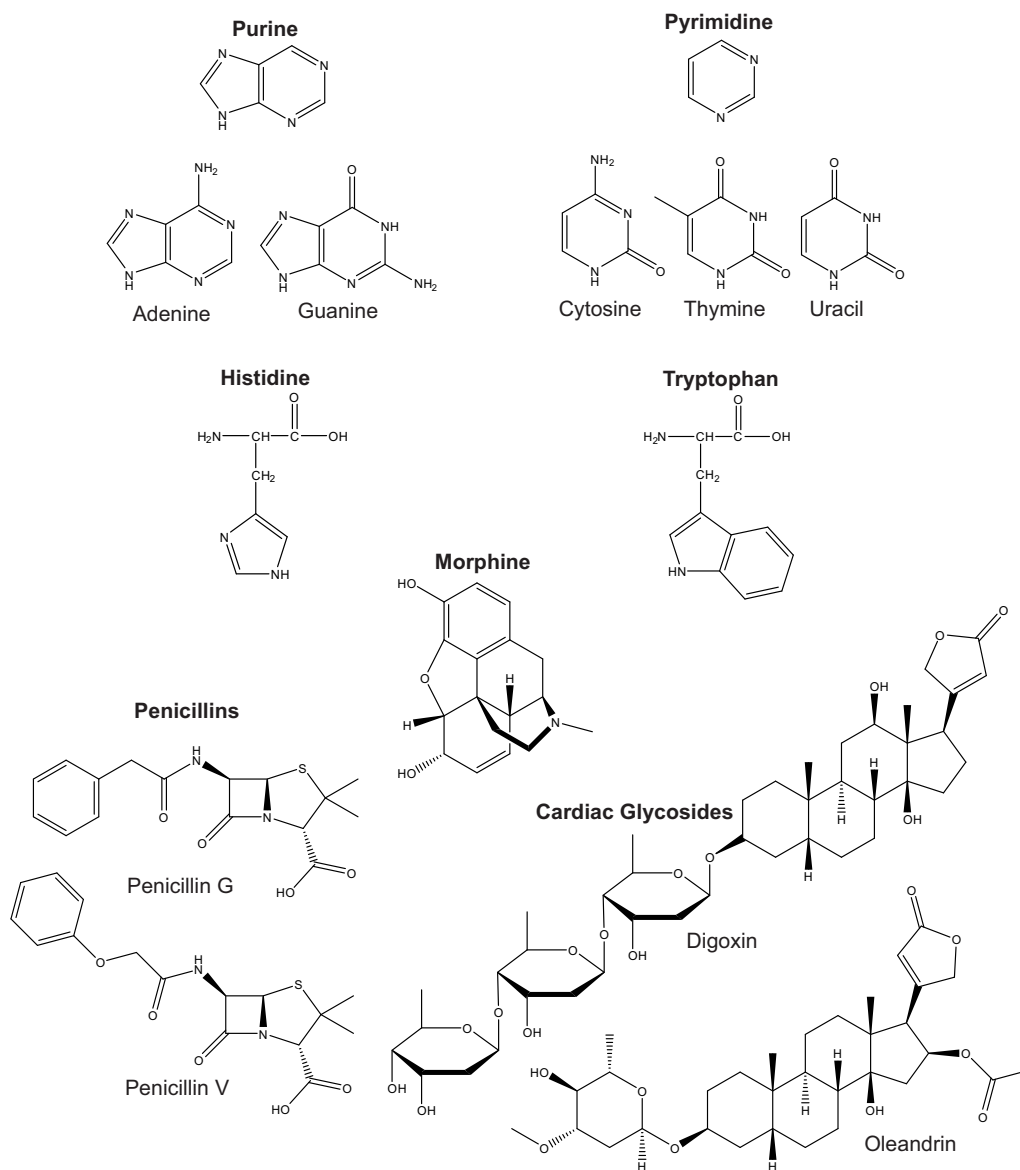
Figure 1.1: Structures of various aromatic natural products.

Within the pharmaceutical industry, aromaticity is often seen in natural product targets and therefore is also desired in natural product mimics. Some of these natural products include antibiotics like penicillins (from the *Penicillium* fungi), alkaloids such as the painkiller morphine (from opium poppies) and cardiac glycosides like digoxin (from foxglove plants) or oleandrin (from the oleander plant), the structures of which can be seen in Figure 1.1.

But aromatic molecules are not just restricted to biological systems. They are

also widespread in dyes, flavourings, polymers, solvents and the rubber industry. Understanding the effect that aromaticity has on these compounds is essential for developing new molecules, rationalising reactivity and explaining mechanisms of action.

1.3   Characterisation of Aromaticity & Antiaromaticity

Since the initial inception of aromaticity, its exact definition has been much debated. A variety of criteria have been used, some more successfully than others, to characterise aromatic systems, but currently, there is no single, universal criterion that works for all molecules. Because aromaticity is a key feature in all branches of chemistry, ranging from organic mechanisms, to stereoselectivity and reactivity, an effective characterisation method is very desirable.

There are four main categories for the criteria used to describe aromaticity. Firstly, there are structural criteria. These include the tendency of aromatic systems to prefer planar, bond equalised structures. Unfortunately, this is not very reliable. For example, borazine, a six-membered ring made up of alternating B and NH components which is isoelectronic with benzene, has completely equal bond lengths but is only weakly aromatic. The low aromaticity in the case of borazine is due to the localisation of the π electrons on the more electronegative N atoms rather than the B atoms. On the other hand, naphthalene is a well known aromatic system, but due to resonance structures, it exhibits a lack of bond equalisation (see Chapter 4).

The next category of aromaticity descriptors are the energetic criteria. Aromatic stabilisation energies are, perhaps, one of the most well known of the aromaticity measures. However, these values are far from trivial to evaluate. They are highly dependent on the choice of reference molecule and equation. A study of the aromatic stabilisation energies of 105 five-membered π electron systems highlighted the many flaws in these kinds of calculations.[39] In particular, the work found that homodesmotic schemes based on acyclic reference molecules were quite unsatisfactory. It is therefore clear that, while useful in some cases, energetic calculations seem to be inappropriate for a universal aromaticity descriptor.

Molecule reactivity has also been used to characterise aromaticity. For example, aromatic molecules typical undergo electrophilic aromatic substitution rather than addition. However, in aromatic systems which lack hydrogens, like the fullerenes,

this is clearly not possible and so the systems undergo addition instead. Interestingly, there is some work which suggests that C_{60} buckminsterfullerene is actually π antiaromatic, which will be discussed later.[40]

Finally, there are magnetic criteria to consider. These include NMR chemical shifts which are commonplace in experimental chemistry. The most frequently used to determine aromaticity are those of ^{1}H nuclei. ^{7}Li NMR chemical shifts can also be used as Li cations are known to complex at ideal positions on aromatic systems, e.g. the aromatic π ring faces.[41,42] The chemical shifts of these nuclei can be used to determine the nature of their environment, including whether they are part of an aromatic, non-aromatic or antiaromatic system. For benzene, the ring current that creates its aromaticity is responsible for a roughly 2 ppm increase in the proton deshielding relative to the vinyl protons in cyclohexene.[41] However, even this is controversial as it has been suggested that arene protons are not deshielded by the ring current but instead are shielded by the currents and deshielded by a mixture of σ CC and π effects.[43,44] Regardless of the true nature of the shielding changes observed, ^{1}H chemical shifts have proved a useful tool. Unfortunately, this strategy only works for molecules which contain hydrogen atoms and those which are easily studied by NMR. Furthermore, these chemical shifts do not depend solely on aromaticity, which again makes them unsuitable for a universal aromaticity descriptor.

It is becoming increasingly popular to evaluate magnetic criteria computationally rather than experimentally. This opens up opportunities for a wide range of new aromaticity measures, the most common of which involve magnetic shielding calculations.

1.3.1   Magnetic Shielding Calculations

Initially, magnetic shielding calculations were performed on nuclei which allowed a direct comparison with experimental NMR results. This made use of the well known relationship between an external magnetic field and that experienced by nuclei within a molecule. This relationship is described by the expression:

$$\mathbf{B}_J = (\mathbf{1} - \boldsymbol{\sigma}_J)\mathbf{B}_0 \tag{2}$$

where $\boldsymbol{\sigma}_J$ is the shielding tensor of nucleus J. This shielding tensor is a 3 $\times$ 3 matrix with rows and columns labelled by the x, y and z coordinates. One

third of the sum of the diagonal elements of this matrix is defined as the isotropic shielding:

$$\sigma_{J,\text{iso}} = \tfrac{1}{3}(\sigma_{J,xx} + \sigma_{J,yy} + \sigma_{J,zz}) \tag{3}$$

Differences between calculated isotropic shieldings correspond to chemical shifts, analogous to those obtained in NMR experiments.

However, in 1958, Johnson and Bovey proposed shielding calculations carried out at off-nucleus positions,[45] and since then this idea has proliferated. The shielding tensor as described before can be calculated at a chosen off-nucleus position $\mathbf{r}$ and the elements of the resulting $\boldsymbol{\sigma}(\mathbf{r})$ can be used to define additional aromaticity criteria. Indeed this is the principle behind the highly popular nucleus-independent chemical shift (NICS) technique which was first published by Schleyer *et al.* in 1996.[42]

One method of carrying out through-space magnetic shielding calculations is to employ a molecular probe. Often, a diatomic hydrogen probe is used and is placed at regularly spaced positions around or above the molecule under investigation, like work by Martin and co-workers.[46–48] The isotropic shielding of one hydrogen in a lone diatomic hydrogen molecule is then subtracted from the shielding of the proximal hydrogen in the diatomic hydrogen probe in order to obtain the through-space isotropic shielding. Unfortunately, the use of a molecular probe perturbs the wave function of the molecule being studied. This was highlighted by work carried out comparing the use of a methane probe (with a similar method to that of a diatomic hydrogen probe) with that of the NICS technique.[49]

1.3.2 NICS Technique

The advantage of the NICS technique over molecular probes is that the shielding calculations carried out in the former method are achieved with the use of ghost atom probes i.e. probes which themselves have no properties. This means that they leave the wave function of the molecule under observation completely unperturbed. Interestingly, in the quantum chemical package Gaussian, these ghost atoms are denoted with the letters 'Bq', so called because of the ghost of Banquo in Shakespeare's play, Macbeth.[41] At each of these ghost atoms, positioned at various places in and around aromatic systems, the isotropic shielding is calculated. Then, in order to correlate with experimental NMR convention, the negative of this shielding is taken and it is this final term that is considered the

NICS value.[42] These NICS values were traditionally computed at ring centres, i.e. the non-weighted mean of the heavy atom positions, for the purpose of probing the ring's aromaticity. A negative NICS denotes an aromatic system while a positive NICS denotes antiaromaticity.

Other advantages of the NICS technique over other aromaticity criteria include no requirement for a reference molecule, which is a problem with energetic calculations, only a moderate ring size dependence, ease of use and good correlation with other criteria.[41] However, it also has limitations. The NICS technique has received criticism because it cannot currently be experimentally determined.[50] There is also debate surrounding the ideal position of the NICS calculation since aromatic systems are known to exhibit paramagnetic vortices around their centre.[51] This means that a single NICS calculation, if not placed in the most appropriate position, could not effectively characterise aromaticity which is intrinsically a global molecular property. There is also disagreement about the propriety of using one third of the trace of the shielding tensor, i.e. the isotropic shielding, as an aromaticity criterion. It has been argued that such methods risk the loss of information about the diatropic nature of aromatic molecules which is vital for a proper understanding of aromaticity.[50]

1.3.3 Other NICS Indices

In order to address some of these limitations, the NICS technique has steadily developed and become far more elaborate. One such development was the introduction of the dissected NICS technique.[52,53] This allowed the assessment of individual contributions from each orbital to the isotropic shielding and therefore the separation of π and σ contributions (with the former denoted NICS(π) or NICS$_\pi$) which is particularly useful for aromaticity studies. A particular focus on the out-of-plane or z-component was also suggested, since this is the direction of the applied magnetic field, and is given the index NICS$_{zz}$.[54] Dissected NICS values were used by Chen *et al.* to study the properties of C_{60} buckminsterfullerene and it was concluded that this system displays spherical antiaromaticity rather than any superaromatic or aromatic character.[40] They found that the antiaromatic five-membered rings and the non-aromatic six-membered rings on the C_{60} surface display local paratropicity and have positive NICS$_{\pi zz}$ values. They used these findings, along with cage strain relief, to rationalise the electrophilicity

of this system with respect to addition reactions. They propose that fullerenes are actually very unstable and their viability is only caused by a lack of decomposition routes to lower energy products that have low activation barriers. This work is an example of shielding calculations being used to explain observed physical properties that were previously poorly understood and highlights the usefulness of such techniques.

Another key improvement in the NICS technique was its application at other positions around aromatic systems, in particular, at 1 Å above the ring centre. This position is given the index NICS(1) while the original placement of a ghost atom at the ring centre is given the index NICS(0). The rationale behind this was that a placement at 1 Å above the aromatic ring excluded any σ contributions to the shielding value and focused primarily on the π electrons which are responsible for the property.[52–54] A comparison of the many NICS indices determined that the best method was the expensive NICS(0)$_{\pi zz}$ but that the cheaper NICS(1)$_{zz}$ was a good compromise of cost and result.[54]

1.3.4   Multiple NICS Calculations

However, the placement of a single NICS calculation is not necessarily enough to fully describe the aromaticity of a molecule. Multiple NICS calculations were carried out by Schleyer *et al.* on benzene and cyclobutadiene as archetypal examples of aromaticity and antiaromaticity.[53] In this work, NICS calculations were carried out across a grid extending from the ring centre to 3 Å above and to the side of the rings with a grid spacing of 0.5 Å.The results highlighted the benefit of NICS(1) over NICS(0) as well as relating paratropic/paramagnetic (associated with antiaromaticity) and diatropic/diamagnetic (associated with aromatic systems) ring currents to the π effects experienced by the molecules. Stanger carried out similar systematic calculations, but this time only extending from the ring centre to 4.9 Å above in a straight line and with spacings of 0.1 Å.[55] He termed this method the NICS-scan technique and separated the values obtained into in-plane and out-of-plane components. These values were then used to indicate diamagnetic and paramagnetic ring currents in the molecules that were investigated which was shown to be more effective than single NICS calculations. It was also found that NICS and NICS-scan results are unable to properly describe local aromaticities within polycyclic systems.

NICS calculations have also been carried out across three-dimensional lattices with the resulting values plotted as isochemical shielding surfaces (ICSSs) by Kleinpeter and co-workers.[56–58] These surfaces have been used to investigate the anisotropy effect of functional groups and stereochemistry as well as aromaticity and antiaromaticity. The distances of ICSS = ± 0.1 ppm from the centres of aromatic rings allowed a qualitative comparison of their relative aromaticities.[57] The authors were also able to compare the effects of various substituents on the through space shielding around various systems. This method was found to be effective in describing and characterising aromaticity and conjugation in a wide range of molecules, but few subtle details could be observed due to the nature of the visualisation and the large 0.5 Å grid step-size. Likewise, little information was obtained on any effects present close to nuclei. However, ICSSs have been used to study the anisotropy effect of multiple bonds and ring currents.[56,59] It was found that the calculated anisotropy effects could be used to help assign experimental ^{1}H chemical shifts in stereoisomers.[56] Furthermore, a study of cyclobutadiene and benzene concluded that for cyclobutadiene, the conventional interpretation of the anisotropic effects of C=C double bonds and antiaromaticity are applicable, but for benzene, the case is not as straightforward.[59] For benzene, the authors found that the π electron effects oppose those predicted by the traditional anisotropy cone depictions and that σ contributions are more influential than previously thought.

This has shown the huge potential of a chemical shielding method to provide insight into a variety of molecular properties, particularly aromaticity and antiaromaticity. It has also been seen that there is scope for some bonding information as well. The development of a technique like this promises to yield significant details of a wide range of systems which would greatly benefit the understanding of key molecules. The investigation of such a technique is the aim of the work contained in this thesis.

1.4   Quantum Chemical Methods

Hartree-Fock (HF) theory approximates the many-electron wavefunction by a Slater determinant, the orbitals in which are optimised through a self-consistent field procedure. This forms one of the most important building blocks of quantum chemistry and has allowed the development of many, more complex theories. The

main limitation of HF calculations is the lack of any inclusion of electron correlation effects, something which the following methods attempt to rectify.

1.4.1   Many-Body Perturbation Theory

Many-body perturbation theory (MBPT) can be viewed as a series of corrections to the simpler HF method. This is used to account for electron correlation effects. A very commonly used approximation is the Møller-Plesset second-order (MP2) perturbation theory.[60] This involves taking the unperturbed HF approximation as the zeroth-order approximation and then applying small first order and second order corrections using MBPT.

Firstly, the many-electron Hamiltonian operator, $\hat{\mathcal{H}}$ is altered according to:

$$\hat{\mathcal{H}} = \hat{\mathcal{H}}_0 + \lambda \hat{V} \tag{4}$$

where λ is a small number, $\hat{V}$ is the Perturbation operator and

$$\hat{\mathcal{H}}_0 = \sum_i \hat{f}_i \tag{5}$$

where $\hat{f}_i$ is the Fock operator. From this, the original Schrödinger equation

$$\hat{\mathcal{H}}\psi = E\psi \tag{6}$$

where E is the energy of the system, becomes

$$(\hat{\mathcal{H}}_0 + \lambda \hat{V})\psi_i = E_i \psi_i \tag{7}$$

Since λ is a small value, the perturbed wavefunction and energy can be expressed as a power series with the first term in each series corresponding to the zeroth order term, the second the first order correction and the third the second order correction etc. Here, the zeroth order wavefunction is the same as the HF wavefunction which means that the zeroth order energy contribution is the sum of the orbital energies

$$E^{(0)} = \sum_{i=1}^{N} \epsilon_i \tag{8}$$

The first order correction is simply the HF energy minus the zeroth order energy

$$E^{(1)} = E_{HF} - \sum_{i=1}^{N} \epsilon_i \tag{9}$$

This first order correction is referred to as MP1, but at least an MP2 energy correction is required to improve upon the original HF energy. The second order correction can be expressed as

$$E^{(2)} = \sum_i \sum_{j>i} \sum_p \sum_{q>p} \frac{(\langle \psi_p \psi_q | \psi_i \psi_j \rangle - \langle \psi_p \psi_q | \psi_j \psi_i \rangle)^2}{\epsilon_i + \epsilon_j - \epsilon_p - \epsilon_q} \tag{10}$$

where p and q are virtual orbitals and i and j are occupied orbitals. The overall MP2 energy is then the sum of $E^{(0)}$, $E^{(1)}$ and $E^{(2)}$ which simplifies to the sum of the HF energy and $E^{(2)}$.

1.4.2   Complete Active Space Self-Consistent Field Approach

The complete active space self-consistent field (CASSCF) approach[61] is a very popular variant of multiconfiguration self-consistent field theory (MCSCF). CASSCF, as the name implies, is a full configuration interaction in the selected active space, i.e. it involves all possible configurations that can be constructed from the active orbitals using the required number of active electrons; all active and core orbitals, as well as the configuration interaction coefficients are optimised simultaneously.

The active space choice is vital for an appropriate calculation. Typically, the active space is chosen according to the area of interest within the system being studied. This could be the π bonds in an aromatic system or bonds involved in a reaction. The number of orbitals and electrons included in an active space is given along with the method e.g. for benzene, a CASSCF(6,6) wavefunction is used which means "6 electrons in 6 orbitals". This allows the π electrons of benzene to make up the active space along with 3 occupied and 3 virtual orbitals in which 6 electrons are distributed between 6 orbitals in all possible ways. This leads to 175 different configurations with doubly and singly occupied orbitals.

1.4.3   Density Functional Theory

In 1964, Hohenberg and Kohn published a paper which proves that the total ground state electronic energy of a system can be calculated by using a functional of the electron density.[62] Shortly after this, Kohn and Sham presented a simpler way to treat electron-electron interactions which involved the definition of a term for the exchange-correlation energy.[63] If a perfect exchange-correlation

functional could be defined, the resultant energy would be exact, however this is impossible to achieve. Instead, an increasing range of approximate functionals are being developed, each with strengths in particular fields.

One very popular hybrid functional is the Becke 3-Parameter Lee-Yang-Parr functional (B3LYP).[64] This involves a non-local correlation provided by the Lee-Yang-Parr expression and a local correlation from the Vosko, Wilk and Nusair 1980 correlation functional(III). Another popular hybrid is the Minnesota 06 (M06) functional by Truhlar and Zhao[65] which is often recommended for use with organometallic, inorganometallic and non-covalent systems. These two density functional theory (DFT) functionals are the only ones which will be mentioned in the following research.

1.4.4   Basis Sets

A basis set is a set of functions that will be used to approximate the orbitals in the calculation being performed. The most commonly used basis set in this work is a Pople basis set denoted 6-311++G(d,p). The 6-311 section refers to the split-valence nature of the basis set which is constructed with six primitive Gaussian-type orbitals for each core orbital and the valence orbitals are contractions of three primitive Gaussian-type orbitals (which approximate one valence Slater-type orbital), one primitive Gaussian-type orbital (which approximates another valence Slater-type orbital) and another primitive Gaussian-type orbital (which approximates the last valence Slater-type orbital). The split-valency allows a lower computational cost while still allowing accuracy of the important valence functions. The ++ in the basis set name denotes the inclusion of diffuse functions. The (d,p) shows the use of polarisation functions of both d-type and p-type.

A few calculations in this thesis made use of one of Dunning's Correlation-Consistent basis sets, specifically the aug-cc-pV5Z basis set. This notation refers to the use of a correlation-consistent, polarised valence quintuple ζ basis augmented with one set of diffuse functions.

1.5   Computational Procedure

The isotropic magnetic shielding values reported in this work were obtained mainly using the Hartree-Fock (HF) method and second-order Møller-Plesset perturba-

tion theory (MP2) with molecular orbitals expanded in terms of gauge-including atomic orbitals (GIAOs). In some cases a complete-active-space self consistent field (CASSCF) method was used and for benzene the DFT functionals B3LYP and M06 were used. All calculations, except those using DFT, were performed within the 6-311++G(d,p) basis by means of GAUSSIAN09[66] or DALTON 2.0 for the case of CASSCF calculations.[67] The DFT calculations were carried out with the aug-cc-pV5Z basis set. For the HF and MP2 calculations the SCF(Tight), NMR and CPHF (Separate) keywords were used. For the DFT methods, the SCF(Tight,NoVarAcc, IntRep), CPHF(Separate), NMR and Int(Grid=-96032) keywords were required in order to correctly recognise molecular symmetry.

In order to study the variations of the isotropic shielding in the regions of space surrounding each molecule, $\sigma_{\mathrm{iso}}(\mathbf{r})$ was evaluated in a variety of planes, each using two-dimensional grids of points with a spacing of 0.05 Å, centered at or directly above the center of mass. Common plane positions are through the molecular plane, 1 Å above this plane or vertical planes bisecting atoms, bonds or both. In cases where the molecule is not planar, multiple grids have been specified, each lying in the plane of a molecular fragment, which have then been compiled into one contour plot. These have been termed 'stitched' plots. For benzene and cyclobutadiene, analogous calculations were performed across a three-dimensional grid, with identical spacing as in the two-dimensional grids. Where further detail was required, usually in the region surrounding a nucleus, an "ultra-fine" grid was used. This is an analogous grid to those mentioned previously but with a 0.001 Å spacing.

The computational effort of this work was reduced by taking into account any symmetry of the systems under investigation. This allows a reduction in the number of calculations which can then be replicated using these symmetry relationships to cover the whole molecule. Where possible, experimental geometries were used. Further details of the geometries used for each molecule can be found in the Introduction of the relevant chapter.

Due to limitations within the GAUSSIAN09 software, it was necessary to restrict the number of ghost atoms (used to perform the shielding calculations) in each input file to fewer than 100. This, therefore, means that each molecule requires multiple input files to be created. An example of the Fortran code used to generate the GAUSSIAN09 input files can be found in the Appendix.

2

Chemical Bonding

"...a bond does not really exist at all: it is a most convenient fiction which...is convenient both to experimental and theoretical chemists."

Charles Alfred Coulson

2.1   Introduction

The concept of chemical bonding has always been complicated and widely discussed, as the quote for this chapter suggests. Popular convention often oversimplifies the nature of bonding by constraining interactions to a formal bond order, localising the region of space that a bond occupies and rigidly assigning bonds as a link between two atomic centres. This definition is satisfactory for many scientific uses, but it is clear that the true character of bonding is far more complex.

Multi-centre bonding, for example, includes interesting interactions like three-centre-two-electron bonds, such as those present in diborane.[13] Originally it was thought that B_2H_6 had a structure similar to that of C_2H_6, but physical data were often in disagreement with each other.[68] The conflict between experimental studies highlights how inappropriate it can be to rigorously assign exact numbers of electrons to orbitals and to localise valence electrons in general. Whilst it can be convenient and effective in simple cases, it is still an approximation and one which is not valid for systems such as diborane. The same is true of viewing Lewis structures as realistic pictures of bonding within molecules. This is eloquently discussed in a review of boron hydrides by Bauer.[68] It is because of these limitations of conventional bonding models that the investigation of diborane with a novel visualisation technique is useful, or even required. A visual representation of the bonding in diborane has been attempted before using a topological analysis of the electron localisation function (ELF) by Silvi,[13] but this lacked any subtle details or information within the structure itself. A similar technique was used by the same author to characterise the strength of hydrogen bonds (H-bonds),[69] something also investigated in this work.

Ring current models have also been used to probe molecular properties like bonding, both in cyclic[70–72] and, recently, acyclic systems.[73,74] Work carried out by Pelloni and Lazzeretti[73] on ethene and ethyne gives an explanation for the magnetic susceptibility and nuclear magnetic shieldings on the carbon and hydrogen atoms. Moreover, stepwise shielding calculations with a coarse, 0.5 Å spacing were used by Kleinpeter *et al.* to investigate ethene, but again, high levels of detail were not obtained.[59] As such, the more detailed, finely space grids used here will produce far greater insight into the properties of small molecules like ethene and can provide information into the bonding and other magnetic characteristics simultaneously.

The geometries of ethane, ethene, ethyne, diborane and the water monomer are all experimentally determined.[75] The acrolein geometry was experimentally determined by microwave spectroscopy[76] and that of *trans*-1,3-butadiene by gas electron diffraction.[77] The allene geometry was obtained by a force field analysis of experimental data.[78] The water dimer structure was optimised at the RMP2(Full)/6-311G** level of theory with the VeryTight convergence criterion.

2.2   Small Hydrocarbon Systems

Ethane (C_2H_6), ethene (C_2H_4) and ethyne (C_2H_2) make up a family of two-carbon hydrocarbons which exhibit single, double and triple C–C bonds, respectively. These simple systems, unperturbed by complicated substituents, allow the dedicated study of C–C bonds of varying formal bond order as well as their influence on C–H bonds.

Table 2.1: Isotropic shieldings for the symmetry-unique nuclei and C–C bonding midpoint values for ethane, ethene and ethyne (in ppm), calculated at the HF-GIAO/6-311++G(d,p) and MP2-GIAO/6-311++G(d,p) levels of theory. Values are also calculated at a position 1 Å above the bond mid-points.

Molecule		$\sigma_{iso}(C)$	$\sigma_{iso}(H)$	$\sigma_{iso}(C–C)$	$\sigma_{iso}(C–C)$ 1 Å Above
Ethane (C_2H_6)	HF	184.03	31.14	52.29	5.96
	MP2	188.14	30.88	52.22	5.92
Ethene (C_2H_4)	HF	61.43	26.31	52.22	16.93
	MP2	75.68	26.37	49.97	15.43
Ethyne (C_2H_2)	HF	117.60	30.63	71.06	15.39
	MP2	128.17	30.51	67.91	14.18

Several interesting trends can be seen in Table 2.1. Firstly, a comparison of HF values with the analogous MP2 values reveals a decrease in consistency between the theory levels as the C–C bond order increases. This highlights the importance of the inclusion of correlation effects in calculations that involve multiple bonds. This trend is most evident for the $\sigma_{iso}(C)$ values which are most affected by the

C–C bond order.
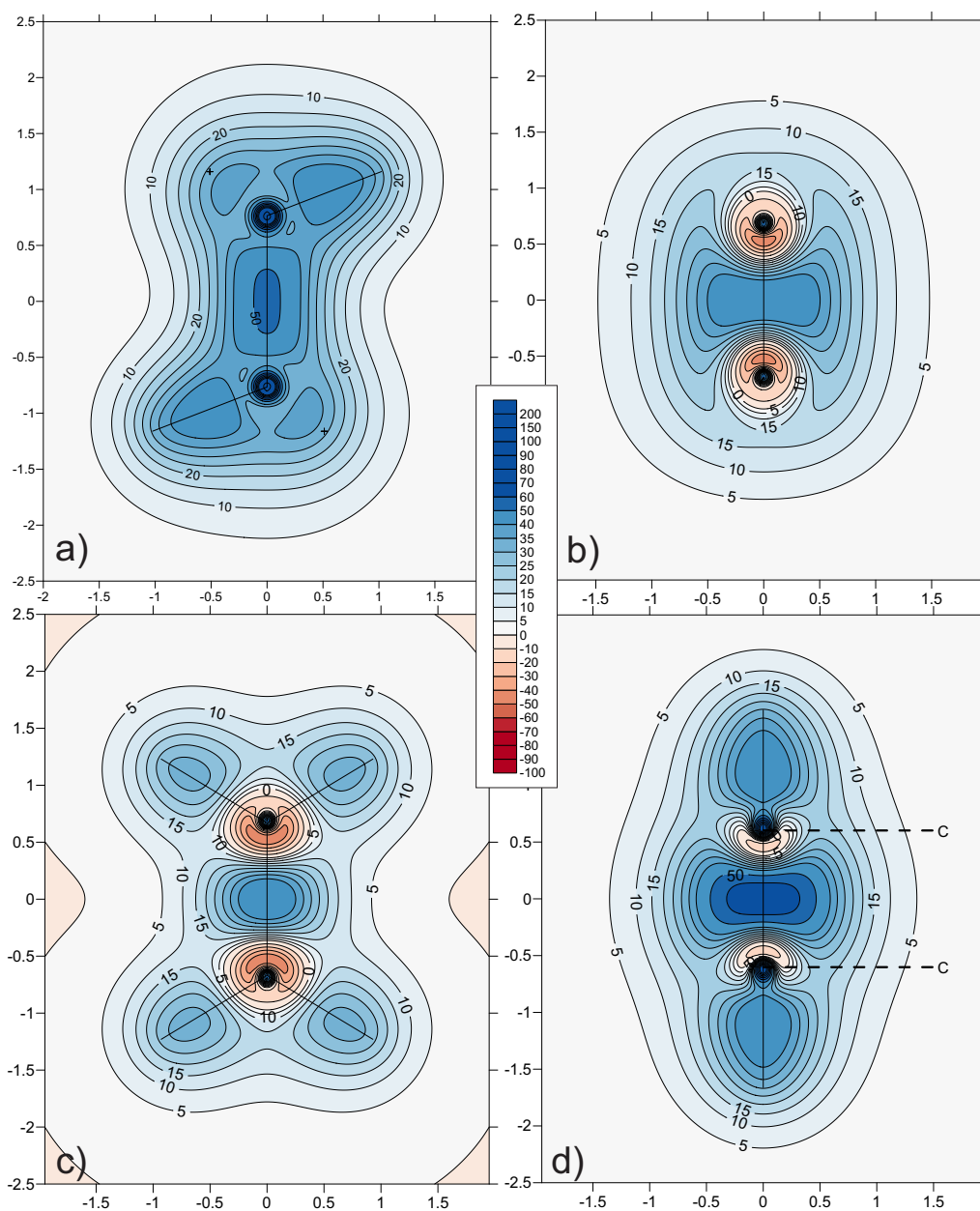
Figure 2.1: Contour plot of the isotropic chemical shieldings (ppm) through the molecular planes of a) ethane, b) ethene (perpendicular to H–C–C–H plane), c) ethene (in the H–C–C–H plane) and d) ethyne calculated at the MP2/6-311++G(d,p) level of theory. The crosses in a) denote the positions of out-of-plane hydrogens.

A second noteworthy point is the trend within each calculated result as the C–C bond order increases. For each value, it might be expected that calculations for ethene, exhibiting a double bond, would lie somewhere between those from ethane, with a single bond, and ethyne, with a triple bond. However, for all four

calculated shieldings, this is not the case. The shieldings on the nuclei in ethene are significantly lower than those of ethane and ethyne. But perhaps the most interesting feature is the bonding region. The shielding at the C–C bond mid-point in ethene is similar, or in the case of the MP2 value, slightly lower than those obtained for ethane. This might also suggest bent-bond character which would not lead to a very high shielding right in the middle of a C=C bond. However, if the shielding values are considered across the whole bonding region, as seen in Figure 2.1, this trend can be rationalised.

Beginning with the C–C single bond in ethane (Figure 2.1a), it can be seen that the shielding along the bonding region is fairly compressed causing a high shielding maximum at the bond mid-point. This is consistent with the localised nature of a σ bond. As the bond order increases to that of ethene (Figure 2.1b & c), the shielding in the internuclear region becomes much wider and slightly more diffuse. This can be seen particularly well in the plane perpendicular to the H–C–C–H plane (Figure 2.1b) where the bond shielding extends significantly above and below the plane of the molecule. This is indicative of the inclusion of π bonds that lie perpendicularly to the molecular plane. Finally, the triple bond of ethyne in Figure 2.1d is visualised and features of both ethane and ethene are evident. There is a similar, if slightly wider shape to the shielding along the bonding region but with a distinct increase in the maximum shielding at the bond mid-point.

This can also be compared to the bond mid-point cross-sections in Figure 2.2 which display a fairly circular shape in both ethane and ethyne, but a more elliptical shape in ethene. This, in combination with the features of the molecular planes seen previously, can be explained by considering the orbitals involved in the C–C bond. In ethene, the π bond is made up of two $2p_z$ orbitals which lie in the plane perpendicular to that of the molecule. This causes the extension of the shielding above and below this plane as seen in Figure 2.1b and the elliptical cross-section. These p orbitals allow diffusion of the bonding electron density which explains the lack of a larger shielding maximum than ethane. However, in ethyne, the π bonds consist of the same two $2p_z$ but also two $2p_y$ orbitals which lie in the molecular plane i.e perpendicular to the $2p_z$ orbitals. This allows the overall C–C bond electron density to spread in three Cartesian directions giving a circular bond cross-section similar to ethane, though with a higher shielding magnitude and a wider diameter.

It is evident from the shielding values in Table 2.1 and the features seen in Fig-

ures 2.1 and 2.2 that it is inappropriate and in some cases, misleading to use a single shielding value as a quantitative measure or indicator of bond order. The magnetic characteristics, and indeed the true nature of bonding, are too complex to allow such simplifications. However, when the shielding in all directions is considered as a whole, a detailed picture emerges. Interestingly, when the molecular isosurfaces obtained here are compared to structures seen in ring current models, several similarities are easily noted.[73]
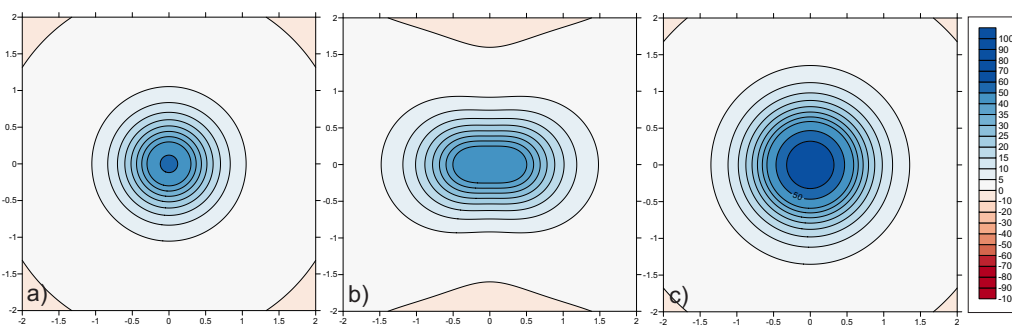
Figure 2.2: Contour plot of the isotropic chemical shieldings (ppm) through the C–C bond of a) ethane, b) ethene and c) ethyne calculated at the MP2/6-311++G(d,p) level of theory.

The high sensitivity of this technique also allows the comparison of C–H bonds, which are frequently overlooked. Figures 2.1a & d show C–H bond shieldings of a fairly similar, slightly arrowhead shape, both with similar magnitudes. On the other hand, ethene displays much rounder C–H bonding regions which are noticeably less shielded than those in ethane and ethyne. Furthermore, the shielding regions along the C–H bonds in ethene are pushed further from the carbon nuclei by the large deshielded features (discussed later).

The shielding present 1 Å above the molecular plane can be used to probe the π density in particular and can be seen in Figure 2.3. The plot over ethane shows no significant shielding features, which is to be expected due to the absence of π bonding. The shielding features visible correspond to the regions around the out-of-plane C–H bonds. Ethene, in comparison (Figure 2.3b) has a more rectangular shape stretching almost to the ends of the C–H bonds with a noticeable region of high shielding directly over the $2p_z$ orbital positions. Ethyne is shown in Figure 2.3c where a lozenge-like shape of shielding is present above the molecule with a circular region of maximum shielding over the C–C bond.
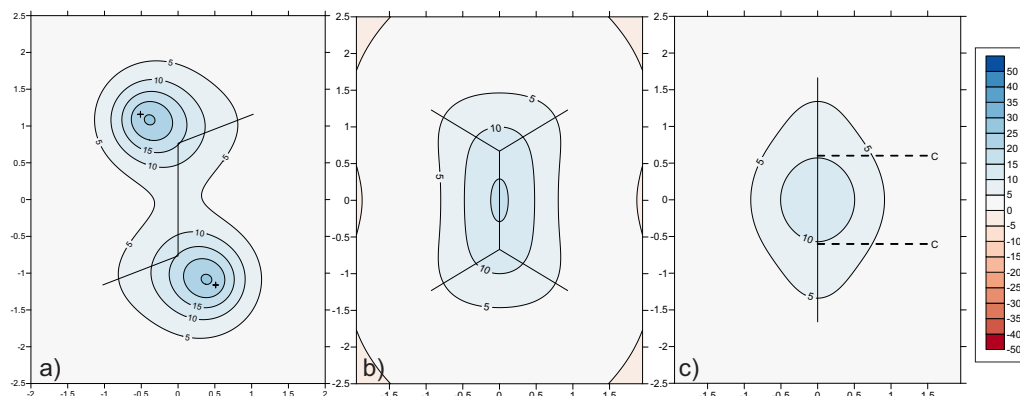
Figure 2.3: Contour plot of the isotropic chemical shieldings (ppm) 1 Å Above the molecular plane of a) ethane, b) ethene and c) ethyne calculated at the MP2/6-311++G(d,p) level of theory.

Alongside the detailed information available in the bonding regions of these hydrocarbons, there are also features surrounding the nuclei that are of great interest (see Figure 2.1). The sp hybridised carbons in ethyne and the sp^2 hybridised carbons in ethene both exhibit regions of deshielding in their immediate surroundings. Analogous features are entirely absent from the sp^3 carbons in ethane, even at very high resolution (0.001 Å grid spacing), suggesting that they are a result of π bonding. It can be seen in the ethene plots that these red, moderately deshielded regions appear in a buffer-like shape between the shielded carbon nuclei and the C–C bond shielding and are wider in the molecular plane than in the vertical plane. When compared to the deshielded features of ethyne, there is a distinct change in shape upon triple bonding. The deshieldings become far less deshielded than in ethene and do not extend around the carbon nuclei as far. Since these features are caused by multiple bonding, it is logical that the difference in magnitude and shape are indicative of the bond order. However, bond length also alters along with bond order, so it is useful to differentiate the effect of bond length from that of the increase in bond order itself.
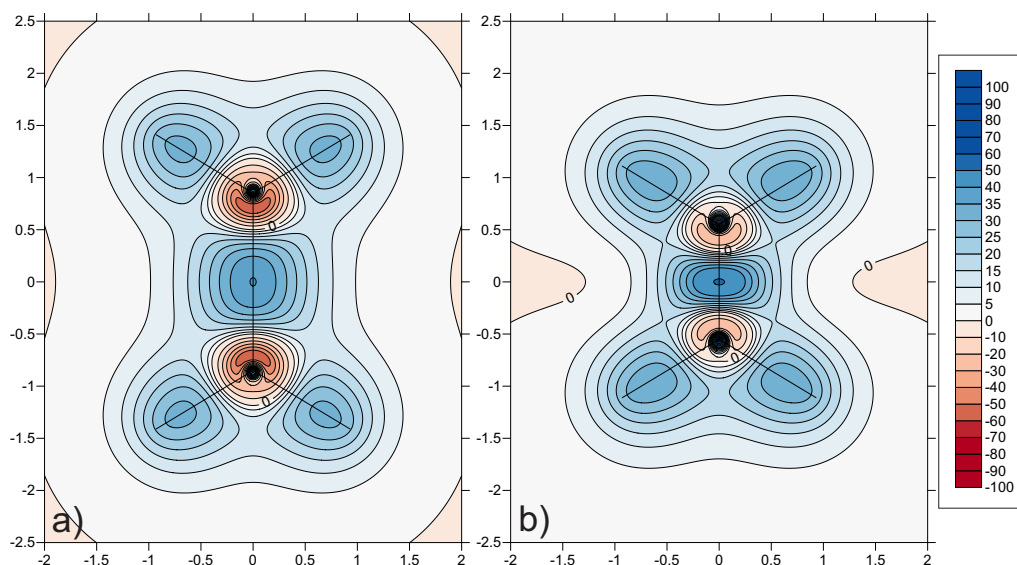
Figure 2.4: Contour plot of the isotropic chemical shieldings (ppm) through the molecular plane of ethene with an altered C–C bond length of a) 1.7 Å and b) 1.1 Å calculated at the MP2/6-311++G(d,p) level of theory.

To attempt to study the effect of bond length, calculations have been repeated on ethene with an increased C–C bond length of 1.7 Å and a decreased C–C bond length of 1.1 Å (for reference, the C–C bond length at the ground state geometry was 1.339 Å), the results of which are shown in Figure 2.4. At first glance, all of the key features present in ground state ethene are replicated upon bond alteration. The main difference is the magnitude of the isotropic shielding surrounding the carbon nuclei and the C–H bonding regions. The bond lengthened ethene is remarkably similar in almost all respects to the equilibrium geometry, with the exception of the magnitude of the deshieldings around the carbon nuclei. The bond shortened structure however, exhibits a shape change of the C–H bond shieldings and a dramatic decrease in the magnitude of the deshielding around the carbon nuclei. In fact, these deshieldings possess values close to those seen in ethyne but with a shape closer to ground state ethene. This suggests that the presence and shape of these deshielded features is due to the bond order, but the magnitude is significantly affected by bond length. This means that accurate geometries are important if the shielding values are to be used for comparative purposes.

2.3   Multiple Double Bonds in a Single System

2.3.1   Allene and 1,3-Butadiene

It is possible to have two double bonds in a three- and four-carbon system in the form of allene (propadiene) and 1,3-butadiene, respectively. The C_{2h} *trans*-1,3-butadiene isomer is considered here as it possesses the lowest energy.

Table 2.2: Isotropic shieldings for the symmetry-unique nuclei and bond maxima in allene (in ppm), calculated at the HF-GIAO/6-311++G(d,p) and MP2-GIAO/6-311++G(d,p) levels of theory.

	$\sigma_{iso}(C_{central})$	$\sigma_{iso}(C_{terminal})$	$\sigma_{iso}(H)$	$\sigma_{iso}(C{=}C)$	$\sigma_{iso}(C{-}H)$
HF	-39.98	115.92	27.19	43.98	37.36
MP2	-18.33	124.48	27.11	43.51	37.18

The shielding values for allene can be seen in Table 2.2 and it is noticeable that the shieldings of the unique carbon environments are hugely different. The $\sigma_{iso}(H)$ values and the C=C bonding maxima are similar to those seen previously in ethene, though the carbon shieldings are distinct. The terminal carbons have a shielding value similar to that seen in ethyne while the central carbon is deshielded, unlike any carbon seen so far. When the contour plot of the isotropic shielding is studied (Figure 2.5), these qualities become even more apparent. The C=C bonding regions are similar in shape and magnitude to those of ethene, including extension of the shielding above and below the molecular plane with the bonding maximum lying at an off-bond position. The regions of space in the vicinity of the carbons, however, are quite unusual. The central carbon possesses a deshielded surrounding of a magnitude without precedent, though the terminal carbons have only very weakly deshielded halos encompassing a well shielded core. This latter structure is most similar to the carbons in ethyne, which is quite unexpected. Although, the C–H bond shielding structures are more suggestive of those seen in ethene, rather than ethyne.
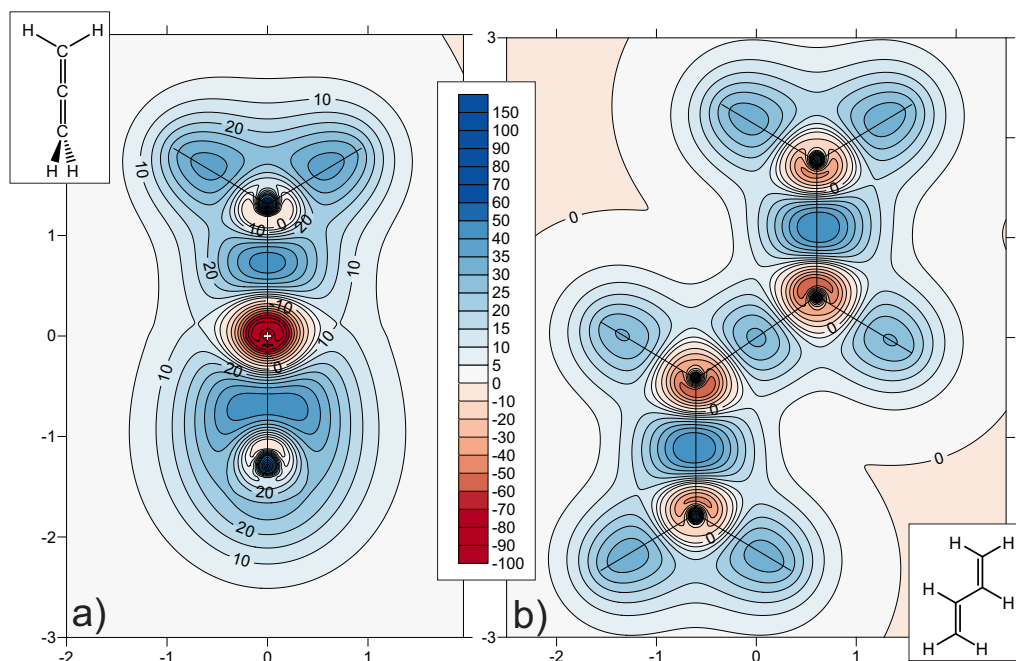
Figure 2.5: Contour plot of the isotropic chemical shieldings (ppm) through the molecular planes of a) allene and b) *trans*-1,3-butadiene calculated at the MP2/6-311++G(d,p) level of theory. The white cross in a) denotes the position of the central carbon.

Table 2.3: Isotropic shieldings for the nuclei and bond maxima in *trans*-1,3-butadiene (ppm), calculated at the HF-GIAO/6-311++G(d,p) and MP2-GIAO/6-311++G(d,p) levels of theory. Subscript *trans* and *cis* refer to positions of hydrogens with respect to the second double bond, with centr and term meaning central and terminal, respectively.

	$\sigma_{\text{iso}}(\text{C}_{\text{centr}})$	$\sigma_{\text{iso}}(\text{C}_{\text{term}})$	$\sigma_{\text{iso}}(\text{H}_{\text{centr}})$	$\sigma_{\text{iso}}(\text{H}_{\text{term}, cis})$	$\sigma_{\text{iso}}(\text{H}_{\text{term}, trans})$
HF	45.52	67.95	25.02	26.10	26.32
MP2	56.90	81.04	25.04	26.06	26.24

	$\sigma_{\text{iso}}(\text{C=C})$	$\sigma_{\text{iso}}(\text{C–C})$	$\sigma_{\text{iso}}(\text{C–H}_{\text{centr}})$	$\sigma_{\text{iso}}(\text{C–H}_{\text{term}, cis})$	$\sigma_{\text{iso}}(\text{C–H}_{\text{term}, trans})$
HF	49.25	29.22	30.48	32.94	33.38
MP2	46.60	31.11	30.37	32.88	33.23

The contour plot of butadiene is perhaps more typical of the results seen for the small hydrocarbons. The two formal double bond regions have similar shapes to those in ethene with maximum shielding values that are only slightly lower than ethene. The C–C single bond region, however, has a shielding maximum that is

lower than the C–H bonds in allene and the terminal C–H bonds in butadiene. The shielded internuclear region is also quite different from the narrow, highly shielded structure in ethane and is more reminiscent of a significantly weakened double bond. These features are a result of the conjugation across the molecular backbone which slightly weakens the double bonds and bestows a degree of double bond character upon the C–C formal single bond.

The carbons have shielding values which straddle the value found in ethene, with the terminal carbons having higher shieldings and the central carbons lower shieldings (see Table 2.3). The red, deshielded halos surrounding the carbons in butadiene are consistent with those in C_2H_4 as well. Overall, butadiene displays expected features, whereas allene is more unique.

2.3.2   Acrolein

Of course, bonding to heteroatoms is essential in most chemically important systems and is therefore worthy of investigation here. A simple example is acrolein (prop-2-enal), a molecule which contains C–C single and double bonds along with their associated C–H bonds, as seen previously, but also contains a carbonyl group. This allows the investigation and comparison of each of these bonds all in one molecule.

Table 2.4: Isotropic shieldings for the nuclei and bond maxima in acrolein (in ppm), calculated at the HF-GIAO/6-311++G(d,p) and MP2-GIAO/6-311++G(d,p) levels of theory. The subscript α, β, *cis* and *trans* denote positions with respect to the carbonyl group.

	$\sigma_{\text{iso}}(C_{C=O})$	$\sigma_{\text{iso}}(C_\alpha)$	$\sigma_{\text{iso}}(C_\beta)$	$\sigma_{\text{iso}}(O)$	$\sigma_{\text{iso}}(H_{C=O})$	$\sigma_{\text{iso}}(H_\alpha)$
HF	− 6.71	47.06	47.09	−344.96	22.75	25.29
MP2	11.87	55.12	65.23	−272.45	22.49	25.40

	$\sigma_{\text{iso}}(H_{\beta\ cis})$	$\sigma_{\text{iso}}(H_{\beta\ trans})$	$\sigma_{\text{iso}}(C=O)$	$\sigma_{\text{iso}}(C\text{–}C)$	$\sigma_{\text{iso}}(C=C)$
HF	25.59	25.36	42.59	20.60	46.16
MP2	25.79	25.54	34.00	21.42	43.67

Table 2.4 shows shielding values for the nuclei in acrolein as well as the shielding maxima along various bonds within the molecule. It should be noted that these

shielding maxima do not necessarily lie at the bond mid-point, nor do they always lie along the line connecting the atoms.

On inspection of the HF values compared with the MP2 values in Table 2.4, it can be seen that, like for the simple hydrocarbons, inclusion of correlation effects makes a significant difference to the calculated shielding magnitudes. But on comparison of the whole molecular plane plots in Figure 2.6a & b, it can be seen that all of the main features are consistent irrespective of theory level. The key differences between the methods are highlighted in Figure 2.6d by a molecular plane plot created from the subtraction of the HF values from the MP2 values.
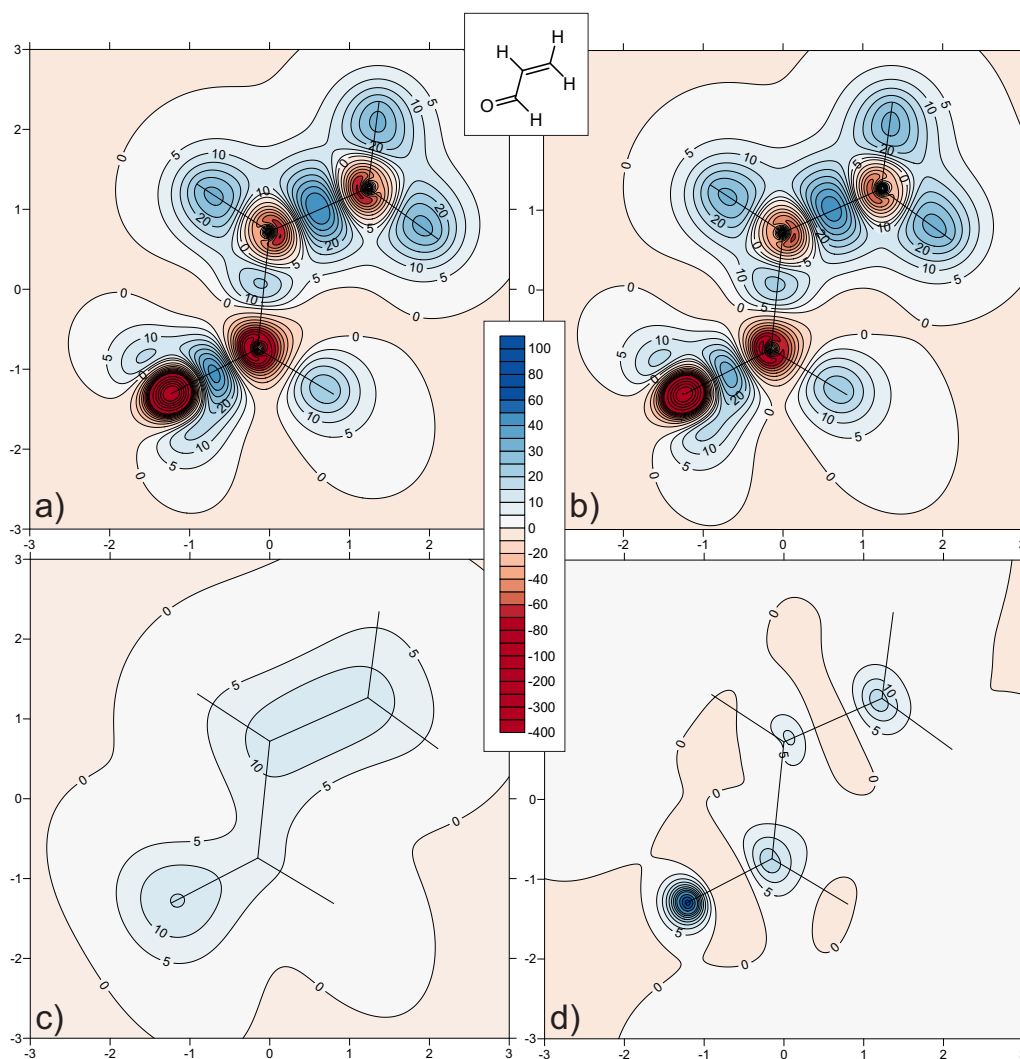
Figure 2.6: Contour plot of the isotropic chemical shieldings (ppm) through a) the molecular plane of acrolein calculated at the HF/6-311++G(d,p) level of theory, b) the molecular plane of acrolein calculated at the MP2/6-311++G(d,p) level of theory, c) a plane 1 Å above the molecular plane of acrolein and d) the difference between the MP2 and HF molecular plane plots.

This difference plot shows that, in general, the main regions where the HF method underestimates the shielding are regions directly surrounding the nuclei, with the electronegative oxygen being the most different. This is because correlation effects are important mostly for π systems and it has been established previously that the π system is responsible for the shielding features around sp and sp^2 hybridised nuclei. It therefore follows that these regions would be most affected by the change in theory level.

Comparison of the $\sigma_{iso}(H)$ values from Table 2.4 shows that, with the exception

of the hydrogen directly bonded to the carbonyl group, all hydrogen shieldings are roughly 25 ppm. On closer inspection, it can also be seen that the hydrogen attached to the α carbon (H_α) has a shielding value closest to the hydrogen on the β carbon which lies *trans* to the carbonyl ($H_{\beta\ trans}$). It can be seen that the $\sigma_{iso}(C)$ results vary far more, which is perhaps expected, and the oxygen nucleus is significantly deshielded.

The bonding regions are perhaps of most interest in acrolein. The shielding maximum of the C–C bond here is *ca* 21 ppm, whereas in ethane, the same C–C single bond reached a shielding of *ca* 52 ppm. Likewise, the C=C in acrolein is around 44 ppm with that in ethene reaching about 50 ppm. There is a large decrease in shielding along the single C–C bond in acrolein compared to ethane which implies a weaker bond strength. The same is true of the C=C bond but to a lesser extent. This is the result of the π conjugation along the whole molecule. This conjugation can be seen in the contour plot positioned 1 Å above the molecular plane (Figure 2.6c). In this figure, there is a small degree of delocalisation across the molecule, but still with moderate localisation over the C=C bond and the oxygen atom. The C=O bond, of the same formal bond order as the C=C bond, has a maximum shielding of approximately 34 ppm, suggesting an intermediate bond strength between that of the C–C single and double bonds.

However, as seen for the hydrocarbon cases, consideration of the bond shielding maximum in isolation is ineffective in fully describing bonding character. For a more detailed analysis, the shape of the shielding regions must also be taken into account and can be seen in Figure 2.6a & b.

The regions surrounding the C–H bonds on the ethene moiety all have similar shapes while the C–H connected to the carbonyl group has a greater degree of roundedness. This reflects the trend in the H nuclei shieldings seen previously. The carbonyl group itself displays a wrapping of the bond shielding around the oxygen nucleus caused by oxygen's electronegativity and the presence of lone pairs. Visualisation of the carbonyl group asymmetry is also possible here and is consistent between the theory levels. The C=C bonding region is very similar to that seen in ethene previously, but the C–C bond is quite different from that seen in ethane, consistent with the difference in shielding maximum values. In acrolein, the C–C bond shielding is fairly small and weak with the maximum shielding lying at an off-bond position nearest C_α. It appears that this distortion is, in part, due to the intense deshielded region surrounding the carbon nucleus

of the carbonyl group. The alkene carbons have only a moderately deshielded surrounding, both of which are fairly similar and with the deshielding maximum lying generally pointed towards the bond, though with a slight rotation off-bond in the case of C_α. This rotation is a result of the π conjugation along the molecule.

2.4   3-Centre-2-Electron Bonding

Diborane (B_2H_6) exhibits an interesting molecular structure containing two bridging hydrogens and four terminal hydrogens. The bridging hydrogens are now commonly considered examples of 3-centre-2-electron bonding. It has been postulated previously that the bonding in diborane could involve an overlapping of π wavefunctions which would effectively create a double bond contribution.[68] However, this would require the BH_3 moieties to have a planar arrangement as opposed to the observed pyramidal structure. It was also proposed by Sidgwick that two of the B–H bonds were one-electron bonds.[79] Pauling agreed and even extended this idea by suggesting that no two particular bonds were permanently of one-electron character but that this fluctuates between the bonds in a kind of resonance.[80] Lewis, however, disagreed due to a lack of observed paramagnetic character.[81] In the same paper, he describes the concept of a three-electron single bond as "unthinkable" but that a three-electron double bond, consisting of two occupied orbitals in one bond and one in another, was more likely, though still did not explain the lack of paramagnetic character. Lewis concluded that the most appropriate description of the bonding in diborane is one similar to that of ethane but with two missing electrons so that each bonding pair, on average, is filled six-sevenths of the time. This would allow the electrons to remain paired, consistent with diborane's diamagnetic properties.

Table 2.5: Isotropic shieldings for the symmetry unique nuclei and bond maxima in diborane (in ppm), calculated at the HF-GIAO/6-311++G(d,p) and MP2-GIAO/6-311++G(d,p) levels of theory.

	$\sigma_{iso}(B)$	$\sigma_{iso}(H_{terminal})$	$\sigma_{iso}(H_{bridging})$	$\sigma_{iso}(B–H–B)$	$\sigma_{iso}(B–H_{terminal})$
HF	102.25	27.86	32.86	38.81	27.11
MP2	98.08	27.42	32.55	38.46	27.34

It can be seen from the σ_{iso} values in Table 2.5 that, with the exception of the value on the boron nucleus, there is negligible difference between the theory levels used. Though even the difference between the boron values is fairly small. This is consistent with the earlier observation that the inclusion of correlation effects only significantly affects atoms with a degree of π bonding character. Another interesting trend is the similarity between the $\sigma_{iso}(H_{terminal})$ and the $\sigma_{iso}(B–H_{terminal})$ values. When this is compared to the two-dimensional plots of σ_{iso} values in Figure 2.7, this trend can be explained by the position of the B–H bond shielding maximum lying very close to the H nucleus, as opposed to lying fairly near the bond mid-point, as it does in ethane, or slightly further from the H in the case of ethene. The region of maximum shielding is also noticeably smaller than in the hydrocarbons seen previously. The bridging hydrogens, however, are more shielded than their terminal counterparts by around 5 ppm. Furthermore, in Figure 2.7b, the B–H–B bridging bond has a shielding maximum positioned central inside the B–H–B angle, rather than along the B–H internuclear distances.

The plots in Figure 2.7 also show weak deshielding around the two boron nuclei, reminiscent of that seen around previous unsaturated carbons. However, the magnitude of these areas is significantly lower than the previous examples where they were products of π bonding. In the case of diborane, the unusual nature of the 3-centre-2-electron bonding has generated slightly similar features to that of a delocalised π system which is fascinating. Interestingly, even at high magnification (see top left of Figure 2.7), there is no evidence of a lobe of deshielding maximum directly around the boron nucleus, something which can be seen for nuclei that are part of a π system. This finding could be used to elucidate the cause of the various features observed in plots of this type, for example, deshielded regions surrounding nuclei seem to be created by delocalised bonding electrons, although there is clearly a difference between π bonding and 3-centre-2-electron bonding.
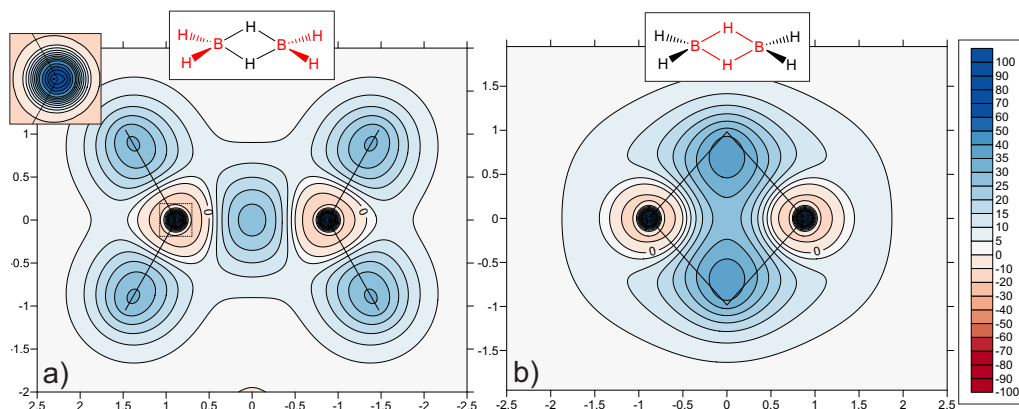
Figure 2.7: Contour plot of the isotropic chemical shieldings (ppm) for diborane a) through the molecular plane (with a close-up of the region surrounding a boron nucleus) and b) through a vertical plane bisecting the bridging hydrogens calculated at the MP2/6-311++G(d,p) level of theory. The red sections of the molecular structures correspond to the sections of diborane that lie in the plane of the plots.

This is a rare example of the visualisation of a bond of this type and demonstrates a degree of bonding character directly between the two B nuclei themselves (also seen in Figure 2.7a). In fact, the shielding between the two B nuclei is not dissimilar in appearance to a weakened version of the C=C bond in ethene. If Lewis' illustration of a three-electron double bond is correct, this could explain the similarity. Moreover, Mulliken likens the electronic structure of diborane to that of O_2, though comments that the idea of formal B=B bond is unreasonable.[82] In fact, Mulliken concludes that the most likely bonding model involves the H atoms being held by two electron-pair bonds and one one-electron bond, like that proposed by Sidgwick and Pauling, though with a degree of π character. The combination of the resemblance to ethene in the B–B region and the B deshielding regions as well as the unusual shielding lying in the centre of the B–H–B angle is all consistent with bonding similar to that which Mulliken describes, complete with features implying a degree of bond delocalisation associated with π bonding.

However, further investigation into the behaviour of boron atoms in work of this type would need to be performed for an absolute conclusion, though it is clear that a traditional skeletal structure of diborane can misrepresent the true nature of the bonding.

2.5 Hydrogen Bonding

The hydrogen bond (H-bond) is arguably the most important of the weak molecular interactions. Perhaps the simplest example of a H-bond can be found in the case of the water dimer. Shielding values for a lone water molecule as well as the water dimer can be found in Table 2.6 with the contour plots shown in Figure 2.8.

Table 2.6: Isotropic shieldings for the symmetry-unique nuclei in water and the water dimer (in ppm), calculated at the HF-GIAO/6-311++G(d,p) and MP2-GIAO/6-311++G(d,p) levels of theory.

		Monomer	H-acceptor	H-donor
$\sigma_{iso}(O)$	HF	325.30	320.29	326.72
	MP2	344.04	339.08	342.92

		Monomer	H-bond	H-acceptor	H-donor
$\sigma_{iso}(H)$	HF	31.26	28.25	30.77	31.86
	MP2	31.42	28.48	30.92	31.91

Several interesting features can be seen amongst the nuclear shielding values in Table 2.6. As seen before, there is very little advantage of including correlation effects when calculating $\sigma_{iso}(H)$ values. However, there is significant impact of this increase in theory level on the $\sigma_{iso}(O)$ calculations. Where previously the main difference has been seen in π bonded systems, here this is not the case. Instead it seems that the correlation effects are important to account for the oxygen lone pairs. In fact, use of the MP2 level of theory changes the ordering of the $\sigma_{iso}(O)$ shielding values compared to the HF calculations. Considering only the MP2 values, it can be seen that, upon H-bonding, the shielding of the oxygen nuclei both decrease slightly from the value in monomeric water, although the oxygen in the H-acceptor molecule is perturbed the most. In Figure 2.8 this alteration upon dimerisation is difficult to see.
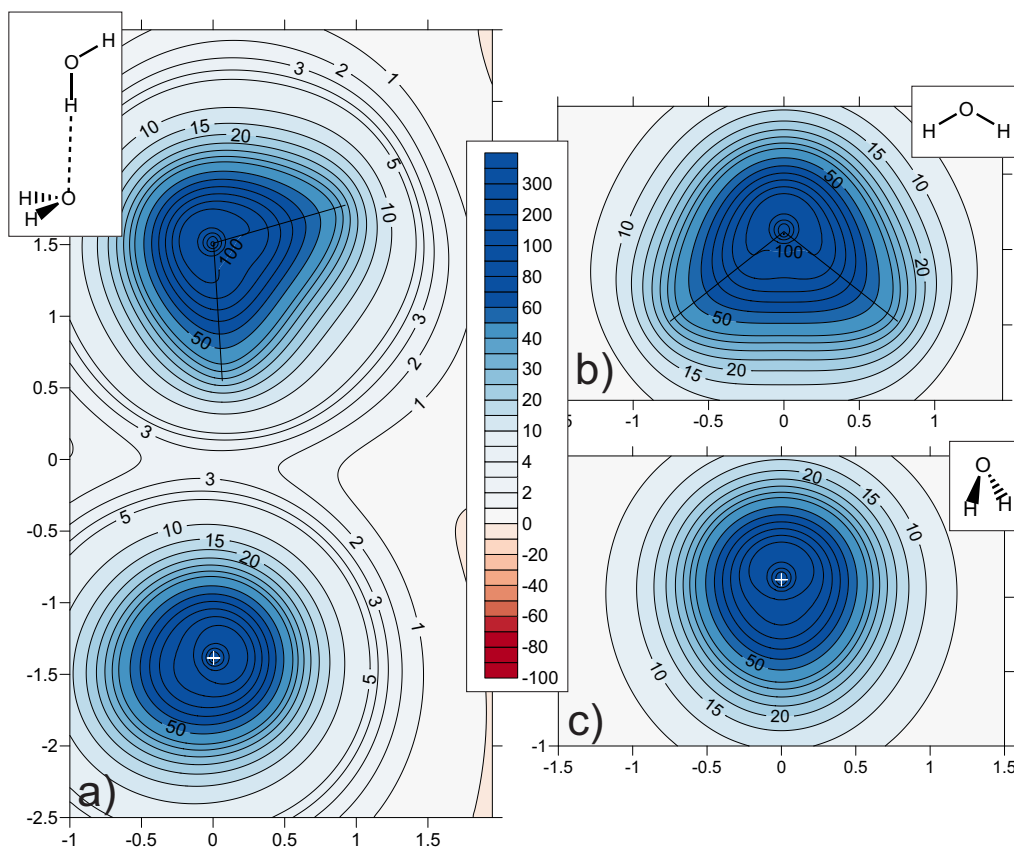
Figure 2.8: Contour plot of the isotropic chemical shieldings (ppm) for water as a) water dimer b) through the molecular plane and c) through the vertical plane calculated at the MP2/6-311++G(d,p) level of theory. The white crosses denote the position of the oxygen nuclei.

The H shielding values also show an interesting pattern. The shielding of the H on the donor water molecule that is not involved directly in the H-bond (labelled H-donor in Table 2.6) is slightly higher than that found in a water monomer whereas the hydrogens on the H-acceptor and that on the donor which is involved in the H-bond are both decreased compared to lone water. The biggest change in shielding upon dimerisation is that of the hydrogen directly participating in the H-bond, which is to be expected. The structures found in the isosurface plots (Figure 2.8) show very little visible difference between the water dimer and a lone water molecule. However, there is perhaps a subtle noteworthy feature directly along the H-bond where there is a slight increase in shielding. This region could potentially be caused by the simple overlap of the shielding of the two single molecules, but because of the importance of this interaction, it is worth further investigation to clarify if a visualisation of H-bonding is possible with this method.

A study of intramolecular H-bonding can also be seen in the section surrounding malonaldehyde and various derivatives in Chapter 7.

2.6   Conclusions

The use of isotropic shielding calculations has proven highly sensitive for the purpose of describing a variety of bonding interactions. It was shown that shielding maxima along bonds cannot be used as a quantitative assessment of bond order on their own. Rather, it is important to take into account the magnitude and shape of the whole bond region. In molecules with a degree of π bonding, the atoms involved exhibit deshielded surroundings of a form and value characteristic of the nature of the nearby bonding. These features combined can allow comparisons between different types of chemical bonding with the two-carbon hydrocarbons used as something of a benchmark. In this manner, the exact nature of bonding can be probed and a more detailed view of multiple bonding can be obtained that does not rely simply on formal bond order.

Cross-sections of the single, double and triple C–C bonds in the small hydrocarbons show an elliptical bond shielding in the double bond but a circular structure in both ethane and ethyne. This can be explained by the nature of the orbitals involved in the triple bond being positioned perpendicular to one another creating a more cylindrical bond than in the double bond of ethene. Shielding plots calculated at 1 Å above these three systems allow a study more directed at the π bonding without inclusion of σ effects. These can also show features characteristic of bond nature and allow a comparison between the double bond of ethene and those in acrolein- with a clear difference visible between the C=C and C=O bonds. These also allow insight into degrees of conjugation across molecules.

In the case of *trans*-1,3-butadiene and acrolein, the extent of delocalisation along each system can be estimated by comparison of the bonding regions which display C–C single bonds with certain properties of formal double bonds. Likewise, this technique has proven sensitive enough to distinguish several key differences between C=C and C=O double bonds. It even allows distinction between C–H bonds which are often overlooked as being standard across molecules. For the results on allene, quite unusual and unexpected features emerge which include terminal carbon environments consistent with those in ethyne, hydrogen environments, C=C and C–H bonds similar to those in ethene and a deshielded central

carbon which is unique to results so far.

More exotic bonding was studied in diborane, which possesses 3-centre-2-electron bonded bridging hydrogens. This yielded very interesting shielding structures which are reminiscent of ethene in the molecular plane, but which are unique when considered through the plane of the bridging hydrogens. The boron nuclei exhibit weakly deshielded halos which are distinct in both structure and magnitude from those seen in other unsaturated systems. The weak intermolecular H-bonding interactions in the case of the water dimer where also investigated. Whilst the isosurfaces did not produce significant regions of interest directly along the H-bond, the subtle effects on the participating molecules were evident and could be used effectively to probe this interaction in other systems.

Throughout, shielding values calculated at both HF and MP2 levels of theory have been compared with a difference isosurface plotted for acrolein (Figure 2.6d). Results show that both methods are in good agreement for hydrogen atoms and sp^3 nuclei, but shielding magnitudes are quite different in π bonded systems when the dynamic correlation effects are included. The difference plot for acrolein shows that the greatest disagreement is present over these unsaturated nuclei, in particular, the oxygen of the carbonyl, while the bonding regions remain mostly unchanged. The effect of geometry was investigated using ethene as a test molecule in Figure 2.4. It was found that accurate geometries are vital in producing accurate shielding features as a relatively small change in bond length dramatically alters the deshielded nuclear regions (although the general bonding features remain consistent).

3

Aromaticity & Antiaromaticity

"I would trade all my experimental works for the single idea of the benzene theory"

August Wilhelm von Hofmann

3.1   Introduction

As discussed in the main introduction, the chemical concept of aromaticity is a common, yet sometimes controversial, topic in modern chemistry. It is also further complicated by the addition of the antithetical antiaromaticity, a concept which is arguably even less well understood. Magnetic shielding calculations are already popular for describing such systems, but it is essential to benchmark these two chemical concepts using our application of this technique before investigating more complex molecules. This is achieved by studying the archetypes of aromaticity and antiaromaticity. Namely benzene and cyclobutadiene, respectively.

Inorganic analogues of benzene are also studied here in order to assess any aromatic properties, but also to probe the effect on bonding and shielding properties of increased atom size. Here hexasilabenzene and hexagermabenzene are investigated. Aromatic stabilisation energy calculations and ring-size-adjusted aromaticity indices have ordered the aromaticity of these three systems as benzene $> Si_6H_6 \approx Ge_6H_6$.[52] A consistent trend is seen with NICS(π) calculations by the same authors. However, it has also been shown that more information can be obtained by using a magnetic shielding calculation technique in a systematic way, like that of the so-called NICS-scan method.[55] This suggests that an even more detailed set of calculations, like those proposed here, would yield significantly more molecular information.

Cyclobutene is also probed in this chapter. A product of the electrocyclisation of butadiene (see previous chapter), this system has the same type of structure as antiaromatic cyclobutadiene, but with one fewer formal double bond. Cyclobutene moieties are rife throughout synthetic and biological chemistry.[83–86] Their high degree of ring strain and multiple bond make them useful synthons which can undergo a huge variety of reactions, including ring-opening electrocyclisations, metathesis-type reactions, epoxidations and cyclopropanations.[86,87] These have been used to produce bicyclic systems for biomolecules in an environmentally benign way,[87] to produce expanded rings of different sizes[88] and to produce useful natural products such as ($\pm$)-sporochnol A,[89] which has fish deterrent properties[90], and β-lumicolchicine, used as a colchicine control in anti-cancer drug studies.[91–93] A deeper understanding of the molecular properties of such a common and important structure would be most welcome.

The structure of benzene used here is the experimentally determined D_{6h} gas-

phase geometry.[94] For cyclobutadiene, the square D_{4h} structure is used as it is the most antiaromatic intermediate between the two rectangular D_{2h} ground states. This geometry was optimised using multireference averaged quadratic coupled cluster (MR-AQCC) calculations with a cc-pVTZ basis set.[95] The C_{2v} structure of cyclobutene was optimised at the MP2/6-311++G(d,p) level of theory using the Tight convergence criterion and a ground state was confirmed by frequency analysis. D_{6h} hexagermabenzene (Ge_6H_6) was optimised at the MP2/6-31G(d,p) level of theory, also with the Tight criterion and frequency analysis. The D_{6h} hexasilabenzene (Si_6H_6) geometry was optimised at the CASSCF(6,6)/6-31G(d,p) level of theory by Karadakov and co-workers.[96] This latter structure was shown to have three imaginary frequencies and analysis showed that a non-planar geometry would have been more stable in this case. However, the planar structure was used as it would display any aromatic qualities, or lack thereof, more than a non-planar geometry. It should be noted that some of the work on benzene and cyclobutadiene has been previously published in the Journal of Physical Chemistry A.[97]

3.2 Benzene

The behaviour of the isotropic shielding around benzene is illustrated, through a variety of planes, in Figure 3.1. These plots were calculated at the CASSCF(6,6) level of theory in order to allow proper comparison with those of cyclobutadiene in the next section. The shielding feature at the ring centre is consistent with results in other work, like that of the NICS technique.[42] However, it is evident that there is far more information available in these shielding plots than simply an indication of aromaticity.

The regions of shielding in the vicinity of the covalent bonds are also of significant interest. The areas directly in between adjacent carbons display strong shielding up to around 44 ppm (exact values calculated at various levels of theory can be found in Table 3.1). As discussed in the previous chapter, the maximum shielding value along a bond cannot be used as a sole indicator of bond order or strength. Instead, this information must be combined with the morphology of the shielded region to give a full description of the bonding character. Bond maxima of around 44 ppm are lower than those seen previously in ethene (a formal double bond) though the shape of the bond shielding is very similar. The same is true of the

double bonds in 1,3-butadiene which exhibits a degree of delocalisation weakening the formal double bonds. This is all consistent with the expected 1.5 bond order for the C–C bonds in benzene.

Even more interesting is the C–C bond cross section. In the case of ethene, an elliptical shape was seen. Here, in benzene, this elliptical shape is still evident, but with a slight indentation visible on the innermost edge. This gives the overall cross-section something of a kidney shape. This perturbation is likely caused by the typical aromatic centre.
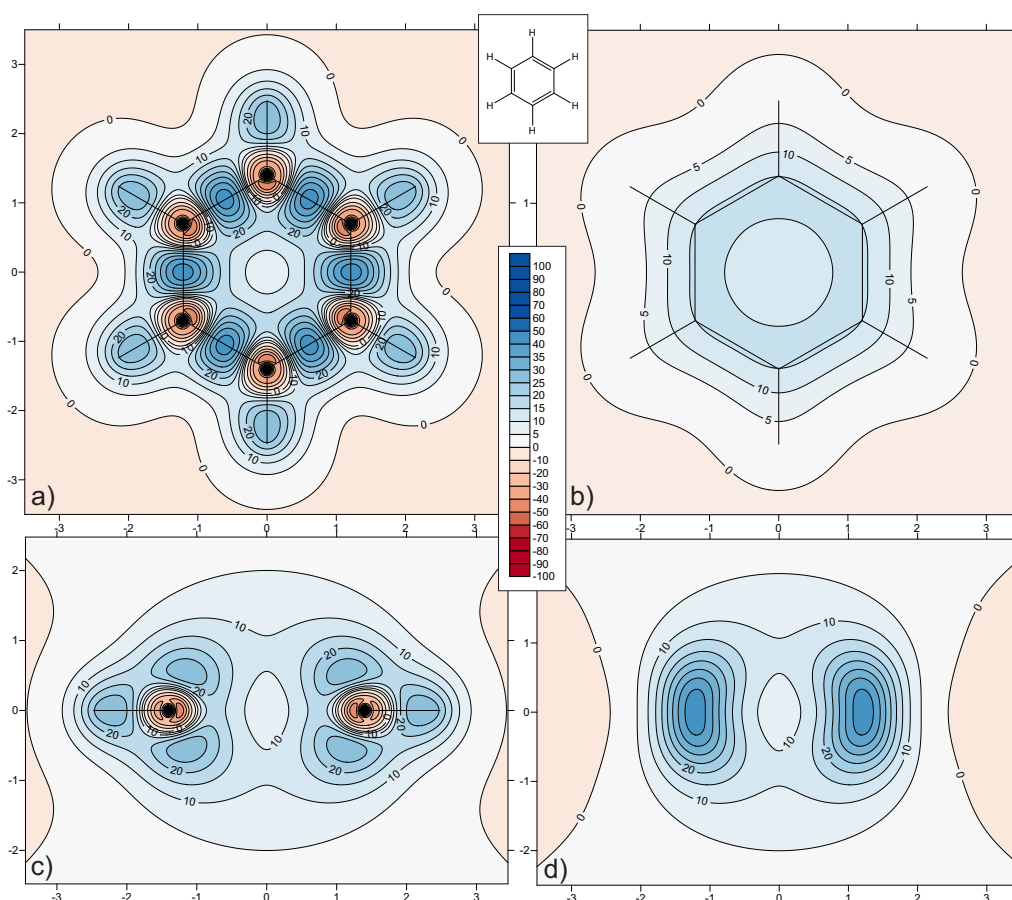
Figure 3.1: Contour plot of the isotropic chemical shieldings (ppm) for benzene through a) molecular plane, b) 1 Å above the molecular plane, c) a vertical plane bisecting C–H bonds and d) a vertical plane bisecting C–C bonds calculated at the MP2/6-311++G(d,p) level of theory.

The σ_{iso}(H) values seen in Table 3.1 are roughly 25 ppm with C–H maxima of around 30 ppm. When this is compared to the σ_{iso}(H) values of the systems in Chapter 2, they are slightly lower than those found in ethene (26 ppm) or 1,3-butadiene (27 ppm). This proton shielding trend is conventionally explained by

the aromatic ring current in benzene, although alternative explanations are available.[43] Interestingly, the C–H maxima are more shielded than the H nuclei themselves.

Table 3.1: Isotropic shieldings for the nuclei and bond maxima in benzene (in ppm), calculated at the HF-GIAO/6-311++G(d,p), MP2-GIAO/6-311++G(d,p), CASSCF(6,6)/6-311++G(d,p), B3LYP/aug-cc-pV5Z and M06/aug-cc-pV5Z levels of theory.

	$\sigma_{\text{iso}}(C)$	$\sigma_{\text{iso}}(H)$	$\sigma_{\text{iso}}(C-C)$	$\sigma_{\text{iso}}(C-H)$
HF	58.00	24.48	44.29	30.09
MP2	69.14	24.25	43.03	29.58
CASSCF	73.85	25.19	44.77	31.29
B3LYP	41.27	23.92	41.76	29.32
M06	33.94	23.94	−	−

The vertical planes slicing through benzene are also interesting. It can be noted that the point of maximum shielding along the normal to the molecular plane passing through the ring centre is not positioned at 1 Å. Instead it appears at around a height of 0.76 Å. This suggests that the use of NICS(0) and NICS(1) values are not ideal for assessing the true shielding at aromatic centres. The vertical plane bisecting the atoms shows a cross-section of two shielded doughnuts above and below the molecular plane. These features are similar to popular images of benzene possessing a ring of π density above and below the ring. Part of this feature can also be seen in the 1 Å above plot.

It is clear from Figure 3.1 that the red regions of deshielding surrounding the sp^2 carbon nuclei are consistent with those seen previously in double bonded systems, like ethene and 1,3-butadiene. This is as expected if still not fully explained. The lobe of lowest shielding around the carbons in benzene is positioned pointing towards the ring centre and reaches values of around -45 ppm. The region directly over the nucleus is, however, shielded. Again, consistent with previous results. It is also useful to note that these deshielded features, while their magnitudes may alter slightly, are present in a very similar form across calculations at various levels of theory (see Figure 3.2). It has been mentioned previously that most existing DFT methods are inappropriate for magnetic shielding calculations such as those performed here. This can be highlighted by inspection of the

B3LYP plot in Figure 3.2 and the B3LYP and M06 shielding values in Table 3.1.
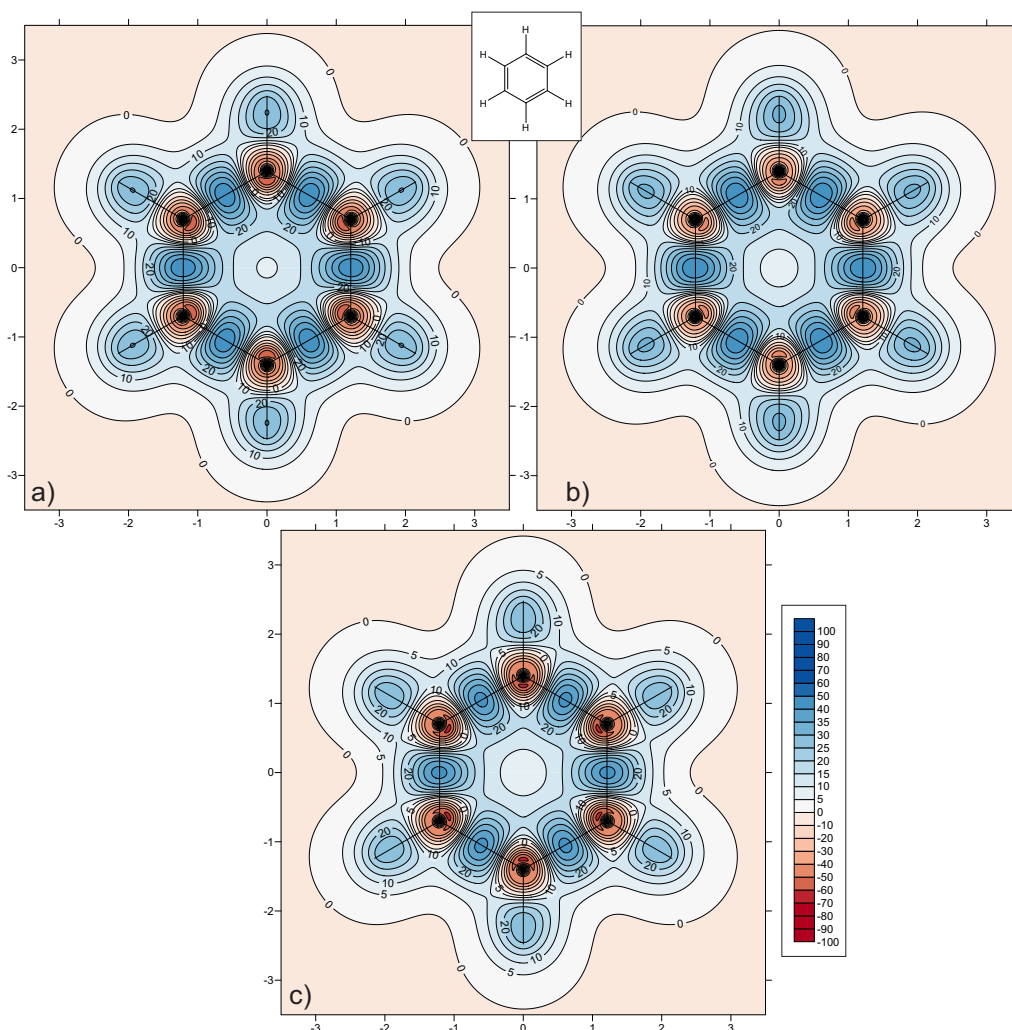
Figure 3.2: Contour plot of the isotropic chemical shieldings (ppm) through the molecular plane of benzene at the a) HF/6-311++G(d,p), b) CASSCF(6,6)/6-311++G(d,p) and c) B3LYP/aug-cc-pV5Z levels of theory.

The DFT calculations utilise a very large aug-cc-pV5Z basis set and require an incredibly fine integration grid. Without these settings, the $\sigma_{iso}(C)$ and $\sigma_{iso}(H)$ values are calculated to be inequivalent. The D_{6h} symmetry of benzene requires all C and all H nuclei to be identical. The values of $\sigma_{iso}(C)$ found in Table 3.1 show reasonable similarity between the MP2 and CASSCF methods, with HF a little lower, as expected. However, the values obtained for the two DFT methods are vastly different. Moreover, on inspection of the B3LYP plot in Figure 3.2, it can be seen that there appears to be an artificial rounding of the shielding features and contours. These calculation settings also dramatically increase the computational

cost. This means that the usual advantage of DFT over post-HF methods is void. In fact DFT calculations with these extra options are dramatically more expensive than HF or MP2 calculations. For this reason, a molecular plane M06 isotropic shielding grid was not obtained. This, combined with the inconsistency of the calculated shielding values means that DFT methods are far from suitable for this kind of work. For these reasons, DFT shall no longer be considered in this work.

3.3   Cyclobutadiene

Isotropic shielding results calculated in and around square cyclobutadiene at the CASSCF(4,4)/6-311++G(d,p) level of theory can be found in Figure 3.3 and Table 3.2. The CASSCF(4,4) level of theory was required for this antiaromatic system in order to correctly describe the antiaromatic character.

Table 3.2: Isotropic shieldings for the nuclei and bond maxima in cyclobutadiene (in ppm), calculated at the CASSCF(4,4)/6-311++G(d,p) levels of theory.

$\sigma_{iso}(C)$	$\sigma_{iso}(H)$	$\sigma_{iso}(C–C)$	$\sigma_{iso}(C–H)$
69.10	27.71	24.89	34.35

On comparison of the values in Table 3.2 with the corresponding CASSCF values for benzene in Table 3.1 several interesting differences can be seen. Firstly, the shieldings on the nuclei themselves are fairly close, with the value of the C lower than in benzene but the H higher by *ca* 2 ppm. The C–H bond shielding maximum is also slightly higher for cyclobutadiene than in benzene. However, perhaps the most interesting comparison should be made between the C–C bonds.

The C–C bond shielding maximum in cyclobutadiene is almost half that of the C–C bond in benzene. This emphasises the dramatic decrease in bond strength on moving to a strained, antiaromatic molecule. When the whole bonding region is considered (see Figure 3.3), it can be noticed that the shielded bonding regions in cyclobutadiene do not lie along the lines connecting the neighbouring carbon atoms. Instead, they lie along off-bond positions and display a significant degree of bent character. Whether this is due to ring strain, antiaromaticity or both will be discussed later in Chapter 5.

Another key comparison with the plots of benzene is the C–C bond cross-section. In the case of benzene, the cross-sections were reminiscent of a kidney i.e. like a slightly distorted double bond. Here, the bond cross-section, apart from being far less shielded (as expected for a weaker bond), the shape is quite different and unlike results seen before. The bonds have a slightly triangular cut-end suggesting a very different nature of bonding to that seen in benzene.
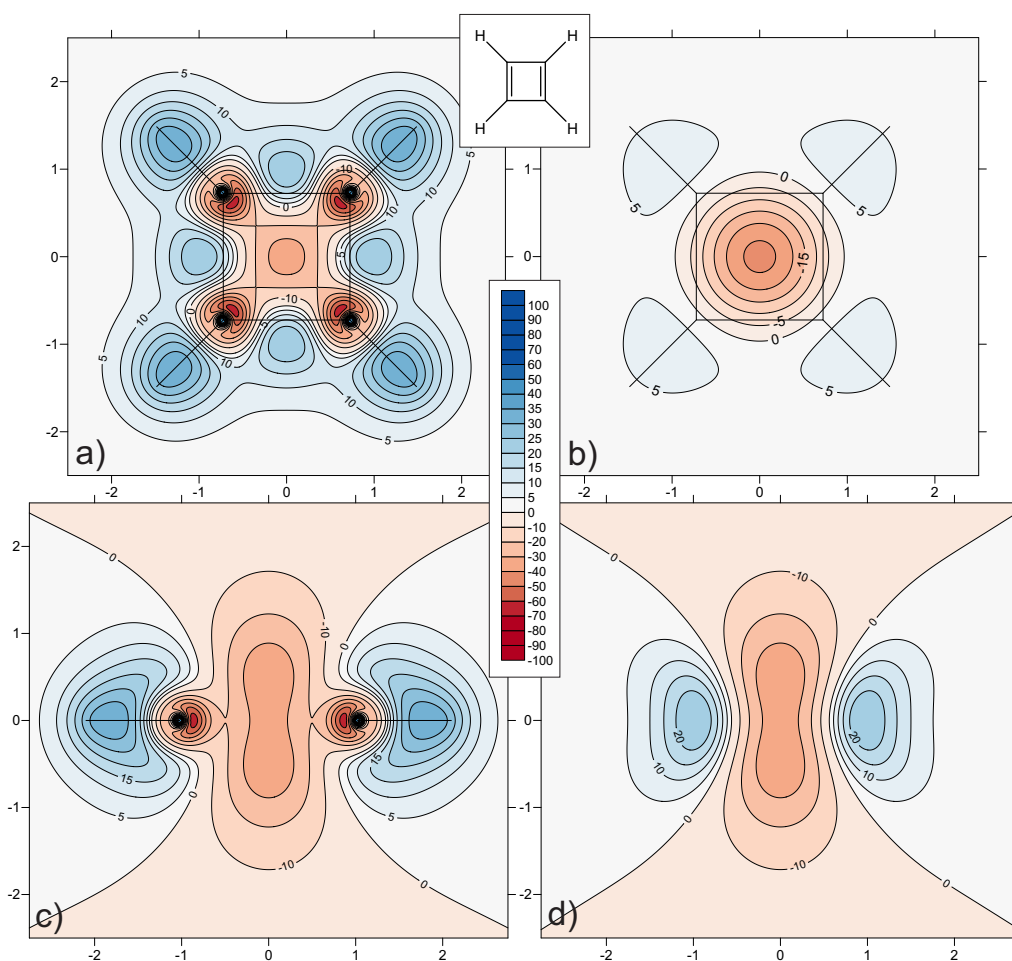
Figure 3.3: Contour plot of the isotropic chemical shieldings (ppm) for square cyclobutadiene through a) molecular plane, b) 1 Å above the molecular plane, c) a vertical plane bisecting C–H bonds and d) a vertical plane bisecting C–C bonds calculated at the MP2/6-311++G(d,p) level of theory.

The regions of deshielding surrounding the sp^2 hybridised carbon nuclei are once again present here, with the lobe of intense deshielding pointing towards the ring centre. However, the magnitude of the deshielding is greater than that in benzene, with values here reaching around -64 ppm compared to -45 ppm in benzene. The same shielded region directly over the nucleus is also evident. Similar

deshielded regions around carbon nuclei in cyclobutadiene can be seen in work by Kleinpeter *et al.* but were not commented upon in that work.[57] There is also an absence of any equivalent of the π doughnut seen in aromatic benzene.

The most striking feature in the cyclobutadiene contour plots, however, is arguably the deshielded 'dumbbell-shaped' region at the ring centre. This feature protrudes significantly above and below the molecular plane, though again, the most intense region does not lie at NICS(0) or NICS(1) positions. This unusual structure is indicative of antiaromatic systems, as shall be seen in later chapters. An analogous feature is also present in the less antiaromatic bond-alternating rectangular cyclobutadiene, though it appears slightly less intense.
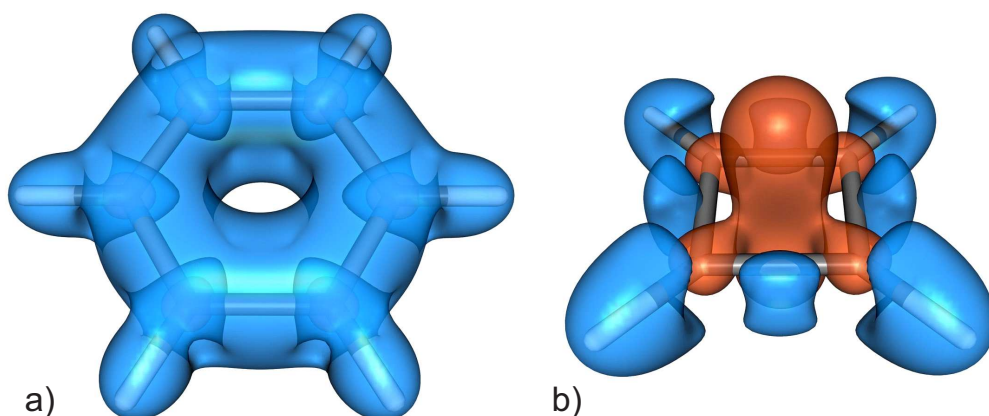
Figure 3.4: Isotropic chemical shielding isosurfaces at $\sigma_{\text{iso}}(r) = \pm$ 16 ppm for a) benzene and b) cyclobutadiene calculated at the CASSCF(6,6)-GIAO/6-311++G(d,p) and CASSCF(4,4)-GIAO/6-311++G(d,p) levels of theory, respectively. Positive isosurfaces are in blue.

The C–H bond shieldings are slightly broader and possess a higher shielding maximum than those in benzene. This suggests that the C–H bonds in cyclobutadiene are stronger than those in its aromatic counterpart. Although the bonds in cyclobutadiene are slightly longer than those in benzene, the small difference in bond length of around 0.7 % is unlikely to cause a *ca* 9 % difference in shielding. An investigation into the effect of geometry was discussed in Chapter 2. Another interesting feature of the C–H bonding regions is that at 1 Å above benzene, the C–H bonds are not visible, whereas in cyclobutadiene, distinct regions of shielding above these bonds is visible at 1 Å above the molecular plane. This is seen perhaps more clearly in the three-dimensional shielding isosurfaces in Figure 3.4.

The overall shape of the shielding surrounding the C–H bonds is quite different in each molecule. Furthermore, the isosurfaces, whilst far more computationally demanding, also give a clearer view of the antiaromatic deshielding feature and its destabilising effect on the carbon bonded framework. These three-dimensional isosurfaces illustrate the stark differences between the archetypal aromatic and antiaromatic systems exceptionally well and give a sound indication of the differences in bonding and behaviour.

3.4 Cyclobutene

Cyclobutene may seem at first glance, unremarkable, but the isotropic shielding calculations carried out in the space surrounding this system suggest otherwise. The $\sigma_{\text{iso}}(C)$ values in Table 3.3 give values slightly lower than those in ethene for the carbons of the double bond and values lower than those in ethane for the singly bonded carbons. In fact, the sp^2 carbons are very similar to the central carbons in 1,3-butadiene illustrating a degree of delocalisation in both molecules. On examination of the bonding maxima, it can be seen that the double and opposing single C–C bonds have very similar values, while the C–C single bonds adjacent to the double bond have slightly lower shieldings. This is reflected in the shielding across the whole molecule as seen in Figure 3.5.

Table 3.3: Isotropic shieldings for the nuclei and bond maxima in cyclobutene (in ppm), calculated at the HF-GIAO/6-311++G(d,p) and MP2-GIAO/6-311++G(d,p) levels of theory. Subscript opposite (opp) and adjacent (adj) refer to the position of the C–C with respect to the double bond.

	$\sigma_{\text{iso}}(C_{C=C})$	$\sigma_{\text{iso}}(C_{C-C})$	$\sigma_{\text{iso}}(H_{C=C})$	$\sigma_{\text{iso}}(H_{C-C})$
HF	45.27	163.97	25.67	29.64
MP2	59.94	163.40	25.70	29.15

	$\sigma_{\text{iso}}(C=C)$	$\sigma_{\text{iso}}(C-C_{\text{opp}})$	$\sigma_{\text{iso}}(C-C_{\text{adj}})$	$\sigma_{\text{iso}}(C-H_{C=C})$
HF	48.25	44.90	41.01	30.65
MP2	44.24	44.10	41.12	30.54

As seen previously, bond maxima cannot be used as the sole indicator of bond-

ing character. In Figure 3.5a, several important bonding features should be noted. Firstly, the C–C single bond opposite the formal double bond, whilst it possesses a shielding maximum comparable to the double bond, is far narrower and more reminiscent of the C–C single bond in ethane. However, this region does not lie directly along the internuclear distance indicating a small amount of bond bending. Alternatively, the C=C is remarkably consistent with that found in ethene, though again with some bond bending. However, it is perhaps the two single C–C bonds adjacent to the double bond which are of most interest.
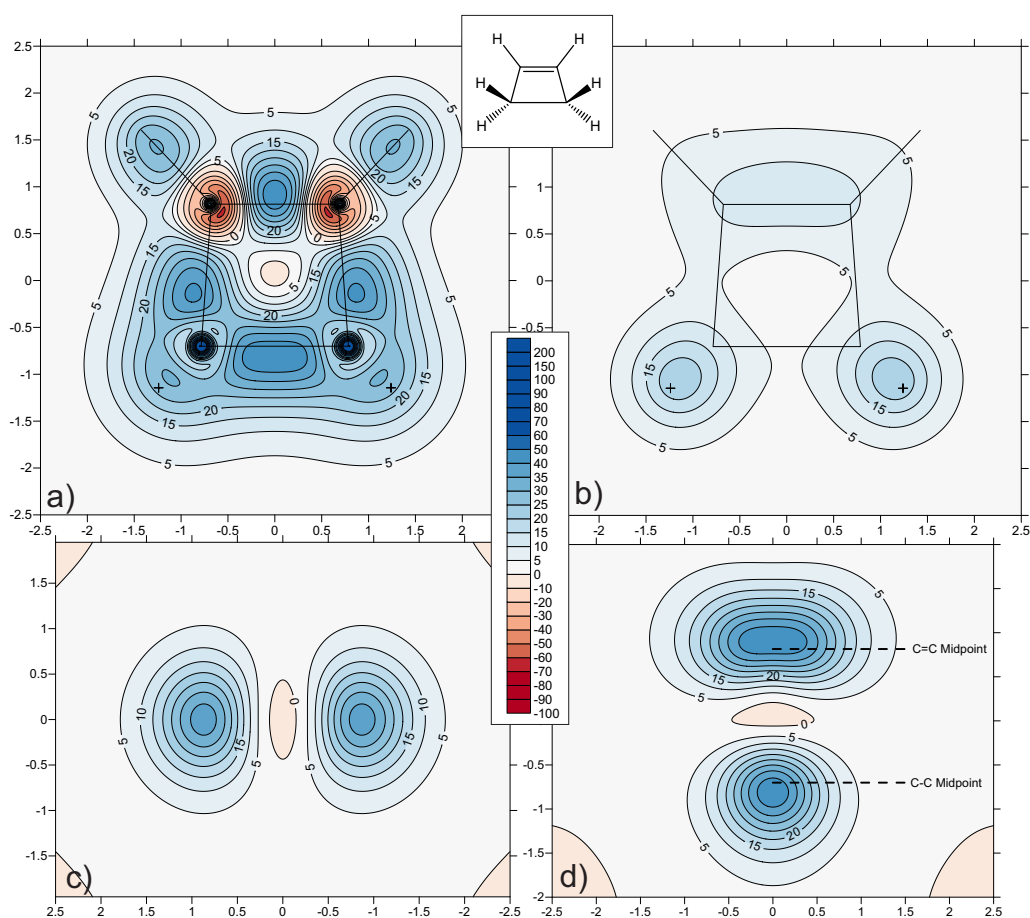
Figure 3.5: Contour plot of the isotropic chemical shieldings (ppm) for cyclobutene through a) molecular plane, b) 1 Å above the molecular plane, c) a vertical plane bisecting C–C bonds and d) a vertical plane bisecting C–C and C=C bonds calculated at the MP2/6-311++G(d,p) level of theory.

These C–C$_{adj}$ bonds have shielding maxima fairly close to the other two bonds, but the structure of the shielded regions is quite different. They have similar contour line shapes to the double bond but with the shielding maxima significantly shifted towards the sp^3 hybridised carbon. These too exhibit some bending but

also a subtle yet noticeable narrowing of the shielding structure around the centre of the bond. When these findings are viewed alongside the 1 Å above plot, an even more comprehensive picture of the bonding character can be obtained.

The 1 Å above plot displays a shielded lobe directly above the C=C bond, similar to that seen above ethene. The C–C$_{opp}$ bond displays a lack of shielding directly over the bond, again, similar to the shielding seen above ethane. The C–C$_{adj}$ bonds, however, rather than displaying a lack of shielding like C–C$_{opp}$, displays a weak shielded feature extending between the C=C double bond and the C–H regions. This extension of the shielded region above the molecule bestows a degree of multiple bond character upon the C–C$_{adj}$ bonds that is perhaps unexpected. This in turn causes the unusual shielding regions along the same bonds in the molecular plane. Further detail can be found in the bond cross-sections seen in Figure 3.5c & d.

The vertical plane bisecting the C=C and opposing C–C bonds (Figure 3.5d) shows an elliptical double bond cross-section, with a very slight indentation on the innermost edge reminiscent of that seen in benzene but to a lesser degree. The C–C cross-section is far narrower and more rounded, like that of ethane, but again with a slight distortion. The C–C$_{adj}$ bonds in Figure 3.5c are most like the C–C$_{opp}$ bond cross-section, although with a very subtle alteration of the overall shape pulling the shielding slightly outwards into a more elliptical form. This in turn allows a more diffuse shielding which causes the lowered bond shielding maximum. Both of these are consistent with double bond character.

However, the most exciting feature of the plots in Figure 3.5 has to be the subtle deshielded region directly at the ring centre. Previously, deshielding has only been seen at the centre of antiaromatic rings. While the feature present in cyclobutene is significantly less intense and far smaller than that seen in cyclobutadiene, its presence at all is intriguing. The deshielding appears fairly cylindrical and does not extend far above the ring like in cyclobutadiene as evident by its absence from the 1 Å above plot. Although, it does have a slight bulge seen in the vertical plane pointing towards the C=C bond and likely impacting on the shape of the double bond cross-section. Whilst cyclobutene is not considered antiaromatic according to traditional Hückel rules (which requires 4n π electrons), it has been seen earlier that some of the 2 electron π bonding associated with the C=C bond is drawn slightly around the sides of the ring. As a result, a hint of antiaromatic character appears to have been induced, though not enough to have a significant

impact on the molecular properties. This is a remarkable finding and seemingly unprecedented.

3.5   Heavy Element Analogues of Benzene

The silicon present in hexasilabenzene (Si_6H_6) and germanium in hexagermabenzene (Ge_6H_6) are the first examples of elements below the second row included in this work. This will allow the study of heavier elements and any effect their increased size and electron density have on the experienced magnetic shielding. The presence or absence of aromatic features in non-carbon benzene analogues can also be investigated.

3.5.1   Hexasilabenzene

The first thing to notice about the nuclear shieldings of Si_6H_6 (Table 3.4) is the almost 5-fold increase in shielding upon moving from carbon to silicon. The $\sigma_{iso}(H)$ values, however, remain mostly unchanged. Likewise, the maximum shielding along the Si–H bond is roughly the same as that along the C–H of parent benzene, though slightly lower in the heavy analogue. The Si–Si bond is just over 10 ppm less shielded than the C–C bond of benzene reflecting the decrease in bond strength. The same trend can also be seen in the molecular plane contour plots (Figure 3.6) where the interatomic regions show far fewer shielding contour lines than those in benzene. The shielded regions are also shifted slightly towards the ring centre. Moreover, the bond cross-sections are less elliptical than those in benzene.

Table 3.4: Isotropic shieldings for the symmetry-unique nuclei and bond maxima in Si_6H_6 (in ppm), calculated at the HF-GIAO/6-311++G(d,p) and MP2-GIAO/6-311++G(d,p) levels of theory.

	$\sigma_{iso}(Si)$	$\sigma_{iso}(H)$	$\sigma_{iso}(Si–Si)$	$\sigma_{iso}(Si–H)$
HF	261.49	25.62	31.35	29.12
MP2	270.85	25.00	30.08	28.17

The region 1 Å above Si_6H_6 still possesses a ring of shielding like that seen in

its lighter parent molecule. However, as the size of the atoms increase, this will start to perturb the features at this level. It is also clear from the migration of the Si–Si bonding regions towards the ring centre and the vertical plane slicing through the Si–H bonds that the shielding doughnut in benzene is not seen here. Instead, rather than a shielding torus above and below the molecular plane, the shielding extends in more of a single surface around the inner circumference of the ring though extending slightly above and below this plane. This suggests some degree of benzene character, but with important differences caused by the increased size and electron density of the larger silicon atoms.
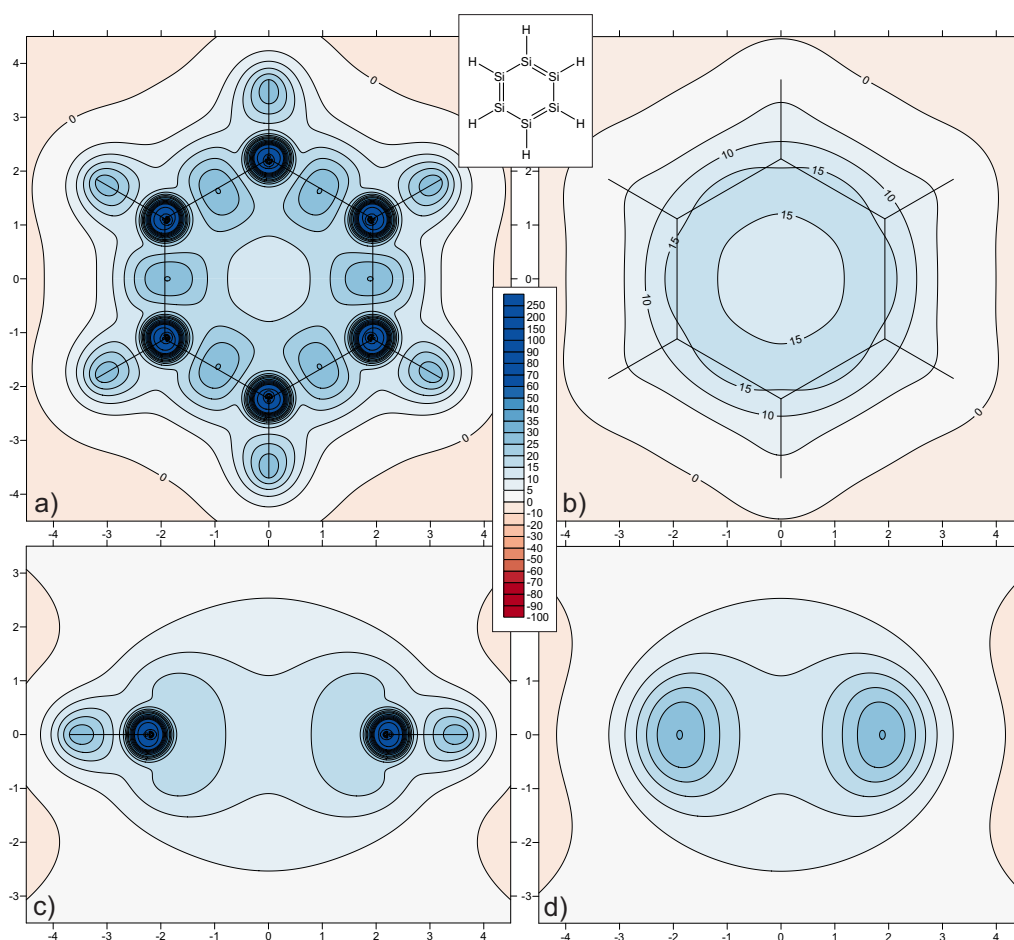
Figure 3.6: Contour plot of the isotropic chemical shieldings (ppm) for Si_6H_6 through a) molecular plane, b) 1 Å above the molecular plane, c) a vertical plane bisecting Si–H bonds and d) a vertical plane bisecting Si–Si bonds calculated at the MP2/6-311++G(d,p) level of theory.

Another striking difference is the apparent absence of the red regions of deshielding surrounding the sp^2 silicon nuclei that have been seen in previous systems.

However, upon closer inspection it can be seen that a semblance of this feature can be seen in the direct locality of the nuclei. In the case of this molecule, while the shielding values decrease in a pattern similar to second row elements seen before, the shielding magnitude does not reach negative values. This is due to the size difference of silicon versus carbon. It appears that the increased electron density and added electron shells of silicon veil the characteristic deshielding around nuclei in an unsaturated system.

3.5.2   Hexagermabenzene

It should be noted that for Ge_6H_6, calculations of the contour plot values have been calculated at HF level of theory only for reasons of computational cost. As seen previously, the features observed can be considered accurate though the shielding magnitudes may differ from those obtained at higher levels of theory. As it happens, in this case, the values seen in Table 3.5 do not show significant difference between the two levels of theory.

Table 3.5:   Isotropic shieldings for the symmetry-unique nuclei and bond maxima in Ge_6H_6 (in ppm), calculated at the HF-GIAO/6-311++G(d,p) and MP2-GIAO/6-311++G(d,p) levels of theory.

	σ_{iso}(Ge)	σ_{iso}(H)	σ_{iso}(Ge–Ge)	σ_{iso}(Ge–H)
HF	1269.24	24.75	35.83	28.59
MP2	1269.78	23.94	–	–

In this case, the σ_{iso}(Ge) values are roughly 20-times the σ_{iso}(C) of benzene. Nevertheless, the σ_{iso}(H) values remain consistent, along with the Ge–H bond maxima. Interestingly, the Ge–Ge bond maxima are slightly higher than the Si–Si values seen in the previous molecule. On inspection of the contour plots in Figure 3.7, it can be noticed that the Ge–Ge bonding areas have slight bulges around their mid-points, though also slightly off-centre towards the inside of the ring. These regions can even be seen at 1 Å above the molecular plane. This type of feature has not been seen in prior results and is most likely due to the dramatic size increase to that of fourth row germanium and the inclusion of d orbitals. Surprisingly, the bond cross-sections are not dissimilar to those seen in

Si_6H_6, as is the shielding bubble-like structure around the inner edge of the ring.
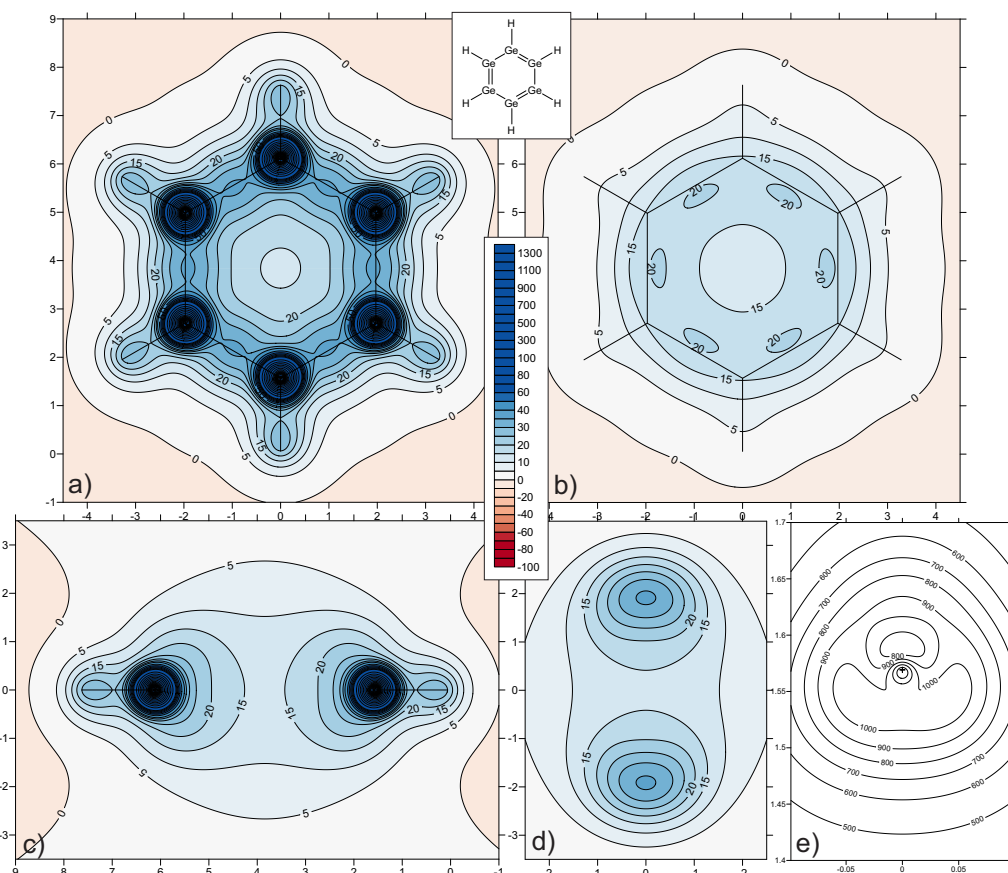
Figure 3.7: Contour plot of the isotropic chemical shieldings (ppm) for Ge_6H_6 through a) molecular plane, b) 1 Å above the molecular plane, c) a vertical plane bisecting Ge–H bonds, d) a vertical plane bisecting Ge–Ge bonds and e) an ultra-fine grid (with 0.001 Å spacing) over a Ge atom calculated at the HF/6-311++G(d,p) level of theory. Note that the contour fill colour has been removed from figure e) for clarity.

The Ge–H bonding regions are quite different shapes to those seen in benzene and hexasilabenzene. Instead of being broad along the internuclear distance and narrowing towards the H nucleus, the shielding feature is almost reversed and is more teardrop-shaped with the widest point at the H end of the bond. This is particularly interesting since the shielding maximum is quite similar across all three benzene-like molecules. This change in shielding behaviour likely results from the altered overlap between a large Ge atom and a small H nucleus as well as the change in electronegativity difference.

Another very important discussion point is the repeated absence of negatively shielded regions enclosing the sp^2 nuclei. Due to the size of the Ge atoms, a

simple close inspection does not suffice. Consequently, an ultra-fine grid (with spacings of 0.001 Å) of $\sigma_{iso}(\mathbf{r})$ calculations was placed directly over the germanium atom lying at approximately (0,1.5) in the molecular plane. The resultant contour plot can be found in Figure 3.7e which shows a subtle area of shielding decrease around the nucleus on the inside of the ring; the same location where the most intense deshielding is found in benzene. A similar, though more subtle decrease can be found in the centre of the lobe encompassed by the 1000 ppm contour line. This corroborates the findings of Si_6H_6 that imply that decreased shielding can be found around all unsaturated nuclei, regardless of size, even if the effect is more understated around larger elements.

3.6   Conclusions

In this chapter the characteristics of aromatic and antiaromatic systems have been explored using magnetic shielding calculations. It was found in aromatic benzene that the C–C bonding regions display similar features to the C=C double bond in ethene (seen in the previous chapter) though with a slight deformation on the inside of the ring caused by the aromatic nature of the molecule. The π doughnuts commonly pictured above and below benzene are seen in shielding plots as a moderately shielded halo. Conversely, for antiaromatic cyclobutadiene, the C–C bonding regions displayed very weak shielding and a distinctly bent form. The bond cross-sections are also unusual with a slightly triangular appearance. A dumbbell-shaped intense deshielding feature was found at the centre of the cyclobutadiene ring and is indicative of antiaromatic character. These features are presented clearly in a three-dimensional shielding isosurface.

Calculations on benzene were also carried out with two DFT methods, both of which proved to be inappropriate for this kind of work. Results produced by these means have features consistent with non-DFT methods, but the shielding magnitudes are highly inconsistent. Furthermore, in order to carry out these DFT calculations on benzene, such fine integration grids and such large basis sets were required that any computational cost advantage of DFT over post-HF methods was removed.

Cyclobutene was also investigated and, on inspection of the $\sigma_{iso}(C)$ values and the contour plots, a degree of π delocalisation was established. As a result of this effect, a small deshielded region was induced at the ring centre suggesting a hint

of antiaromatic character within the system.

Finally, two heavy atom analogues of benzene, Si_6H_6 and Ge_6H_6, were studied. Results have shown that the bonding in each ring is noticeably different, with Si_6H_6 displaying a weakened version of the bonding character in benzene but with Ge_6H_6 exhibiting shielding bulges at bond mid-points and an inversion of the shielding pattern along the bonds to hydrogen. It was also observed that while the shielding values of C, Si and Ge were hugely different, as expected, the values of $\sigma_{iso}(H)$ between all three systems were remarkably similar. Most importantly, however, was the finding that despite an apparent absence of deshieldings around the sp^2 nuclei in these heavy atom alternatives, the same features are still present, though less intense, requiring closer inspection or even ultra-fine grid calculations.

This detailed study of aromaticity and antiaromaticity provides a vital baseline with which to explore the properties of increasingly complicated systems.

Multiple Ring Systems

4

"You could call your thesis "Lord of the Rings"..."
James Perry

4.1   Introduction

Naphthalene is the smallest of the polycyclic aromatic hydrocarbons. It is an ideal system for studying the effect of benzene annelation on aromatic properties. Azulene can be studied for similar reasons but, unlike its isomer naphthalene, possesses rings of different sizes. Azulene is known to be highly aromatic with its high degree of conjugation evident by its striking blue colour.

Benzocyclobutadiene is formed by the joining of benzene and cyclobutadiene, the archetypal aromatic and antiaromatic systems, which have been studied in a previous chapter. The overall resulting molecule possesses 8π electrons and so investigation of any overall aromatic/antiaromatic properties is important. Likewise, the addition of a second cyclobutadiene moiety results in benzodicyclobutadiene, which is equally, if not more, interesting. Benzodicyclobutadiene can exist in several isomeric forms, two of which will be studied in this work. The two bond stretch isomers considered here differ only slightly by the length of the bridging C–C bonds but, in having this structural difference, can exhibit quite different properties.

Finally, three fulvalene molecules will be studied for the purpose of exploring the possibility of charge transfer between two rings over a central C=C double bond. Currently, it is not clear whether the rings are sufficiently conjugated to allow any transfer of electron density across the system which would increase aromatic properties in one or both of the rings. In the case of fulvalene-3, both rings would be competing for extra electron density in order to gain stability so the potential aromaticity of this system will hopefully be determined.

The structure of naphthalene was calculated with a mixture of ultrahigh-resolution laser spectroscopy and *ab initio* calculations.[98] The geometry of azulene was optimised at the MP2/6-31G(d,p) level of theory and that of benzocyclobutadiene at the CASSCF(8,8)/6-31G(d,p) level of theory. The two benzodicyclobutadiene structures were optimised by Cooper and Karadakov with the CCSD(T)/6-31G(d) method.[99] Finally, the fulvalene structures were optimised by Stanger at the B3LYP/6-311G(d) level of theory ensuring C_{2v} symmetry.[100]

4.2   Naphthalene

Naphthalene is an annelated ring system consisting of two benzene moieties with one C–C bond common to both. The calculations on this molecule were only obtained for the HF level of theory due to computational costs but, as seen previously, the results are qualitatively identical to MP2.

Table 4.1: Isotropic shieldings for the symmetry-unique nuclei and bond maxima in naphthalene (in ppm), calculated at the HF-GIAO/6-311++G(d,p) level of theory. C_1 refers to the outermost carbons while C_3 corresponds to the carbons common to both rings.

	$\sigma_{iso}(C_1)$	$\sigma_{iso}(C_2)$	$\sigma_{iso}(C_3)$	$\sigma_{iso}(H_1)$	$\sigma_{iso}(H_2)$	$\sigma_{iso}(C_1–C_2)$
HF	54.90	57.90	53.90	24.12	23.88	47.39

	$\sigma_{iso}(C_2–C_3)$	$\sigma_{iso}(C_1–C'_1)$	$\sigma_{iso}(C_3–C'_3)$	$\sigma_{iso}(C_1–H_1)$	$\sigma_{iso}(C_1–H_1)$
HF	37.13	41.12	43.46	29.75	29.43

The isotropic shielding values obtained for the nuclei and bonding regions in naphthalene can be seen in Table 4.1. Both the carbon nuclear shieldings and the C–C bonding maxima exhibit the same trend in values. The outermost carbons (C_1) and C–C bond (denoted $C_1–C'_1$) have values intermediate between the other two. However, the C–C bonding regions are perhaps of most interest, both from the values in the table but also the contour plots in Figure 4.1. It can be seen from the latter that there is clear bond alternation with the $C_1–C_2$ bond possessing more double bond characteristics than the two peripheral C–C bonds. The C–C bond common to both rings ($C_3–C'_3$) also displays slightly more double bond character than the opposing or connecting C–C bonds, though not as much as $C_1–C_2$.
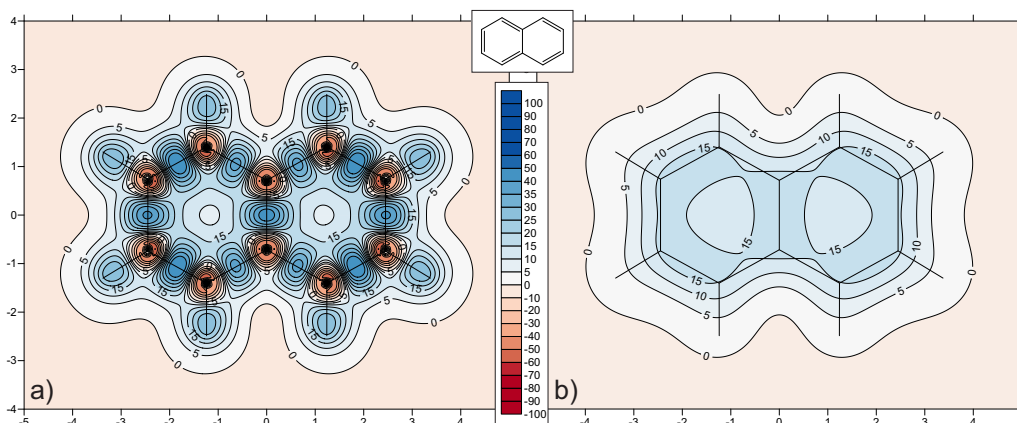
Figure 4.1: Contour plot of the isotropic chemical shieldings (ppm) for naphthalene through a) molecular plane and b) 1 Å above the molecular plane calculated at the HF/6-311++G(d,p) level of theory.

This bond alternation is not normally seen in aromatic systems (in fact, it is usually associated with antiaromaticity), but for the case of naphthalene, it can be rationalised by considering resonance structures like those seen in Figure 4.2. From these structures, it is clear that the C_1–C_2 bonds are formal double bonds for two out of three of the resonance structures, hence leading to bond alternation. This is also seen in the bond lengths, relative bond orders[101] and traditional bond orders.[102]
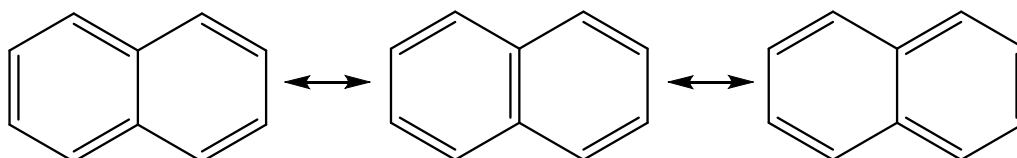
Figure 4.2: Resonance structures of naphthalene.

The shielding observed at 1 Å above the molecule is mostly homogeneous, as expected from an aromatic system, but with slight deviation from this trend over the C_2–C_3 bonds. These bonds also possess the lowest shielding maxima of the C–C bonds in the molecular plane. This finding implies that the aromaticity of naphthalene will be lower than that of lone benzene. Using the popular, and related, NICS technique, the NICS(0) for naphthalene has been calculated to be −9.9 ppm compared to −9.7 ppm for benzene.[42] The NICS(1) value of naphthalene was found to be −10.8 compared to −10.6 ppm for benzene.[43,53] (Note that the NICS(0) and NICS(1) values were calculated with different methods so

comparison between the two indices is not useful. However, the two NICS(0) values are comparable, as are the two NICS(1) values.) These NICS values suggest that naphthalene is slightly more aromatic than benzene, however, despite NICS values being often described as a local aromaticity indicator, it has been found that NICS values actually reflect global π aromaticity and therefore are not so straightforward to analyse.[103] Through space NMR shielding surfaces have been calculated by Kleinpeter *et al.* but the subtle changes in bonding and aromaticity are not clearly observable there.[57]

4.2.1   Azulene

Azulene is another interesting polycyclic system under investigation. Here the calculations are mostly performed at the MP2 level of theory, with the exception of the 1 Å above plot, which was carried out using the HF method for similar reasons as for naphthalene. A table of shielding values is not given for certain cases, including azulene, for simplicity and because it adds nothing valuable to the discussion.
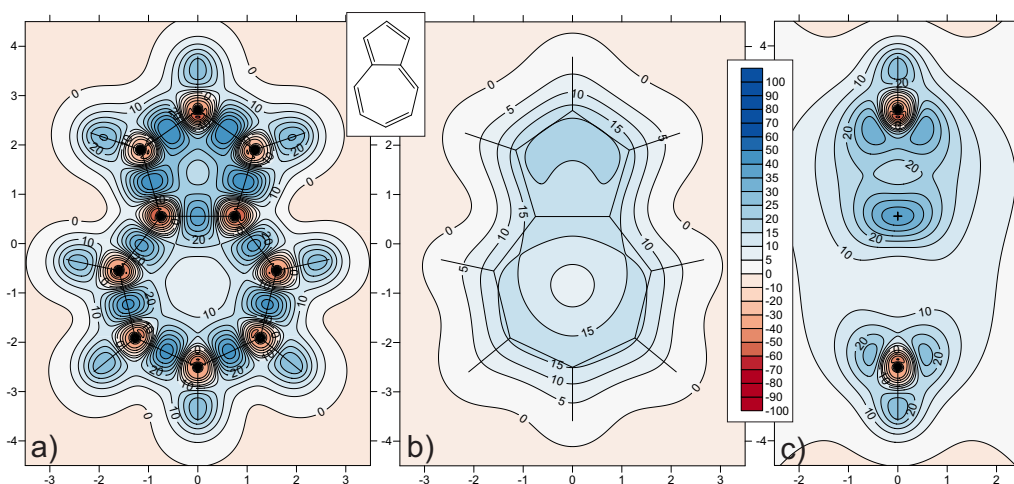
Figure 4.3: Contour plot of the isotropic chemical shieldings (ppm) for azulene through a) molecular plane, b) 1 Å above the molecular plane and c) a vertical plane bisecting two C–H bonds and the central C–C bond calculated at the MP2/6-311++G(d,p) level of theory (except for b, which used the HF/6-311++G(d,p) level of theory).

The isotropic shielding in and around azulene can be seen in Figure 4.3. For this molecule, bond alternation is not observed in the shielding along the C–C bonds as it was in naphthalene. This is consistent with bond lengths and bond orders

found in azulene which show far less variation than those in naphthalene.[102] It does however show notably stronger C–C bonds in the five-membered ring compared to those in the larger ring. This is mirrored by the shielding at 1 Å above the ring which shows a moderate shielding over the whole of the five-membered ring but with an increased shielding region localised over the non-bridging C–C bonds. The seven-membered ring, on the other hand, is very similar to that seen in naphthalene with a reasonably shielded, delocalised area around the circumference of the ring but with distortion over the C–C bonds connecting to the five-membered ring.

NICS(1) values for azulene have been calculated to be -7.5 ppm above the seven-membered ring and -17.7 ppm above the five-membered ring.[104] This suggests that the smaller ring displays significantly higher aromaticity than the larger ring and this is consistent with the findings in Figure 4.3b. A ring current study of azulene found that the five-membered ring current is slightly diatropic while the seven-membered ring current is slightly paratropic.[103] Although the same study also determined that the current around the whole periphery of the molecule was highly diatropic and dominated the two individual ring currents. This means that interpretation of NICS values in multiple ring systems in non-trivial.

The vertical plane through azulene, seen in Figure 4.3c, shows the typical features of aromaticity, though with a subtle distinction between the two rings. The smaller ring (viewed at the top of Figure 4.3c) has a more substantial π doughnut visible above and below the bisected carbon compared to that seen in the larger ring. Furthermore, the cross-section of the bridging C–C bond displays a flattening on the edge on the side of the five-membered ring which denotes a higher degree of aromaticity in that ring compared to the larger one.

Overall, the five-membered ring displays a greater degree of aromaticity than the seven-membered ring, but if the two rings are considered as a whole, the difference exhibited between the two suggests a lower overall aromaticity than naphthalene caused by the inhomogeneity across the entire system.

4.3   Benzocyclobutadiene

Benzocyclobutadiene is formed from both benzene and cyclobutadiene moieties. This should display both aromatic and antiaromatic characteristics in one molecule. It should be noted that while the results presented here were carried out at the

HF level of theory, CASSCF(8,8) calculations were also performed with almost identical results. The results obtained can be seen in Figure 4.4.
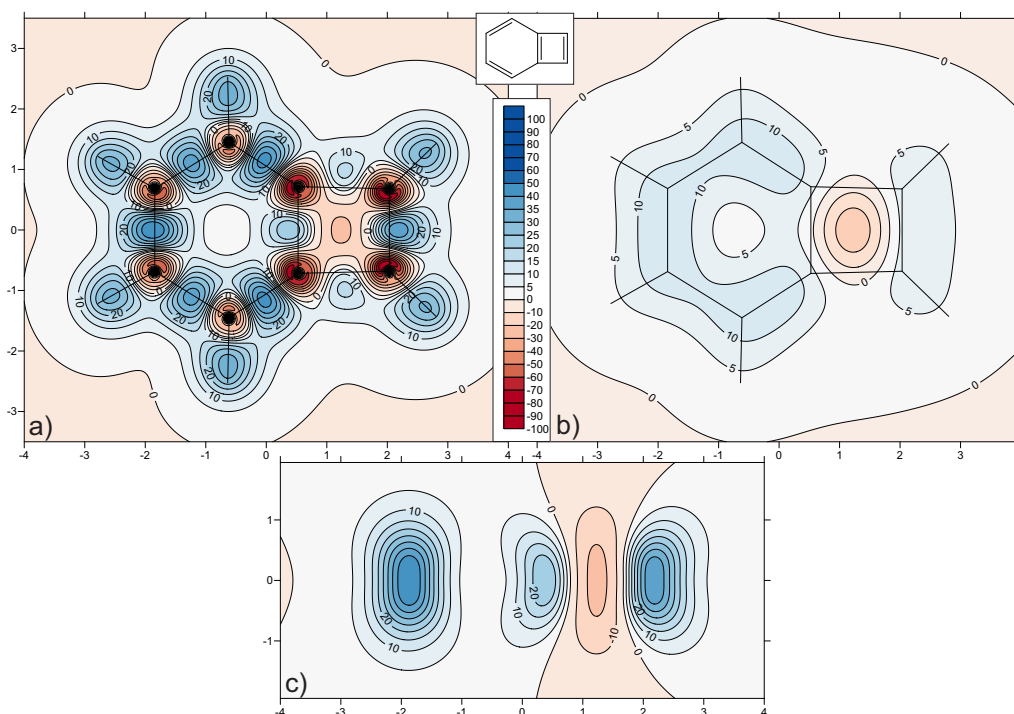
Figure 4.4: Contour plot of the isotropic chemical shieldings (ppm) for benzocyclobutadiene through a) molecular plane, b) 1 Å above the molecular plane and c) a vertical plane bisecting three C–C bonds calculated at the HF/6-311++G(d,p) level of theory.

On first inspection, many features are common to those seen in the benzene and cyclobutadiene plots. However, there are some subtle differences worth noting. The carbons around the benzene moiety are distinctly inequivalent as seen by the red regions of deshielding around the nuclei. This, along with the inhomogeneous region of shielding 1 Å above this section of the molecule, implies lower aromaticity than lone benzene. Moreover, the C–C bonding regions around the same framework display subtle differences, with the C–C bond opposite the cyclobutadiene moiety appearing the strongest and those adjacent to the bridging C–C bond being slightly distorted. All of these features denote less aromaticity than benzene, which is as expected.

The cyclobutadiene ring in benzocyclobutadiene also exhibits several key differences from lone cyclobutadiene. Firstly, the deshielded feature at the ring centre is more cylindrical here than in square cyclobutadiene. This shows a decrease in antiaromaticity compared to cyclobutadiene. This is, in part, due to the rectangu-

lar configuration of the cyclobutadiene moiety, which will lower the antiaromaticity and can be seen by the dramatic differences in the C–C bonding regions around the four-membered ring. The two 'single' C–C bonds are typical of the weak, bent bonds in cyclobutadiene, though with a slight distortion. The C–C bond opposite the bridging C–C bond is far stronger and is more consistent with a strained double bond like that seen in and around the double bond in cyclobutene or cyclopropene. This similarity can also be seen in the 1 Å above plot. The bridging C–C bond is an intermediate between the other two unique C–C bonding regions in the four-membered ring.

Finally, the vertical plane through benzocyclobutadiene can be seen in Figure 4.4c and shows three C–C bond cross-sections. The bond on the far left of the plot corresponds to the C–C bond of the six-membered ring and is quite oval in appearance. The lack of the indentation on the innermost edge shows a lower aromaticity than benzene. The bridging C–C bond cross-section is quite similar to those seen in cyclobutadiene, though the far right C–C bond cross-section is more typical of a strained double bond.

All of this isotropic shielding analysis leads to the conclusion that whilst the benzene and cyclobutadiene moieties do display features of aromaticity and antiaromaticity, respectively, they each weaken the properties of the other. Through-space NMR shielding surfaces have been performed for this molecule and the authors found very few changes compared to the lone constituents.[57] However, they did note that the properties of aromaticity and antiaromaticity were present though, as seen in the calculations here, were both weaker than in the lone molecules. This highlights the extra information and sensitivity obtained over the through space NMR shielding method.

4.4   Benzodicyclobutadiene

In this section, two bond stretch isomers of benzodicyclobutadiene are studied-benzodicyclobutadiene-1 possesses an annelated C–C bond length of 1.414 Å and benzodicyclobutadiene-2 has the same bond length of 1.553 Å.[99]
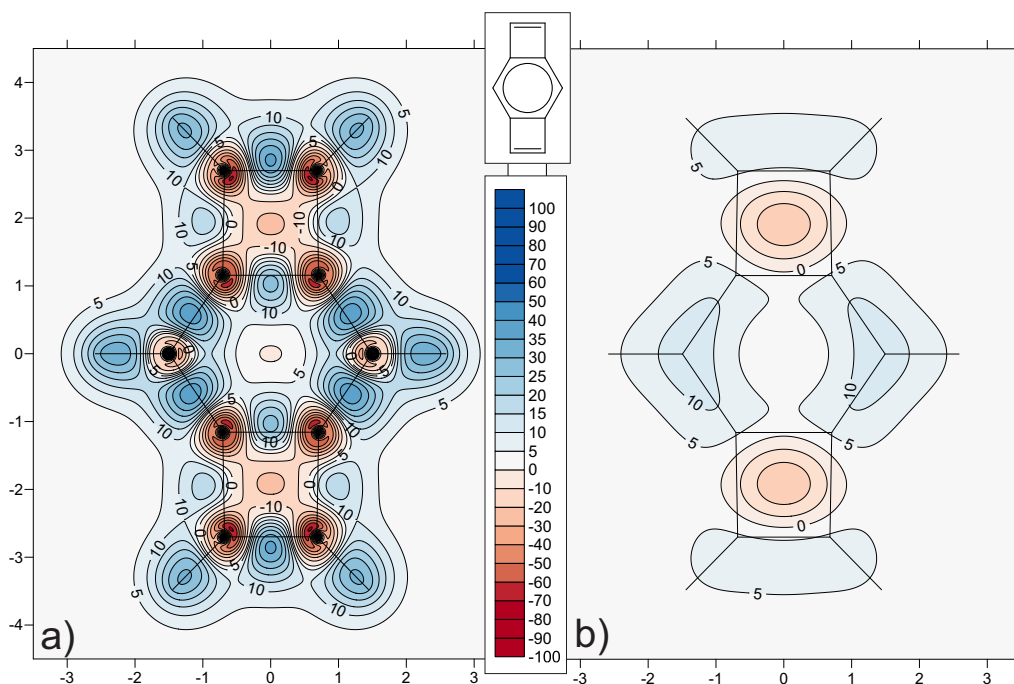
Figure 4.5:   Contour plot of the isotropic chemical shieldings (ppm) for benzodicyclobutadiene-1 through a) molecular plane and b) 1 Å above the molecular plane calculated at the MP2/6-311++G(d,p) level of theory.

Despite the fairly small variation in geometry between the two isomers, there is a striking difference between the two when the isotropic shielding is considered (see Figures 4.5 & 4.6). As the skeletal structure for benzodicyclobutadiene-1 suggests, the molecule is primarily the same as benzocyclobutadiene, as seen in the previous section, but with an extra cyclobutadiene moiety. It displays many of the same features as those seen in benzocyclobutadiene and, by association, benzene and cyclobutadiene. However, it can be seen that the benzene moiety displays far less aromaticity than in the other cases just mentioned. The central carbons only possess weakly deshielded surroundings and the shielding 1 Å above this section displays only small, localised shielded regions. Moreover, at the centre of the six-membered ring there is a very small, slightly deshielded area which is normally seen in antiaromatic molecules rather than aromatic systems.

The cyclobutadiene moieties display more significantly deshielded features at the ring centres than seen in benzocyclobutadiene, denoting a higher degree of antiaromaticity in this molecule. However, the outermost C–C bonds still show similarities, both in the molecular plane and above, with the double bond in cyclobutene. This all signifies weak aromaticity in the central ring and antiaro-

maticity in the outer rings that is intermediate between benzocyclobutadiene and square cyclobutadiene.
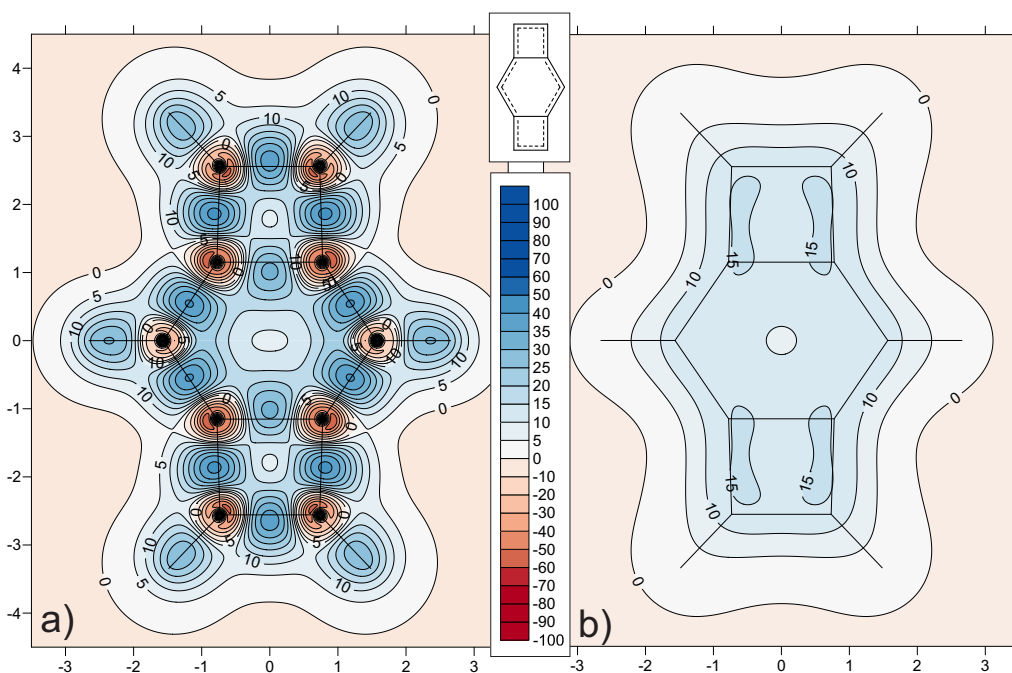
Figure 4.6:   Contour plot of the isotropic chemical shieldings (ppm) for benzodicyclobutadiene-2 through a) molecular plane and b) 1 Å above the molecular plane calculated at the MP2/6-311++G(d,p) level of theory.

The structure of benzodicyclobutadiene-2 implies more π delocalisation over the whole system as opposed to the distinct environments found in benzodicyclobutadiene-1. This results in a very different shielding surface as seen in Figure 4.6. In this instance, there is significant shielding delocalised over the whole molecule, as seen at 1 Å above the molecular plane. It also possesses small areas of slightly higher shielding localised over the C=C double bonds within the four-membered rings. Furthermore, the C–C bonding regions all show fairly similar shielding in the molecular plane with much less bent bonding than was seen in benzodicyclobutadiene-1. It is known from other chapters that a significant portion of the bent bonding is caused by antiaromaticity which explains the decrease in bending for this molecule. The two central carbons still display weak deshieldings around their nuclei, as in benzodicyclobutadiene-1, but the other carbons are reasonably similar to each other which allows higher aromaticity.

It is clear from the isotropic shielding plots that a slight alteration in geometry makes a very important impact on the properties and nature of benzodicyclobuta-

diene. Benzodicyclobutadiene-1 exhibits distinct aromatic and antiaromatic sections, though with fairly weak aromaticity in the benzene section. On the other hand, benzodicyclobutadiene-2 displays significant aromaticity across the whole polycyclic system. Profound differences between these systems have also been seen with a modern valence bond approach with some similar conclusions.[99]

4.5 Fulvalenes

In this section, three fulvalenes are studied i.e. systems which are comprised of two conjugated rings joined together by a double bond. Molecule naming is as follows: [3,5]-fulvalene is referred to as fulvalene-1, [3,3]-fulvalene as fulvalene-2 and [3,7]-fulvalene as fulvalene-3.
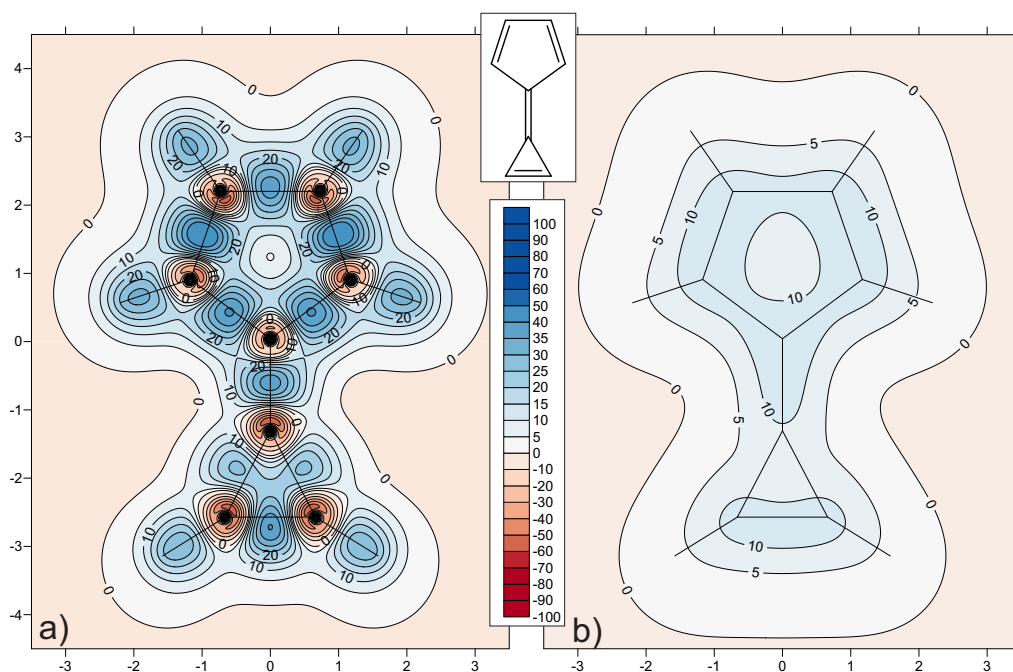
Figure 4.7: Contour plot of the isotropic chemical shieldings (ppm) for fulvalene-1 through a) molecular plane and b) 1 Å above the molecular plane calculated at the MP2/6-311++G(d,p) level of theory.

Fulvalene-1 results can be seen in Figure 4.7. The molecular plane isotropic shielding and the shielding 1 Å above display strong similarities between the three-membered ring here and the analogous plots for cyclopropene and the cyclopropenyl cation. The C–C bonding regions adjacent to the exocyclic double bond are consistent with those seen in $C_3H_3^+$ while the C=C bonding region is

close in character to the double bond in cyclopropene. The lobe of shielding present above the formal double bond is also similar to that seen above cyclopropene.

The deshielded regions surrounding the carbon nuclei of the three-membered ring are intermediate in shielding magnitude between cyclopropene and the cyclopropenyl cation, though closer to those seen in cyclopropene. This, along with the bonding regions, suggests that, while there is delocalisation over the ring and across the exocyclic double bond, any aromaticity displayed by that part of the fulvalene is significantly lower than in $C_3H_3^+$.

In the five-membered ring of fulvalene-1 some typical aromatic features can be seen. For example, at 1 Å above the ring, there is a region of moderate shielding encompassing the whole circumference and even extending over the exocyclic double bond. This shows a better conjugation around the five-membered ring than around the smaller ring and also shows that it delocalises more over the joining double bond than the smaller ring. In delocalising over the central double bond, the five-membered ring gains extra π electron density bringing it closer to aromaticity. This additional conjugation is also shown by the along-bond position of the deshielding maximum around the carbon that is common to both the three-membered ring and the exocyclic double bond. If the three-membered ring had been sufficiently conjugated, the deshielding maximum would not lie in this position. The bonding regions within the largest ring display a degree of bond alternation, though this does not perturb the shielding 1 Å above the ring so has little impact on any aromaticity of the system.

It has been suggested in other work that the aromaticity displayed by fulvalene-1, and its large dipole moment, can be explained by charge transfer from the three-membered ring to the five-membered ring creating a partial aromaticity in both sides.[58,100] This has been shown by calculation of through-space NMR shielding surfaces which concluded that the three-membered ring was close in nature to the cyclopropenyl cation.[58] In this work, similarities are evident with $C_3H_3^+$ but many differences are also observed highlighting the sensitivity and additional information afforded by this technique. Furthermore, typical characteristics of charged cycles, namely significant alterations in carbon deshielding and bond shielding magnitudes, were not observed in these results which discounts any charge transfer large enough to impose formal charges on the two rings. From this evidence, the most realistic view of the aromaticity of fulvalene-1 is a de-

localised 6π electron system over the five-membered ring and exocyclic double bond, which exhibits aromaticity, and a three-membered ring which primarily displays a localised double bond but with a slight delocalising effect which alters the other C–C bonds in the ring.
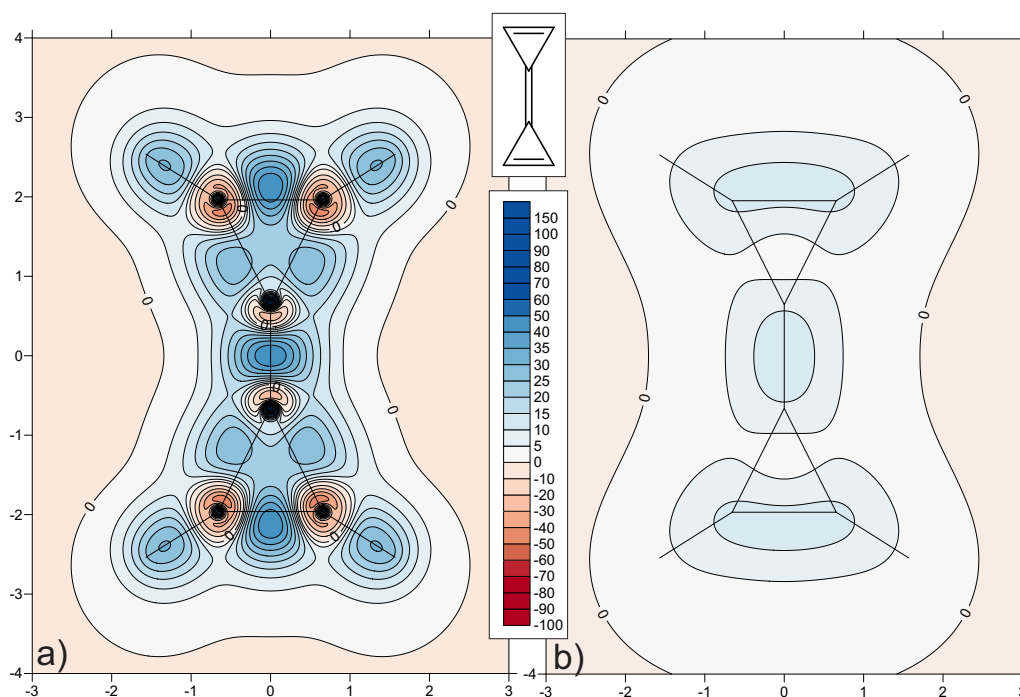
Figure 4.8: Contour plot of the isotropic chemical shieldings (ppm) for fulvalene-2 through a) molecular plane and b) 1 Å above the molecular plane calculated at the MP2/6-311++G(d,p) level of theory.

Fulvalene-2 can be seen in Figure 4.8 and displays quite different properties to those seen in fulvalene-1. The bonding regions around the two rings are consistent with those seen in cyclopropene without the changes to the C–C 'single' bonds that were seen in fulvalene-1. This gives these C–C bond shielding regions an appearance which is more consistent with the analogous bonds in cyclopropene than those seen in $C_3H_3^+$. This shows that the three-membered rings in fulvalene-2 exhibit less aromatic tendencies than the three-membered ring in fulvalene-1. Moreover, the central double bond between the rings is quite locailsed as evident by the localised shielding at 1 Å above the double bond but also the position of the carbon deshieldings which face into the double bond and away from the terminal rings.
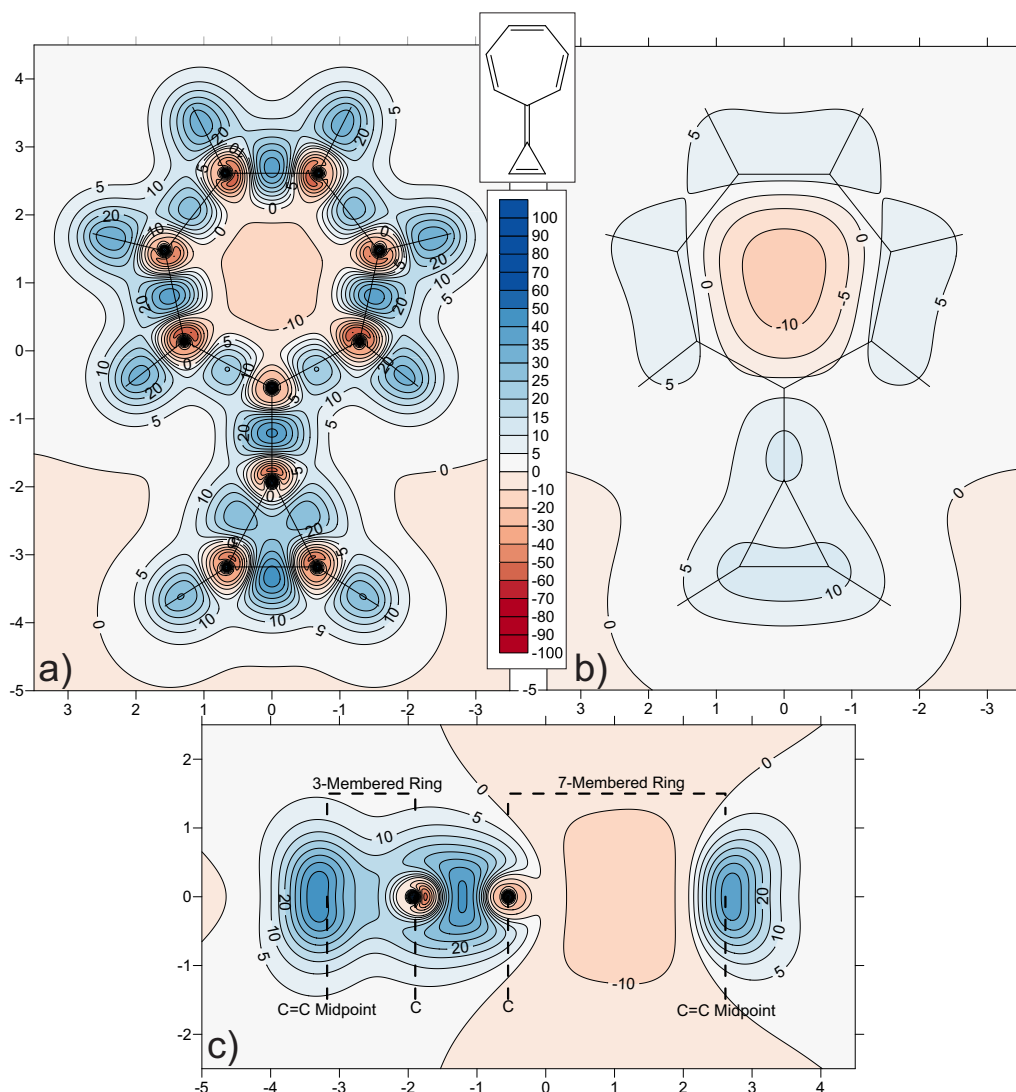
Figure 4.9: Contour plot of the isotropic chemical shieldings (ppm) for fulvalene-3 through a) molecular plane, b) 1 Å above the molecular plane and c) a vertical plane perpendicular to the molecular plane calculated at the MP2/6-311++G(d,p) level of theory.

Work carried out by Stanger concluded that for fulvalene-2, the rings push electron density into the C=C π^* orbital which would suggest a degree of conjugation and should result in a weakening of the C=C bond, neither of which are seen in these results.[100] In work by Kleinpeter and co-workers, they determine that occupation of the C=C π^* orbital has little to no effect on bonding due to conjugation of this orbital across the fulvalene system.[58] So, for the case of fulvalene-2, there is little electron donation from the rings into the central double bond, and, what donation there is, has been conjugated partially across the system causing

no real change in bonding. The lack of π acceptance by the central double bond and the olefinic nature of the three-membered rings are also seen in the same work by Kleinpeter.[58] This all suggests quite localised π density in fulvalene-2 and therefore very little, if any, aromatic nature.

Finally, the isotropic shielding in and around fulvalene-3 can be seen in Figure 4.9. On inspection of the three-membered ring, it can be seen that the C–C bonding regions are fairly similar to those seen in fulvalene-2. The same is true of the shielding directly above the ring. This suggests a similar nature to that seen in fulvalene-2.

The seven-membered ring, however, is quite different and exhibits typical antiaromatic properties. The deshielded feature at the ring centre, indicative of antiaromaticity, is quite large, though not very intense. It does not form a dumbbell shape as seen in cyclobutadiene but a more cylindrical shape like that seen in neutral COT and benzocyclobutadiene. This is a result of the large ring size and the antiaromaticity being weaker than that seen in square cyclobutadiene.

Of particular interest are the C–C bonds in the seven-membered ring. A subtle bond alternation is observed but, more importantly, the bond shieldings are atypical of previously studied antiaromatic systems. There is only slight evidence of bond bending demonstrated by the shielded regions along the internuclear distances being positioned outwards, away from the ring centre. Moreover, excluding the C–C bonds adjacent to the central double bond, the C–C bonding regions all show moderate to strong bonding. On inspection of the cross-section of a C–C bond in the seven-membered ring (see Figure 4.9c), the triangular shape associated with other antiaromatic systems is only slightly visible. All of this can be used to conclude that the seven-membered ring only exhibits a subtle degree of antiaromaticity, similar to that displayed by cyclobutene.

The central double bond in fulvalene-3 has a bonding region typical of a double bond, and the carbon attached to the three-membered ring is also quite typical of this environment. However, the carbon attached to the larger ring possesses a slightly unusual halo of deshielding in that there is no visible maximum. The shielding plot positioned 1 Å above the molecule shows that the shielding over the double bond is highly localised and positioned closer to the three-membered ring than the seven-membered ring. This will allow slightly more conjugation with the three-membered ring and will be the cause of the slight reminiscence of the

C–C 'single' bonds with those seen in more conjugated systems. The shielding around the seven-membered ring is quite disjointed as the weak shielding visible is pushed significantly away from the ring centre by the deshielded protrusion. In cyclobutadiene, the shielding is only located over the C–H bonds at this distance above the molecule but here there is more delocalisation of the shielding between neighbouring C–H bonds. This is consistent with the weak antiaromaticity suggested earlier for the case of fulvalene-3.

Work on fulvalene-3 was carried out by Stanger, who suggested that the seven-membered ring in this molecule is stabilised by 19.5 kcal mol^{-1} due to possession of 4n π electrons i.e. by antiaromaticity.[100] The results in this work suggest only a very slight antiaromatic character; a property which is responsible for the ring stability. In the same work, Stanger also suggests that there is charge transfer from the seven-membered ring to the three-membered ring making the latter more aromatic. However, the results in this work do not display noticeable aromatic properties with any aromaticity being far less significant than for fulvalene-1. The similarity between the three-membered ring in this fulvalene with that in fulvalene-1 is noted in work by Kleinpeter *et al.* as is the evidence of partial, but not full, antiaromaticity.[58] Importantly, Kleinpeter and co-workers note that the aromatic character of the three-membered ring is noticeably greater in fulvalene-1 than in fulvalene-3, which is consistent with the findings in this work.

4.6 Conclusions

In this chapter a variety of polycyclic systems have been investigated with isotropic shielding calculations. In the case of naphthalene, aromatic properties coincided with visible bond alternation caused by the resonance structures of the molecule. Azulene, another annelated ring system, was studied and it was found that the five-membered ring displayed a greater degree of aromaticity than the seven-membered ring. However, it was also concluded that the system should also be considered as a whole and, when this is done, azulene can be considered as less aromatic than naphthalene.

Benzocyclobutadiene was found to possess characteristics of both aromaticity, in the benzene moiety, and antiaromaticity, in the cyclobutadiene moiety, though each weakens the other one. This was then extended to investigate two bond stretch isomers of benzodicyclobutadiene. Each isomer displayed dramatically

different properties of the surrounding magnetic shielding. Benzodicyclobutadiene-1, with shorter bridging C–C bonds, appeared like benzocyclobutadiene with both aromatic and antiaromatic properties, though with more pronounced antiaromaticity than benzocyclobutadiene. On the other hand, benzodicyclobutadiene-2, with longer bridging C–C bonds, exhibited no signs of antiaromaticity and instead showed aromatic characteristics across the whole molecule.

Finally, three fulvalenes were investigated with fulvalene-1 displaying the most aromatic character of the three systems. It was found that fulvalene-1 should be considered as a delocalised $6\,\pi$ electron system consisting of the five-membered ring and the exocyclic double bond along with a three-membered ring which is primarily cyclopropene-like (though with some conjugation to the other ring). Fulvalene-2, however, is made up of significantly localised three-membered rings and a joining double bond, with little evidence of any conjugation between the components. The last fulvalene, fulavalene-3, displays weak antiaromaticity in the seven-membered ring and no real aromatic character in the three-membered ring which is consistent with through-space NMR shielding studies.[58]

This section has given insight into the additive nature, of lack thereof, of combining aromatic/antiaromatic rings together in two different ways- by direct sharing of a C–C bond or by linking together with a double bond. The interactions between the various moieties has been discussed and several interesting effects have been noted.

Charged Cycles

"What we observe is not nature itself, but nature exposed to our method of questioning."
Werner Heisenberg

5.1   Introduction

Charged, cyclic systems are commonplace in a variety of fields, particularly in organometallic chemistry, where the effects of metal complexation to aromatic rings is of great interest. Moreover, the effects of charges on these molecules is also important. Previously, only neutral aromatic rings have been studied, but in this chapter, a range of charged, cyclic systems will be investigated, including one antiaromatic ring.

Cyclopropane is a fascinating three-membered ring with unusual properties for a saturated and highly strained system. It has a surprisingly low strain energy and C–C bond lengths that are shorter than expected for an alkane. It can even take part in reactions that are more often associated with alkenes. There has also been much debate about the possibility of σ aromaticity being present in cyclopropane, a concept which may explain its unusual properties.[29,105,106] The idea of σ aromaticity involves σ bond delocalisation, something which is distinct from σ conjugation and σ electron delocalisation since all molecules with three or more atoms contain σ conjugation and all σ electrons can be considered as delocalised.[107] Whether any of these properties manifest themselves in interesting shielding properties will be investigated and results compared to those for cyclopropene and the cyclopropenyl cation.

A range of charged cycles of different sizes and charges will also be studied. In addition to $C_3H_3^+$, $C_5H_5^-$, $C_7H_7^+$, $C_8H_8^{2-}$ and $C_8H_8^{2+}$ will be seen. Special investigation will be undertaken of the 8-membered ring, cyclooctatetraene (COT), including the neutral, antiaromatic form and the disodiated dianion along with the two ions mentioned previously. Other work concluded that COT does not show significant antiaromatic destabilisation in its neutral, planar form[108] and this will be tested with isotropic shielding plots which have previously been shown to be highly sensitive.

All charged cycle geometries were optimised at the CASSCF(m,n) level of theory and a 6-311G(d,p) basis set. The cyclopropenyl cation required a CASSCF(3,2) wavefunction, while the C_4H_4 dication used CASSCF(2,4), the cyclopentadienyl anion used CASSCF(6,5), the tropylium cation used CASSCF(6,7), COT dication CASSCF(6,8) and COT dianion CASSCF(10,8). The structure of cyclopropene was also optimised, this time at the MP2/6-31G(d,p) level of theory with a ground state confirmed by frequency analysis. Cyclopropane calculations used a struc-

ture determined experimentally by microwave spectroscopy.[109] Neutral D_{8h} COT was optimised at the CASSCF(8,8)/6-31G* level of theory. The Na_2COT geometry was optimised at the AE-CCSD(T)/aug(H,Na)-cc-pCVTZ level of theory by Sokolov and co-workers.[110]

5.2   Cyclopropane, Cyclopropene & Cyclopropenyl Cation

This section focuses on three-membered rings with varying degrees of saturation. Cyclopropane, which is completely saturated, displays carbon nuclear shieldings (Table 5.1) at values about 13 ppm higher than those seen in the small, linear hydrocarbon ethane in Chapter 2. However, the hydrogen shielding and C–C bond shielding maxima are only about 2 ppm higher than those in ethane. These similarities with ethane are not unexpected, but the bonded regions seen in Figure 5.1 are quite different.

Table 5.1: Isotropic shieldings for the symmetry-unique nuclei and C–C bonding midpoint values for cyclopropane (in ppm), calculated at the HF-GIAO/6-311++G(d,p) and MP2-GIAO/6-311++G(d,p) levels of theory.

	σ_{iso}(C)	σ_{iso}(H)	σ_{iso}(C–C)
HF	199.33	32.41	54.25
MP2	201.40	32.05	54.17

The shielding along the C–C bonds in cyclopropane is noticeably wider than that seen in ethane. Furthermore, the shielding has been pushed outwards, away from the ring centre, showing a degree of bond bending, like that seen in cyclobutadiene, though not quite as pronounced. This suggests that the ring strain is not the only reason for the bent bonding in cyclobutadiene, as alluded to previously. See the later section on COT for further discussion.
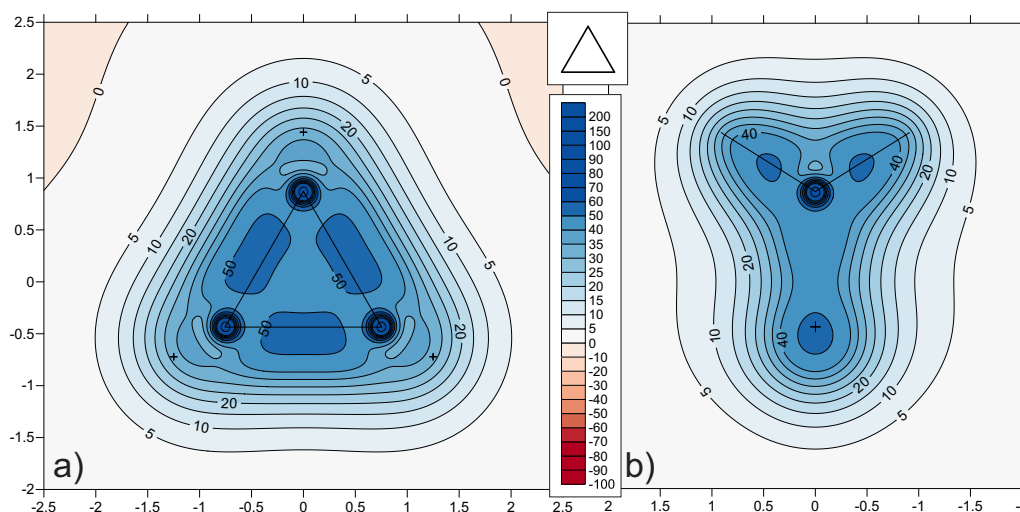
Figure 5.1: Contour plot of the isotropic chemical shieldings (ppm) for cyclopropane through a) molecular plane and b) a vertical plane bisecting the C–C bond calculated at the MP2/6-311++G(d,p) level of theory.

The vertical plane through cyclopropane in Figure 5.1b shows C–H bonds that are similar, though slightly more strongly shielded than those in ethane. This could be due to the C–H bonds being formed by atomic orbitals with unusually high s character.[29] It also displays a complete absence of any pertinent feature at the ring centre. It has been suggested that cyclopropane exhibits σ aromaticity, a property in this molecule which involves increased stabilisation caused by 3-centre-2-electron delocalisation.[106,107] This kind of delocalisation has been studied with magnetic shielding for the case of diborane in Chapter 2. Cyclopropane is devoid of any similarities with the diborane plots which is inconsistent with the presence of 3-centre-2-electron bonding in the three-membered ring. The same conclusion has been drawn by work using modern valence bond theory.[111] The question surrounding the validity of σ aromaticity as a concept is not considered here, but these results certainly distinguish between the types of bonding interaction present in cyclopropane versus diborane. Interestingly, when using the popular ring current method, a well-defined distinction between σ and π aromaticity cannot be obtained, but using the isotropic shielding plots in this work, the systems display clear differences.[112]

For the partly saturated case of cyclopropene, the sp^3 carbon, denoted C_1, exhibits very similar shielding to the carbons in cyclopropane. The same is true of the associated hydrogen nuclei. The shielding of C_2, on the other hand, varies greatly with theory level and is dissimilar from any of the linear hydrocarbon val-

ues obtained previously. The same is true of the C=C and C–C bond shielding maxima. But perhaps the most interesting results are found in the contour plots in Figure 5.2.

Table 5.2: Isotropic shieldings for the symmetry-unique nuclei and C–C bonding mid-point values for cyclopropene (in ppm), calculated at the HF-GIAO/6-311++G(d,p) and MP2-GIAO/6-311++G(d,p) levels of theory. C_1 refers to the sp^3 carbon.

	$\sigma_{iso}(C_1)$	$\sigma_{iso}(H_1)$	$\sigma_{iso}(C_2)$	$\sigma_{iso}(H_2)$
HF	193.90	31.03	73.01	24.40
MP2	195.14	31.03	92.46	24.92

	$\sigma_{iso}(C{=}C)$	$\sigma_{iso}(C{–}C)$	$\sigma_{iso}(C{–}H_1)$
HF	56.61	39.21	31.38
MP2	53.03	40.15	32.45

The C–C bonding regions in cyclopropene are very different from those in cyclopropane. The shielding along the C–C internuclear distance is concentrated nearest the sp^3 carbon to such an extent that both C–C bond shieldings merge around C_1. Furthermore, the shielding maxima are lower than those seen in cyclopropane with quite a different shape to the contours. The C=C bond, on the other hand, is reminiscent of a distorted version of a typical double bond. The shielding maximum is higher than for a typical double bond due to the squashed nature of the shielded region and again, bond bending is noticeable.

The vertical plane through cyclopropene shows slight differences in the C_1–H_1 bonding regions and an oval C=C bond cross-section which is typical of a double bond like that in ethene. There is also the hint of a lowered shielding feature at the ring centre which was not present in cyclopropane. This region in the vertical plane does not match up with a small shielding hole in the surface 1 Å above the molecule.

The final three-membered ring under investigation is the cyclopropenyl cation which is formed by deprotonation of cyclopropene. The results for this molecule can be seen in Table 5.3 and Figure 5.3.
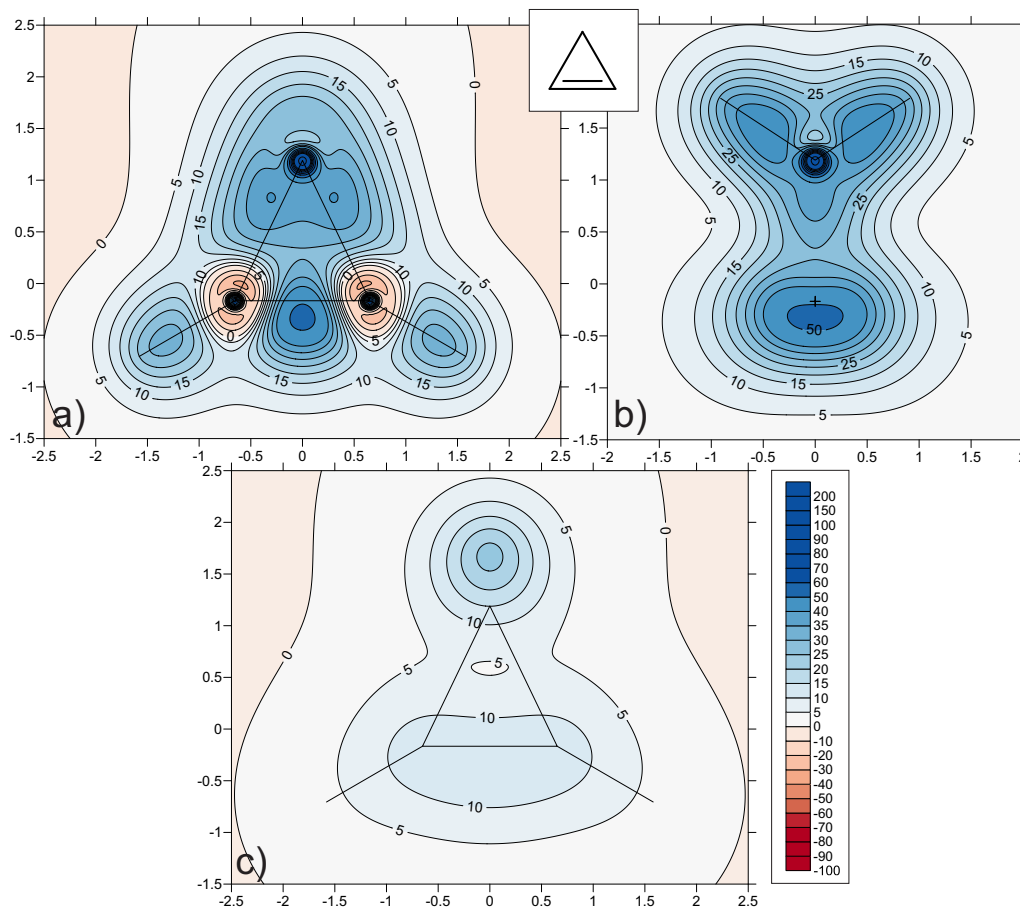
Figure 5.2: Contour plot of the isotropic chemical shieldings (ppm) for cyclopropene through a) molecular plane, b) a vertical plane bisecting the C=C bond and c) a plot 1 Å above the molecular plane calculated at the MP2/6-311++G(d,p) level of theory.

Table 5.3:   Isotropic shieldings for the symmetry-unique nuclei and C–C bonding mid-point values for the cyclopropenyl cation (in ppm), calculated at the HF-GIAO/6-311++G(d,p) and MP2-GIAO/6-311++G(d,p) levels of theory.

	$\sigma_{iso}(C)$	$\sigma_{iso}(H)$	$\sigma_{iso}(C–C)$	$\sigma_{iso}(C–H)$
HF	26.75	21.82	30.63	28.04
MP2	26.98	21.46	27.86	27.17

The carbon shieldings in the cyclopropenyl cation are unlike those in any of the linear hydrocarbons and are closer to, although a little lower than, those seen in systems like benzene. The is consistent with the introduction of aromaticity into the cyclopropenyl cation but the low value can be accounted for by the positive

charge. In fact, most of the features in all of the contour plots of this system are similar to those seen in other aromatic rings. The positive charge results in more intense deshieldings around the carbon nuclei than seen in neutral systems and the ring size and strain distorts the C–C bonding regions, but otherwise the features are consistent.
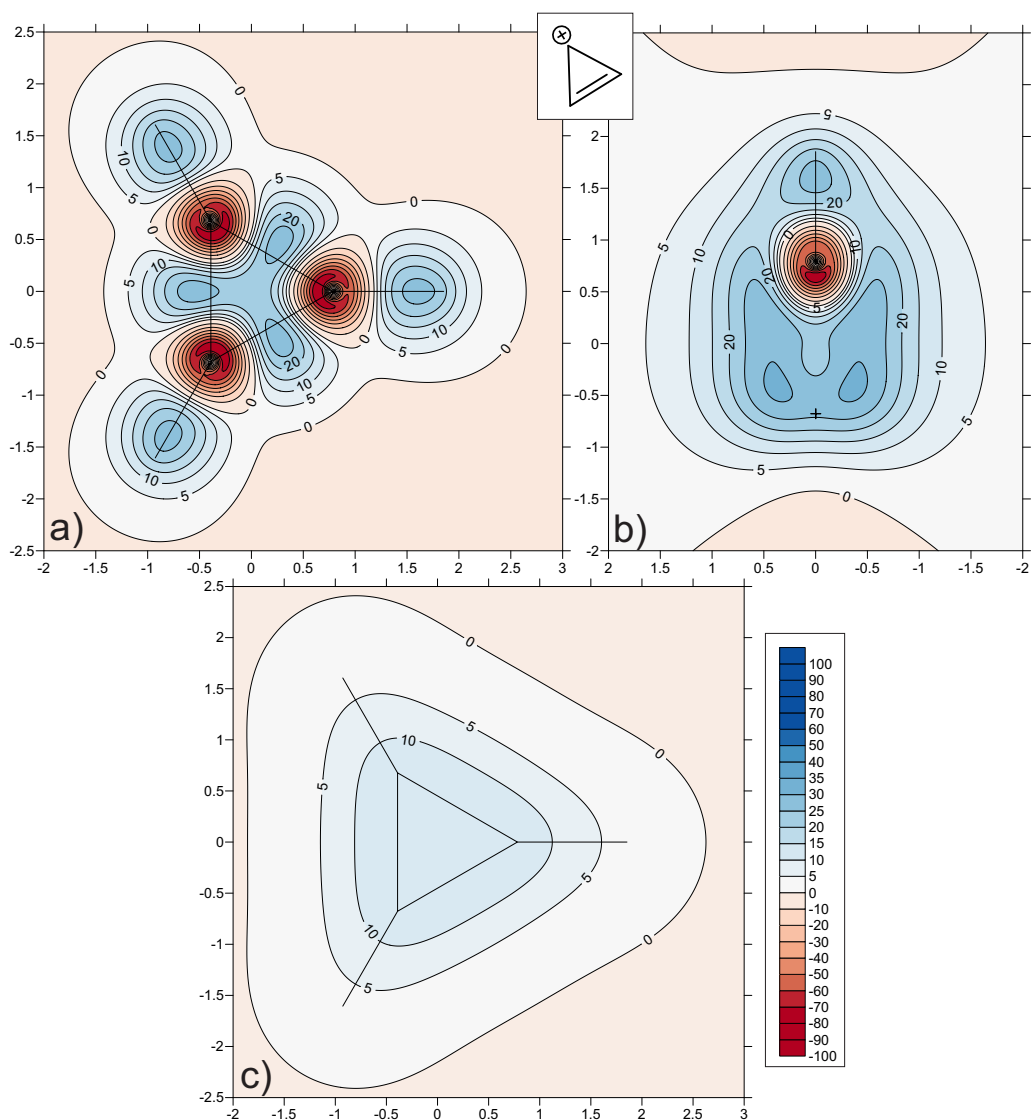
Figure 5.3: Contour plot of the isotropic chemical shieldings (ppm) for the cyclopropenyl cation through a) molecular plane, b) a vertical plane bisecting the C–C bond and c) a plane 1 Å above the molecular plane calculated at the MP2/6-311++G(d,p) level of theory.

In the vertical plane through the cyclopropenyl cation, a form of the π doughnut seen in other aromatic rings is present, although due to the small ring size, it is less well defined than in previous examples. For the same reason, the C–C bond cross-section is not distinct from the π doughnut.

The impressive change of features between these three three-membered rings is a reflection of the detail and sensitivity afforded by this method and results in great insight into a variety of molecular properties, particularly bonding.

5.3   Cyclopentadienyl Anion

The five-membered cyclopentadienyl (Cp) anion is a very commonly used system, especially as a ligand in organometallic complexes. Just like the cyclopropenyl cation, it is classed as a Hückel aromatic system, but possesses an overall negative charge rather than the positive charge in the cyclopropenyl cation. The investigation of this anion yielded the results in Table 5.4 and Figure 5.4.

Table 5.4: Isotropic shieldings for the symmetry-unique nuclei and C–C bonding midpoint values for the cyclopentadienyl anion (in ppm), calculated at the HF-GIAO/6-311++G(d,p) and MP2-GIAO/6-311++G(d,p) levels of theory.

	$\sigma_{iso}(C)$	$\sigma_{iso}(H)$	$\sigma_{iso}(C–C)$	$\sigma_{iso}(C–H)$
HF	89.98	26.39	53.17	33.09
MP2	99.49	25.91	51.50	32.54

The carbon shieldings in the Cp anion are higher than those in aromatic benzene which is likely due to the negative charge. This charge also results in less intense deshieldings around the carbon nuclei- the opposite of the effect of the positive charge seen in the cyclopropenyl cation, which is reasonable. The C–C bonding regions have the characteristic shape of bonds of 1.5/2 bond order, but with a higher shielding maximum which lies roughly at the bond mid-point, though with a little movement off-centre. This increased bond shielding can again be explained by the negative charge on the system.

The vertical plane through the Cp anion is typical of many other aromatic systems studied with a π doughnut above and below the ring and a slightly deformed oval C–C bond cross-section. The plane 1 Å above the ring is slightly different from that seen in benzene as the delocalised shielding ring above the molecule is not of an even width around the whole circumference of the ring. It exhibits bulges in the shielding at positions directly over carbon nuclei. This indicates a slightly lower aromaticity than that of benzene along with the C–C bond cross-section

which only displays a slight flattening on the inside rather than the distinctive kidney-shape of more aromatic compounds.
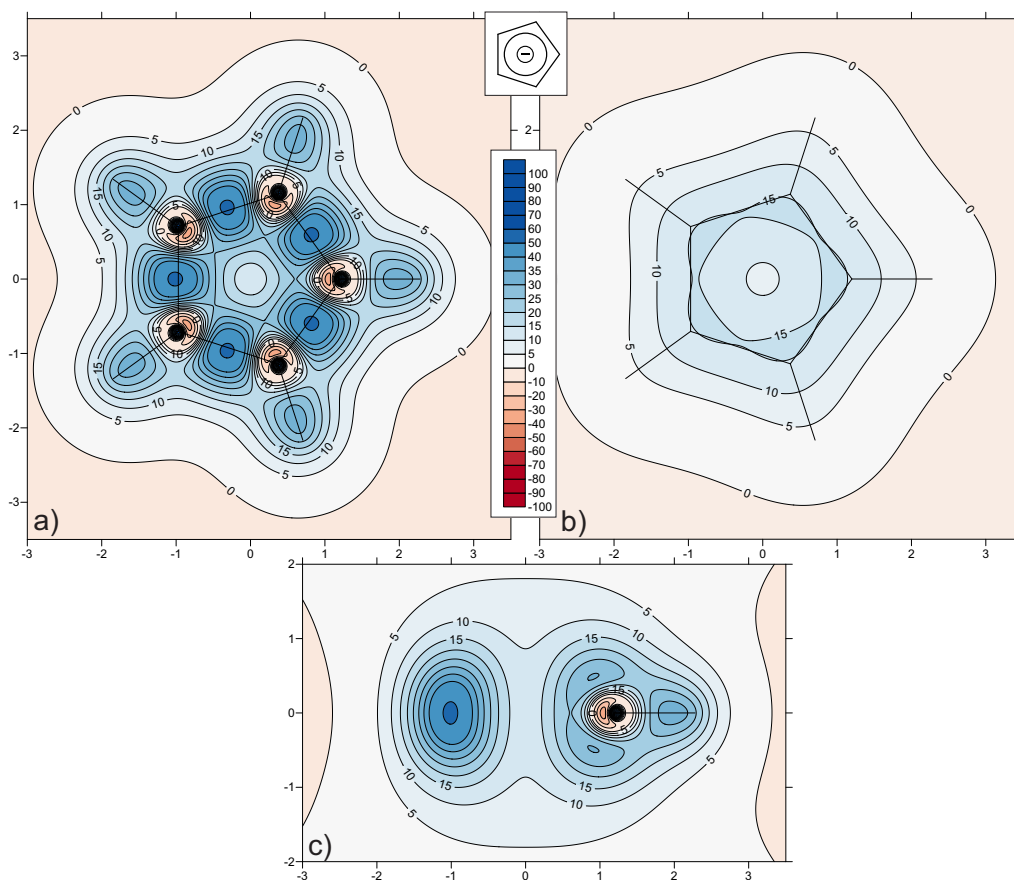
Figure 5.4: Contour plot of the isotropic chemical shieldings (ppm) for the cyclopentadienyl anion through a) molecular plane, b) a plane 1 Å above the molecular plane and c) a vertical plane bisecting a C–H bond calculated at the MP2/6-311++G(d,p) level of theory.

Overall it has been seen that a positive charge on a Hückel aromatic system results in intense carbon deshielded surroundings whereas a negative charge produces weakly deshielded regions. There are also effects on the C–C bond shielding maxima, with a negative charge producing more shielded bonds. However, typical aromatic characteristics are still visible in both cases.

5.4   Tropylium Cation

The tropylium cation, $C_7H_7^+$, another Hückel aromatic system, is frequently encountered in mass spectrometry. It commonly forms from fragmentation of molecules which contain a benzene moiety. Just like the cyclopropenyl cation, it is a posi-

tively charged aromatic system, but with the absence of the ring strain present in the three-membered ring.

Table 5.5: Isotropic shieldings for the symmetry-unique nuclei and C–C bonding midpoint values for the tropylium cation (in ppm), calculated at the HF-GIAO/6-311++G(d,p) and MP2-GIAO/6-311++G(d,p) levels of theory.

	$\sigma_{iso}(C)$	$\sigma_{iso}(H)$	$\sigma_{iso}(C–C)$	$\sigma_{iso}(C–H)$
HF	33.34	22.76	37.94	27.86
MP2	43.82	22.58	37.29	27.42

The positive charge for $C_7H_7^+$ is responsible for the same increased deshieldings around the carbon nuclei as seen in $C_3H_3^+$. It is obvious, however, that the shieldings directly on the carbon atoms can vary widely between systems as the values for the tropylium cation are quite unlike other rings. The same is true of the C–C bonding regions too, but this has been previously established.

More importantly, the contour plots show significant similarities with other aromatic systems. For example, the vertical plane seen in Figure 5.5c is entirely consistent with typical aromatic systems with the characteristic π doughnuts above and below the ring plane and the distinctive kidney-shaped distortion of the C–C bond cross-section. In fact, the bond cross-section possesses a greater distortion than that seen in the Cp anion, which is also aromatic. However, it is difficult to determine from this alone whether $C_7H_7^+$ is more aromatic than the Cp anion, hence the more kidney-shaped bond slice, or whether the increased electron density afforded by the negative overall charge in the Cp anion alters the bond shielding, covering the kidney-shape. It could be argued that, if the latter instance is true, this very effect could decrease the extent of the aromatic properties hence decreasing the overall aromaticity, but the current investigation remains inconclusive on this matter so far.

The C–C and C–H bonding regions are as expected when compared to previous work and the plot positioned 1 Å above the ring shows an homogenous shielding band encircling the ring, again, as expected. It seems that the tropylium cation exhibits very typical isotropic shielding features of a positively charged, aromatic system including some evidence that it may be considered more aromatic that the Cp anion.
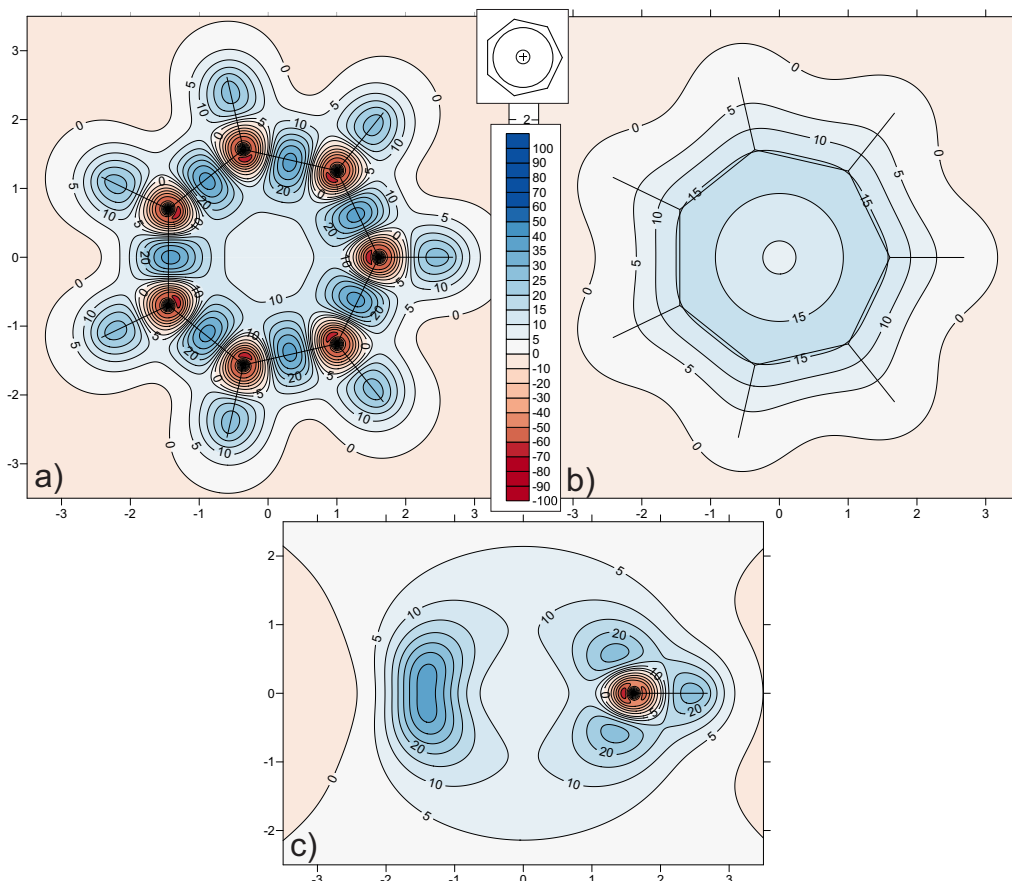
Figure 5.5: Contour plot of the isotropic chemical shieldings (ppm) for the tropylium cation through a) molecular plane, b) a plane 1 Å above the molecular plane and c) a vertical plane bisecting a C–H bond calculated at the MP2/6-311++G(d,p) level of theory.

5.5 Cyclooctatetraene

Cyclooctatetraene (COT) is an interesting and versatile system, both as a planar, aromatic dianion/dication, as part of a variety of metal complexes or just in its neutral, antiaromatic form. This latter instance does not exist in a planar geometry at its energetic ground state, however, for the purposes of this work, the planar, D_{8h} structure has been used to maximise the antiaromatic properties under investigation.

The data in Table 5.6 allows comparison of nuclear and bond shieldings for each of the COT forms explored here. It should be noted that the CASSCF method was used for neutral COT in order to properly describe the antiaromaticity of the molecule. The carbon shieldings of the neutral COT are just over 20 ppm lower than those in the dianionic and disodiated forms. In fact, the values obtained

for the dianion and Na$_2$COT are fairly similar but the neutral COT values are all distinct. This suggests little influence on the shieldings of the ring by the two sodium atoms. The dication values are also quite different from the other COT forms but not too dissimilar from those in the tropylium cation.

Table 5.6: Isotropic shieldings for the symmetry-unique nuclei and C–C bonding midpoint values for neutral COT, COT dianion and Na$_2$COT (in ppm), calculated at the CASSCF(8,8)/6-311++G(d,p), HF-GIAO/6-311++G(d,p) and MP2-GIAO/6-311++G(d,p) levels of theory.

Molecule		σ_{iso}(C)	σ_{iso}(H)	σ_{iso}(C–C)	σ_{iso}(C–H)
Neutral COT	CASSCF	69.48	31.35	26.51	38.24
COT Dication	HF	19.81	21.17	33.01	26.01
	MP2	30.11	20.96	32.39	25.49
COT Dianion	HF	93.90	26.40	54.47	32.84
	MP2	93.39	26.03	49.82	32.03
Na$_2$COT	HF	105.57	25.66	57.32	33.31
	MP2	113.01	25.12	55.00	32.45
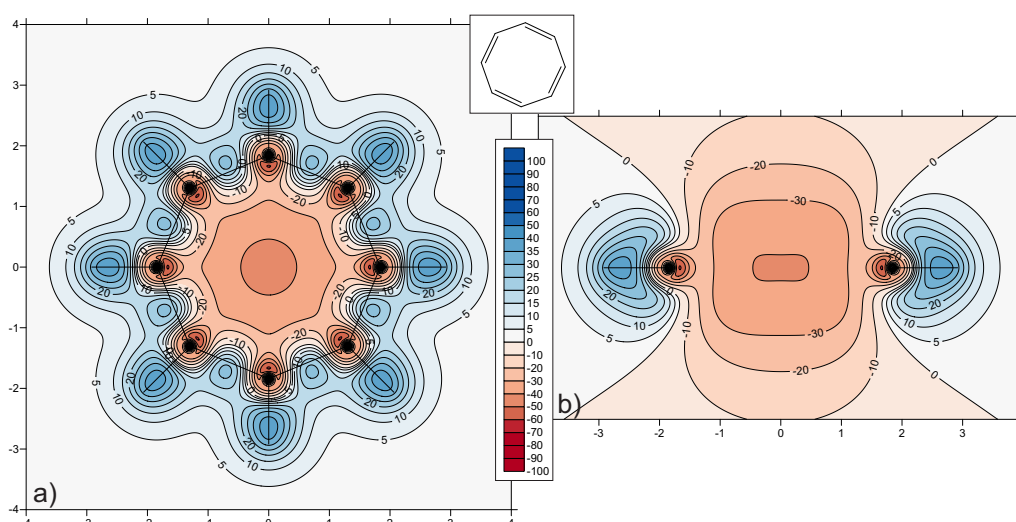
Figure 5.6: Contour plot of the isotropic chemical shieldings (ppm) for COT through a) molecular plane and b) a vertical plane bisecting two C–H bonds calculated at the CASSCF(8,8)/6-311++G(d,p) level of theory.

Figure 5.6 shows the molecular and vertical planes through neutral, planar COT. Distinctive antiaromatic features, such as those seen for cyclobutadiene, are evident including the weak C–C bond shieldings and the deshielded feature at the ring centre which extends above and below the ring. Unlike in cyclobutadiene, this deshielded region in the ring centre is more cylindrical than the dumbbell shaped. This will be caused by the increased ring size of COT over C_4H_4.
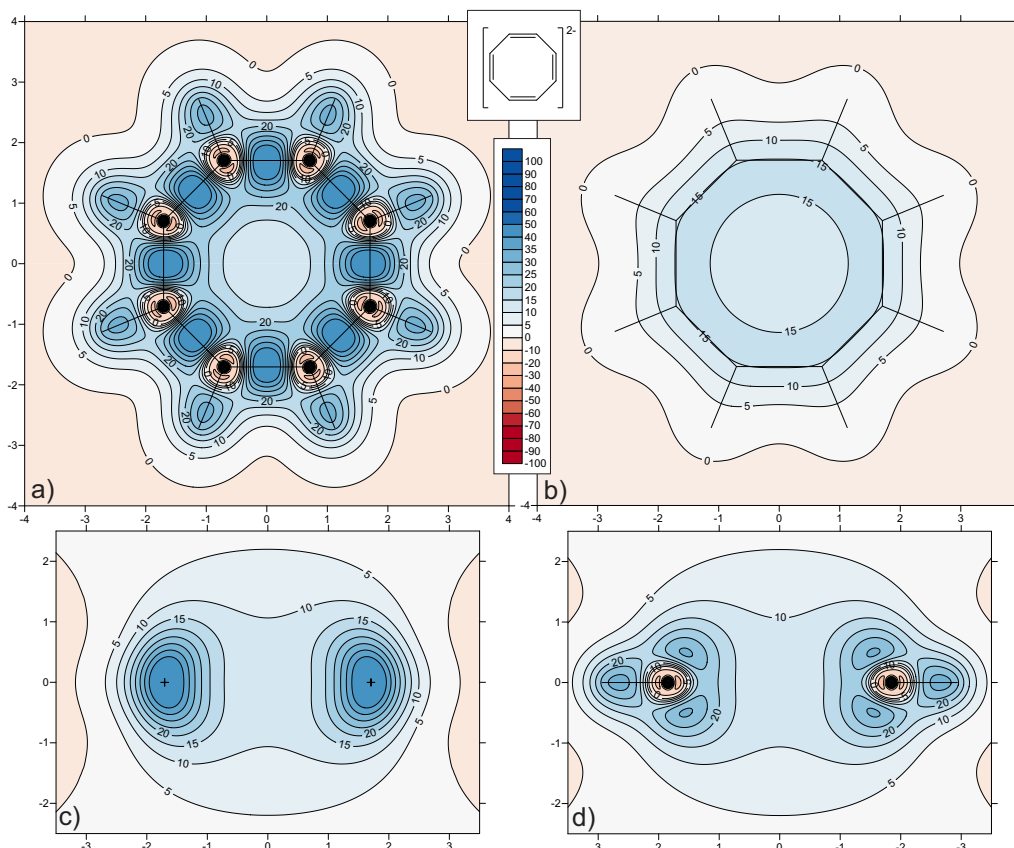
Figure 5.7: Contour plot of the isotropic chemical shieldings (ppm) for the COT dianion through a) molecular plane, b) a plane 1 Å above the molecular plane, c) a vertical plane bisecting two C–C bonds and d) a vertical plane bisecting two C–H bonds calculated at the MP2/6-311++G(d,p) level of theory.

However, perhaps of most interest are the C–C bonding regions. The shieldings around the internuclear regions are very similar in magnitude and shape to those seen in cyclobutadiene, including the weakness of the shielding and the bond bending that forces the shielding maximum to lie off-centre, outside the ring. In cyclobutadiene, this could have been attributed to ring strain, but with a system as large as COT, and the continued presence of bond bending, it is more likely that this is, at least in part, caused by the antiaromaticity in the molecule. It seems that

the deshielded central feature, formed in antiaromatic systems, is affecting the C–C bonding regions and forcing them outwards away from the ring centre. An analogous, but more subtle, effect has been seen in aromatic systems where the bonds have been drawn into a deformed shape by the aromaticity giving the bond cross-sections a kidney-shaped appearance. Moreover, this all shows a degree of ring destabilisation caused by the antiaromaticity of the system, something which other work had not found.[108]
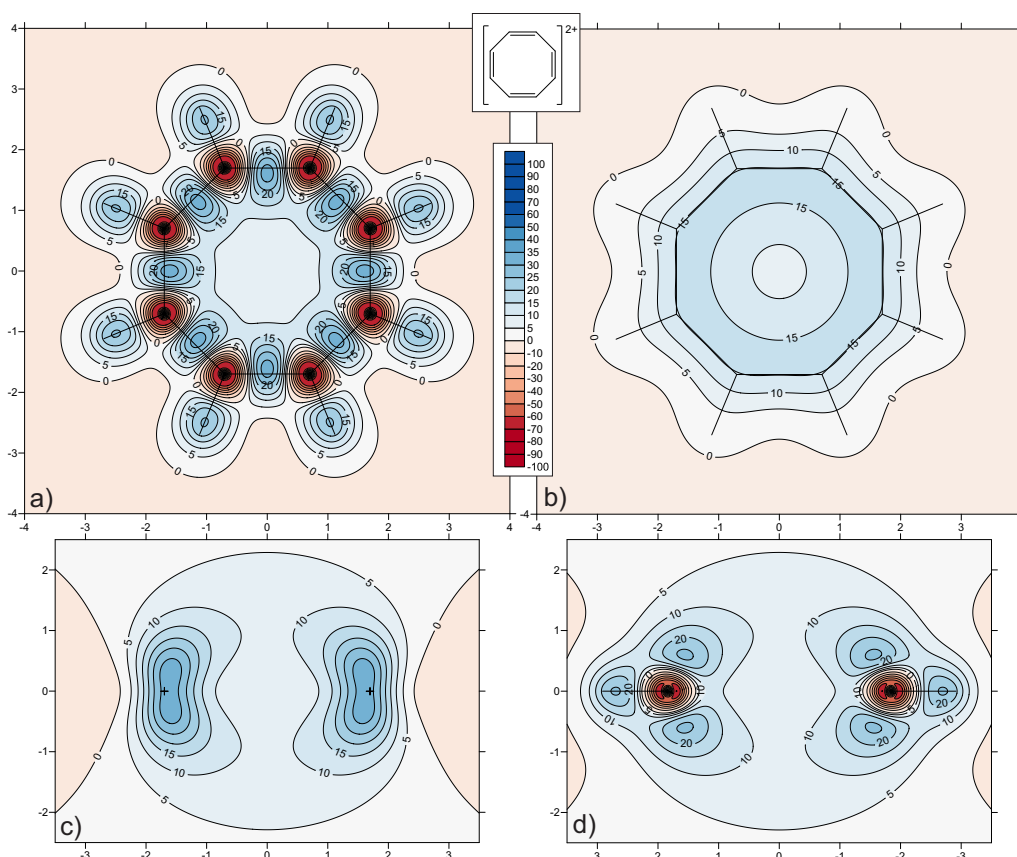
Figure 5.8: Contour plot of the isotropic chemical shieldings (ppm) for the COT dication through a) molecular plane, b) a plane 1 Å above the molecular plane, c) a vertical plane bisecting two C–C bonds and d) a vertical plane bisecting two C–H bonds calculated at the MP2/6-311++G(d,p) level of theory.

In the dianionic and dicationic forms of COT (Figures 5.7 & 5.8), typical aromatic features are observed with the same alterations caused by charge as seen in previous examples, though to a greater extent since the charges in these cases are doubled. The π doughnuts are clear for both molecules in the vertical plane and 1 Å above the rings. The C–C bond cross-sections are more kidney-shaped in the dication, similar to the results for $C_7H_7^+$ while the bonds in the dianion

exhibit a flattening on the inside of the ring and a slight bulge on the outside. This implies that the aromaticity which causes the indentation on the inner edge, is still present in this example, but that the increased electron density through a 2− charge has caused the bulging on the outside edge. This latter effect has not been seen in the Cp anion, possibly due to the smaller charge. This, along with the more homogeneous shielding at 1 Å above the ring, suggests that COT^{2-} should be considered as more aromatic than the Cp anion, a finding which is consistent with other work.[113]
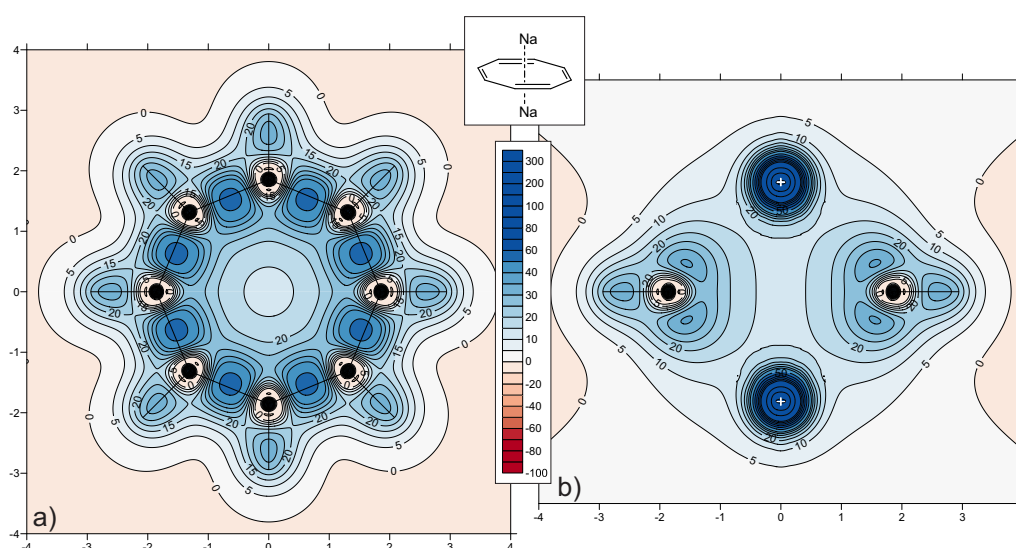
Figure 5.9: Contour plot of the isotropic chemical shieldings (ppm) for Na$_2$COT through a) molecular plane and b) a vertical plane bisecting two C–H bonds calculated at the MP2/6-311++G(d,p) level of theory.

Finally, Figure 5.9 shows the results for Na$_2$COT. It can be seen from the molecular plane plot that most of the features within the ring are identical to those seen in the naked dianion with the exception that the carbon deshielded surroundings are slightly less intense and the C–C bonding regions are slightly more shielded. The vertical plane is also remarkably similar to that of the lone dianion. These findings show only subtle shielding perturbations upon disodiation, but the strengthening of the C–C bond shieldings suggest a significant impact on the structural properties of the ring itself which could provide greater understanding of metal complexation with aromatic systems.

5.6   Conclusions

A variety of charged systems have been studied including some with multiple charges. A study of three-membered rings showed significant changes in shielding features upon moving from saturation, to partial saturation and finally to full unsaturation. This demonstrated a high degree of sensitivity of the method used here as well as the high level of detail that can be obtained.

The effect of charge on aromatic rings has also been investigated and it has been found that an overall positive molecular charge causes an increase in the magnitude of the deshielded regions around carbon nuclei as well as a slight weakening of the C–C bond shieldings. Conversely, a negative overall charge weakens the deshieldings around the conjugated nuclei and strengthens the C–C bonding regions. Furthermore, the C–C bond cross sections display a more pronounced kidney-shape in cationic systems than in anionic systems. In the case of the COT dianion, this C–C cross-section even exhibited a bulge on the outside of the ring along with the deformation on the inner edge.

Finally, a variety of COT variants have been explored. Disodiation of dianionic COT revealed little impact on the ring itself with the exception of a slight C–C shielding increase and a decrease in the carbon deshielded surroundings. Planar, neutral COT, which can be considered antiaromatic, displays a deshielded region at the ring centre, similar to the case of cyclobutadiene, although the shape is more cylindrical for COT. Most importantly, significant bond bending is displayed in neutral COT which can now be attributed to the effect of antiaromaticity rather than purely ring strain, as was considered for cyclobutadiene.

6

Heterocycles

"An enormous mass of information was reduced to a well-ordered system
through the aid of a few simple principles."
Gilbert N. Lewis

6.1   Introduction

Thousands of key chemical compounds contain aromatic moieties, most of which contain one or more heteroatoms. There has also been much debate over the years about the correct ordering of aromaticity for even the most common heterocycles. The use of off-nucleus magnetic shielding calculations has already been shown to successfully describe aromaticity and antiaromaticity as well as chemical bonds, so in this chapter, the same technique is used to investigate a range of heterocycles both to study their molecular properties but also to attempt to define an aromaticity order.

Furan, pyrrole and thiophene are three of the most commonly studied heterocycles. They are all five-membered aromatic rings with a single heteroatom. Early computational work on these molecules by Cordell and Boggs determined that pyrrole was the only one of the three systems that could be considered truly aromatic.[114] They suggested that the nitrogen of pyrrole was ideal for ring conjugation while the oxygen in furan and the sulphur in thiophene were too small and too large, respectively. However, work carried out a few years before used seven different aromaticity criteria to establish that thiophene and furan could be considered aromatic.[115]

Oxazole, imidazole and thiazole are identical to these molecules but with structures that each possess one extra nitrogen atom within the ring. A study of these azoles concluded that the so-called 'first heteroatom' (O, S or NH), which donates two π electrons, will have the greatest impact on the molecule's aromaticity.[116] The shielding around the azoles in this work can be compared to their single-heteroatom analogues to determine the overall effect of the second heteroatom.

Finally a selection of heavier heteroatoms, such as Se and P, can be explored along with larger, six-membered heterocycles. This will allow the investigation of the effect of atom size on aromaticity, conjugation and bonding as well as ring size on the shielding plots. For example, it is known that the popular NICS technique is moderately dependent on ring size,[42] but the application of shielding calculations across large areas, such as the method used in this work, should remove ring size dependence.

The geometries of furan,[117] pyrrole[118] and thiophene[119] are all experimentally determined gas-phase, ground-state structures. The structure of selenophene[120]

and thiazole[121] were experimentally determined by microwave spectroscopy. Oxazole and imidazole were optimised at the MP2/aug-cc-pVTZ level of theory and the ground-state was confirmed by frequency analysis. The geometries of phosphole, phosphabenzene and the pholide ion were also optimised but at the MP2/6-31G(d,p) level of theory. The structures of pyridine[122] and pyrimidine[123] were experimental determined by a combination of methods.

It should be noted that the work on furan, pyrrole and thiophene has been previously published.[124] The work on the azoles is also in preparation for publication at the time of writing.

6.2   Five-Membered, Single Heteroatom Heterocycles

6.2.1   Furan, Pyrrole & Thiophene

Table 6.1 shows the isotropic shieldings for the nuclei in furan, pyrrole and thiophene as well as the NICS(0) and NICS(1) values. It can be seen from this table that the carbons adjacent to the various heteroatoms (denoted C_1) are less shielded than the other carbons (denoted C_2). As seen in previous chapters, the theory levels both have the same trend, though different shielding magnitudes.

The comparison of the C_1 shieldings with those of C_2 across the three molecules is very interesting. There is a difference of around 35 ppm between the two carbons in the case of furan, but this gap closes to around 6 ppm in pyrrole and is only 0.4 ppm for thiophene. This pattern can be seen even more clearly in the contour plots in Figures 6.1a, 6.2a and 6.3a. It is evident that the carbon environments are most distinct in furan and are far more equivalent in thiophene, with pyrrole as an intermediate. This is a key indicator of the degree of π delocalisation and therefore the degree of aromaticity in each of these molecules.

This is illustrated beautifully by the planes 1 Å above the molecules, seen in Figures 6.1b, 6.2b and 6.3b. In the case of furan, there are two lobes of moderate shielding positioned over the two "double bonds". As the molecule changes to pyrrole, these two lobes spread and join together forming a larger, banana-shaped region of shielding covering half of the ring. Finally, in thiophene, the whole ring is enclosed by this region of shielding, demonstrating the highest level of delocalisation around the ring, and therefore the highest degree of aromaticity. Furan, with the very localised π density, can be considered the least aromatic.

Table 6.1: Isotropic shieldings for the symmetry-unique nuclei and NICS(0), NICS(0.5) and NICS(1) values for furan, pyrrole and thiophene (in ppm), calculated at the HF/6-311++G(d,p) and MP2/6-311++G(d,p) levels of theory. C_1 is the carbon adjacent to the heteroatom Z.

	Furan (Z = O)		Pyrrole (Z = N)		Thiophene (Z = S)	
	HF	MP2	HF	MP2	HF	MP2
$\sigma_{\text{iso}}(Z)$	57.70	56.29	109.10	117.76	333.73	314.05
$\sigma_{\text{iso}}(H_Z)$	–	–	24.85	24.19	–	–
$\sigma_{\text{iso}}(C_1)$	41.80	54.55	68.16	83.13	55.47	73.61
$\sigma_{\text{iso}}(C_2)$	78.88	89.39	79.48	89.18	62.74	73.97
$\sigma_{\text{iso}}(H_1)$	24.49	24.31	25.15	25.12	24.66	24.59
$\sigma_{\text{iso}}(H_2)$	25.64	25.41	25.67	25.41	24.92	24.62
NICS(0)	−12.18	−12.64	−14.80	−14.14	−19.64	−19.43
NICS(1)	− 9.20	− 9.70	−10.42	−10.25	−11.35	−11.68

This same ordering is obtained by the NICS(0) and NICS(1) values in Table 6.1. Interestingly, this is in contrast to the HF/6-31+G* and HF/6-31G* NICS(0) results produced by Schleyer and co-workers which predicts the aromaticity to decrease in the order pyrrole > thiophene > furan.[42] This suggests that the use of extended basis sets is beneficial when calculating NICS values.

These plots also afford a great deal of bonding information. Firstly, it is interesting to note that the plots are consistent with the widely accepted view that the C_1–C_2 "double" bonds are stronger than the C_2–C_2' "single" bonds. However, from viewing the plots and the data in Table 6.2, it is clear that this distinction is fairly subtle. Moreover, bond equalisation is frequently used as an aromaticity indicator, with a greater amount of equalisation meaning a greater amount of aromaticity. Because the introduction of a heteroatom into the ring creates perturbation of the ring as well, it is important to consider the carbon-heteroatom bonds rather than just comparing the carbon-carbon bonds.
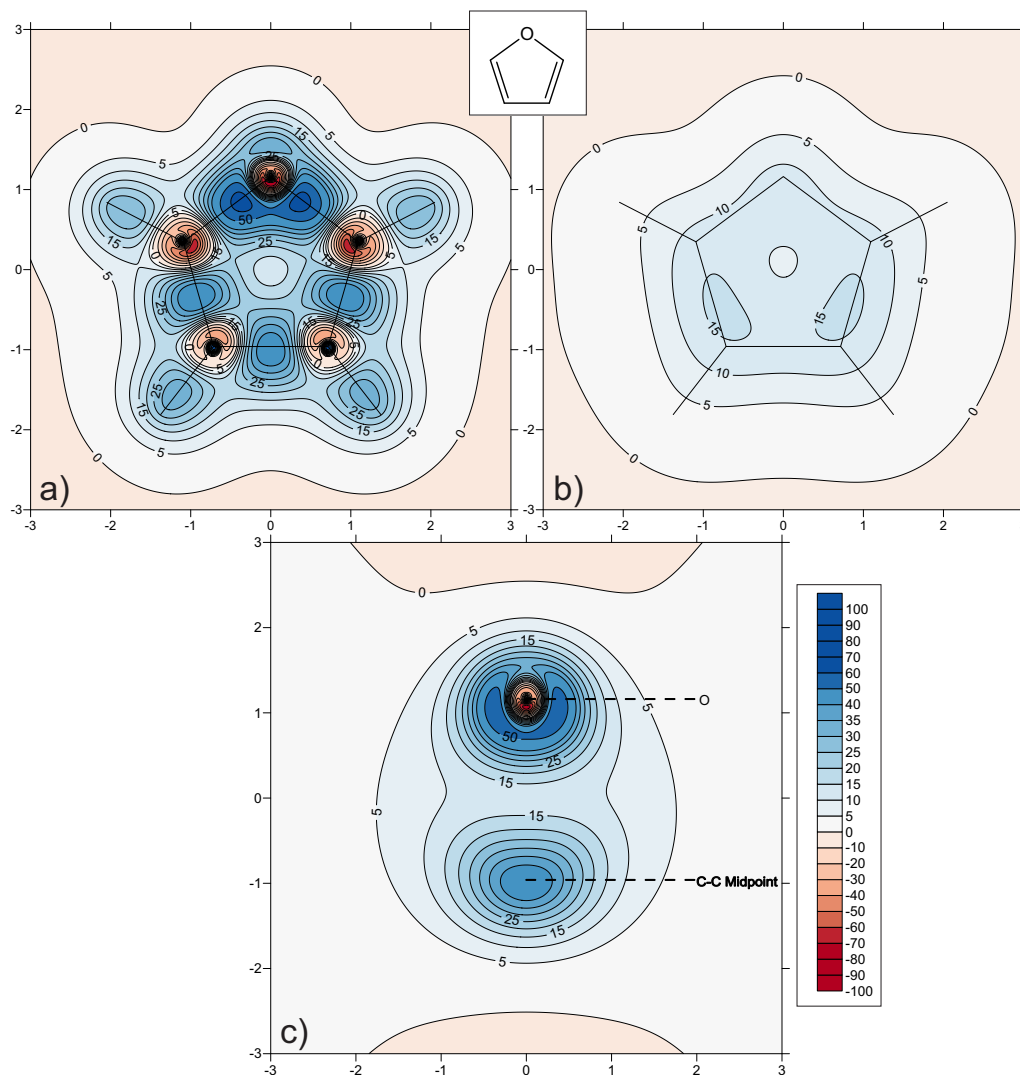
Figure 6.1: Contour plot of the isotropic chemical shieldings (ppm) for furan through a) molecular plane, b) 1 Å above the molecular plane and c) a vertical plane bisecting the O atom and the C–C bond calculated at the MP2/6-311++G(d,p) level of theory.

On inspection of the contour plots, and with the previous comment in mind, it can be seen that the most equalised bond distribution is found in thiophene, with the least equal found in furan. Considering the values in Table 6.2, the same trend can be seen, with the C_1–X and C_1–C_2 bond shielding maxima being only 5 ppm apart in thiophene compared to about 11 ppm in pyrrole and 17 ppm in furan. These observations are consistent with the aromaticity order provided earlier by the NICS values calculated in this work, carbon nuclear shieldings and inspection of the 1 Å above plots.
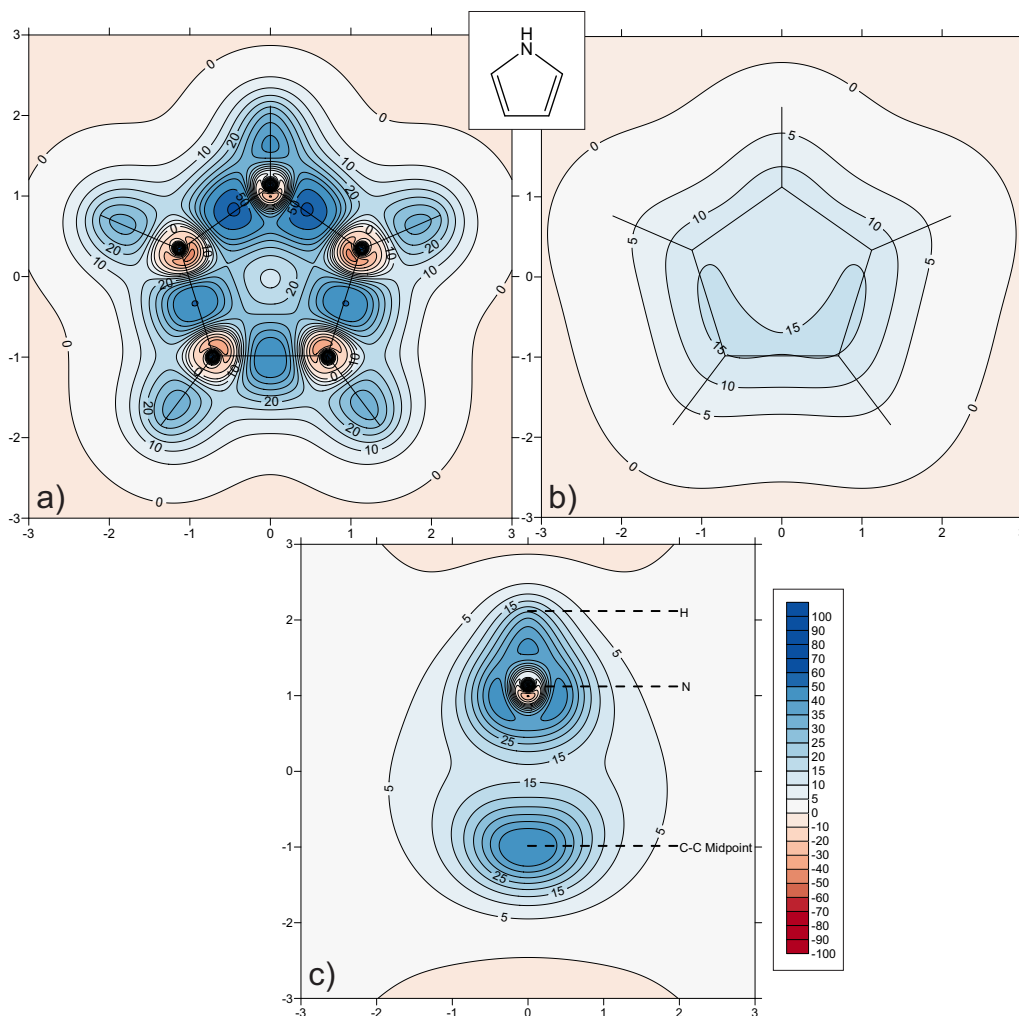
Figure 6.2: Contour plot of the isotropic chemical shieldings (ppm) for pyrrole through a) molecular plane, b) 1 Å above the molecular plane and c) a vertical plane bisecting the N–H and the C–C bond calculated at the MP2/6-311++G(d,p) level of theory.

The red regions of deshielding surrounding the sp^2 hybridised nuclei also exhibit the same trend of carbon environment equivalence as the carbon nuclear shieldings. The regions surrounding the heteroatoms are less useful for comparison in this manner due to the effect of changing atomic structure between the elements. The sulphur atom does not appear to have a deshielded surrounding, but as seen in previous chapters, larger nuclei require a closer inspection to see this feature. This will be seen in greater detail in the section on thiazole (*vide infra*).

Table 6.2: Highest isotropic shieldings within regions corresponding to carbon-heteroatom and carbon-carbon bonds in furan, pyrrole and thiophene (in ppm). Approximate values taken from the $\sigma_{iso}(\mathbf{r})$ grids in the respective molecular planes calculated at the MP2/6-311++G(d,p) level of theory.

| | Highest $\sigma_{iso}(\mathbf{r})$ value | | |
	Furan (Z = O)	Pyrrole (Z = N)	Thiophene (Z = S)
C_1–Z	64	61	54
C_1–C_2	47	50	49
C_2–C_2'	45	48	44

The bond cross-sections, seen in the vertical plane plots (Figures 6.1c, 6.2c and 6.3c) are also useful. Whilst at first glance, all three cross-sections look very similar, a closer inspection of the bond in thiophene reveals a slight kidney-shaped shielded region. This same shape has been seen previously in benzene which again places thiophene as the most aromatic of these three heterocycles.

Cordell and Boggs calculated electron density plots of these three systems at the HF level of theory, and the vertical planes they produced have quite similar features to those presented here, though the shielding plots differentiate between bonds more clearly.[114] Kleinpeter *et al.* have published iso-chemical shielding surfaces (ICSSs) which correspond to "through-space NMR shieldings" for furan, pyrrole and thiophene.[57] However, the use of very coarse grid spacings (ten times larger than those used in this work) causes subtle details to be missed, even if the overall aromaticity trend is the same.

In can be concluded, from studying bonding regions, nuclei and shielding 1 Å above these heterocycles that the order of aromaticity increases from furan < pyrrole < thiophene, which is consistent with established experimental evidence. It has also been seen that this method provides a great deal more information than previously established methods such as ICSSs, NICS values or electron density plots.
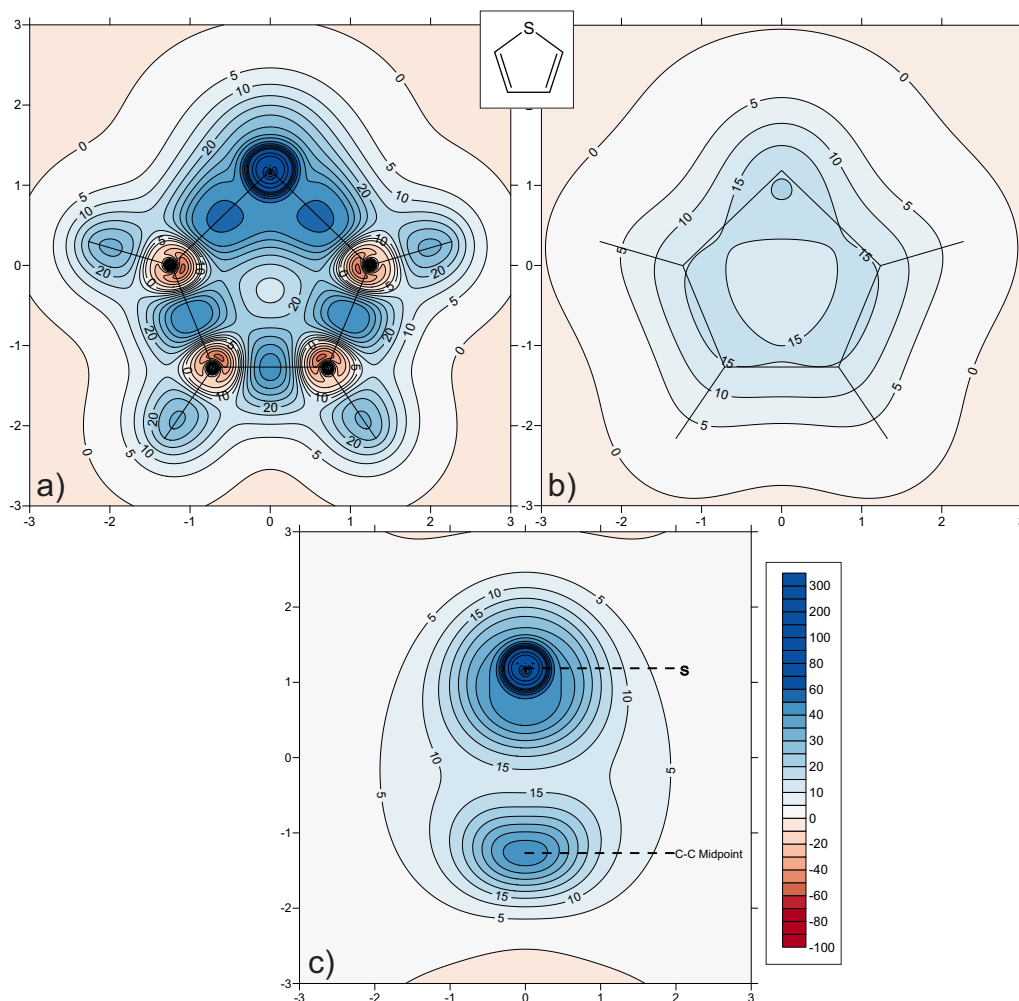
Figure 6.3: Contour plot of the isotropic chemical shieldings (ppm) for thiophene through a) molecular plane, b) 1 Å above the molecular plane and c) a vertical plane bisecting the S atom and the C–C bond calculated at the MP2/6-311++G(d,p) level of theory.

6.2.2 Selenophene

Selenophene is a heavier analogue of furan and thiophene from the same periodic group. The contour plots of various planes through selenophene can be seen in Figure 6.4 with nuclear shielding values and bond maxima in Table 6.3.

Table 6.3: Isotropic shieldings for the symmetry-unique nuclei and bond maxima in selenophene (in ppm), calculated at the HF-GIAO/6-311++G(d,p) and MP2-GIAO/6-311++G(d,p) levels of theory. C_1 refers to the carbon adjacent to the Se.

	$\sigma_{iso}(Se)$	$\sigma_{iso}(C_1)$	$\sigma_{iso}(C_2)$	$\sigma_{iso}(H_1)$	$\sigma_{iso}(H_2)$
HF	1378.71	45.60	57.39	24.16	24.87
MP2	1338.35	65.68	69.12	24.16	24.59

	$\sigma_{iso}(C_1\text{–}C_2)$	$\sigma_{iso}(C_2\text{–}C'_2)$	$\sigma_{iso}(C_1\text{–}H_1)$	$\sigma_{iso}(C_2\text{–}H_2)$
HF	50.96	37.64	30.35	30.90
MP2	48.42	41.32	30.71	30.56

It can be seen from the data in Table 6.3 that the shielding on the heavy selenium atom is far higher than the oxygen or sulphur atoms seen in previous heterocycles. Interestingly, the C_1 isotropic shielding is intermediate between those in furan and those in thiophene while the value of the C_2 atom in selenophene is lower than both of the lighter heterocycles. However, the most useful comparison is between the two unique carbon environments in each molecule. In furan this difference was around 35 ppm, in thiophene it was 0.4 ppm indicating, along with other results, an increase in aromaticity moving from furan to thiophene. In the case of selenophene, this shielding difference is roughly 3.5 ppm which is intermediate between pyrrole and thiophene. Just as in the previous heterocycles, this small difference is reflected in the contour plot in Figure 6.4a where the carbon nuclei display significant equivalence in their surroundings.

The selenium surrounding is well shielded, like that seen around the sulphur in thiophene, except that in this case, the shielding extends over the region of intense shielding along the C–X bonds so that the two features are no longer distinct. The C_2–C'_2 bond cross-section in Figure 6.4c shows a fairly oval shape with a slight deformation on the inner edge reminiscent of the kidney-shaped bond cross-section in benzene. This is very similar to that seen in thiophene and is generally an indicator of a degree of aromaticity higher than that seen in pyrrole and furan which do not exhibit this deformation.
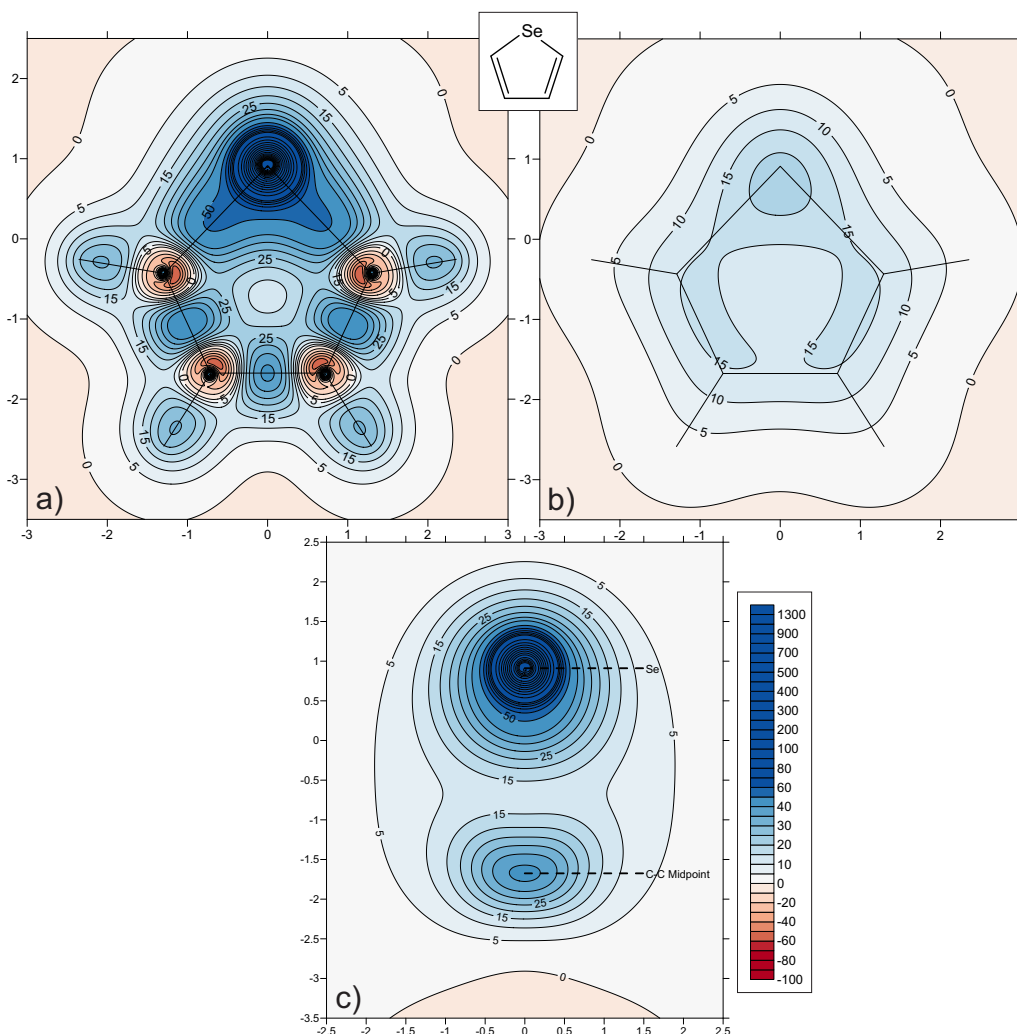
Figure 6.4: Contour plot of the isotropic chemical shieldings (ppm) for selenophene through a) molecular plane, b) 1 Å above the molecular plane and c) a vertical plane bisecting the Se atom and the C–C bond calculated at the MP2/6-311++G(d,p) level of theory.

The comparison between the shielding maxima along the C–C bonds in the heterocycles seen so far is also interesting. In furan and pyrrole the difference is only 2 ppm, but in thiophene this increases to 5 ppm and in selenophene this increases still to around 7 ppm. This further highlights the importance of caution when considering the bond shielding maxima in isolation as these results suggest that the least aromatic heterocycle, furan, has the least diene-character which is in contradiction with well-known experimental evidence. The C–X bond must be compared to these values and the shape of the shielding surfaces should be factored into the analysis. The C–C bond shielding contours in selenophene are very similar to those seen in thiophene. This, along with the previous evidence

suggests that selenophene is quite similar to thiophene in aromaticity.

However, the shielding at 1 Å above selenophene also provides useful information. The delocalised shielding around the ring in Figure 6.4b, whilst fairly similar to that in thiophene, also displays a discontinuity above the C_2–C'_2 bond. This disruption will result in a lower aromaticity than thiophene for which the delocalisation extends around the whole ring. This is caused by the increased size of the heteroatom and the resultant change in its ability to overlap with and delocalise into the rest of the ring. As the size of the heteroatom increases, this becomes a more limiting factor. Sulphur, for example, is less electronegative and bigger than the oxygen of furan making its electron density more diffuse. This allows less perturbation of the ring's π density which results in thiophene being more aromatic than furan. However, the size of selenium means that these effects are negated by the poor overlap that is inherent in large elements bonded to carbon. This is seen in a study of furan, thiophene, selenophene and tellurophene by Fringuelli and co-workers.[115]

In conclusion, the shielding at 1 Å above the ring, the carbon shielding values and the bond cross-sections all indicate that selenophene exhibits an aromaticity that is intermediate between furan and thiophene, in agreement with other work.[115] It also appears to be slightly more aromatic than pyrrole, which is again, in agreement with the literature.[38]

6.2.3 Phosphole & Pholpholide Ion

Having considered heavy analogues of other heterocycles, it is worth considering those of pyrrole (and later, pyridine). Here the phosphorus-containing 5-membered ring of phosphole is investigated along with its planar, anionic form (the pholpholide ion). The results for these can be seen in Figures 6.5 & 6.6 and Tables 6.4 & 6.5.

Neutral phosphole is not planar, hence there is disagreement about whether it can exhibit aromaticity. The phosphorus atom exists in a pyramidal conformation, which some suggest will prohibit aromatic characteristics. An investigation into this by UV photoelectron spectroscopy and theoretical studies concluded that, despite its non-planar conformation, phosphole can be considered aromatic.[125] This was found to be due to nπ* conjugative and P–C/π* hyperconjugative interactions between the *cis*-butadiene and PH moieties. However, the authors

found little evidence of any π electron delocalisation which they ascribe to the electron-accepting nature of the phosphorous d orbitals. Though the effect of the phosphorus lone pair cannot be excluded as it has also been found to be key in the aromaticity of phosphole.[126] Other work on heterocycle aromaticity suggests that inclusion of phosphorus within small rings helps to reduce ring strain which can also add to the stabilisation of these systems.[116]

The popular NICS technique establishes phosphole as a borderline aromatic system (NICS(6-31+G*) = -5.3 ppm, NICS(6-31G*) = -5.9 ppm), similar to cyclopentadiene.[42] By considering stabilisation energies, diamagnetic susceptibility exaltations and geometries, a similar conclusion can be drawn, though suggesting that phosphole is slightly more aromatic than cyclopentadiene.[127] Upon removal of the proton on the phosphorus to form the phospholide anion, the structure becomes planar and more conjugated, therefore increasing the aromaticity.[128]

Table 6.4: Isotropic shieldings for the symmetry-unique nuclei and bond maxima in phosphole (in ppm), calculated at the HF-GIAO/6-311++G(d,p) and MP2-GIAO/6-311++G(d,p) levels of theory. C_1 refers to the carbon adjacent to the P.

	$\sigma_{iso}(P)$	$\sigma_{iso}(C_1)$	$\sigma_{iso}(C_2)$	$\sigma_{iso}(H_1)$	$\sigma_{iso}(H_2)$	$\sigma_{iso}(H_P)$
HF	420.82	51.31	46.60	25.12	24.77	27.31
MP2	410.26	67.44	60.02	24.99	24.54	26.84

	$\sigma_{iso}(P-C_1)$	$\sigma_{iso}(C_1-C_2)$	$\sigma_{iso}(C_2-C'_2)$	$\sigma_{iso}(C_1-H_1)$	$\sigma_{iso}(C_2-H_2)$
HF	38.72	49.59	30.70	31.37	30.21
MP2	40.15	46.53	34.12	31.40	29.93

In work by Chesnut *et al.*, the formal single and double bond lengths in phosphole were found to be close to ordinary single and double bond lengths, with the C–P bond close to a C–P single bond.[128] However, upon enforcing planarity or deprotonation of phosphole to form the phospholide ion, there was shortening of the C–P and C_2–C_2' bonds and lengthening of C_1–C_2 bonds suggesting increased conjugation. The findings of that work can be compared to the results of the isotropic shielding calculations performed here.

The maximum shielding values obtained along the various bonds can be found

in Table 6.4 and show some interesting features. Firstly, the maximum shielding along the formal C–C single bond and the formal C=C double bond differ by about 13 ppm, with the value along the double bond being similar to that obtained along the C=C bond in ethene previously. However, the C–C bond of ethane exhibited a shielding maximum of *ca* 52 ppm which is significantly higher than the C–C single bond in phosphole. Since it has already been established that shielding magnitude alone is insufficient to describe bond order, the overall shielding surface around the various bonds must also be compared. These can be seen in Figure 6.5.
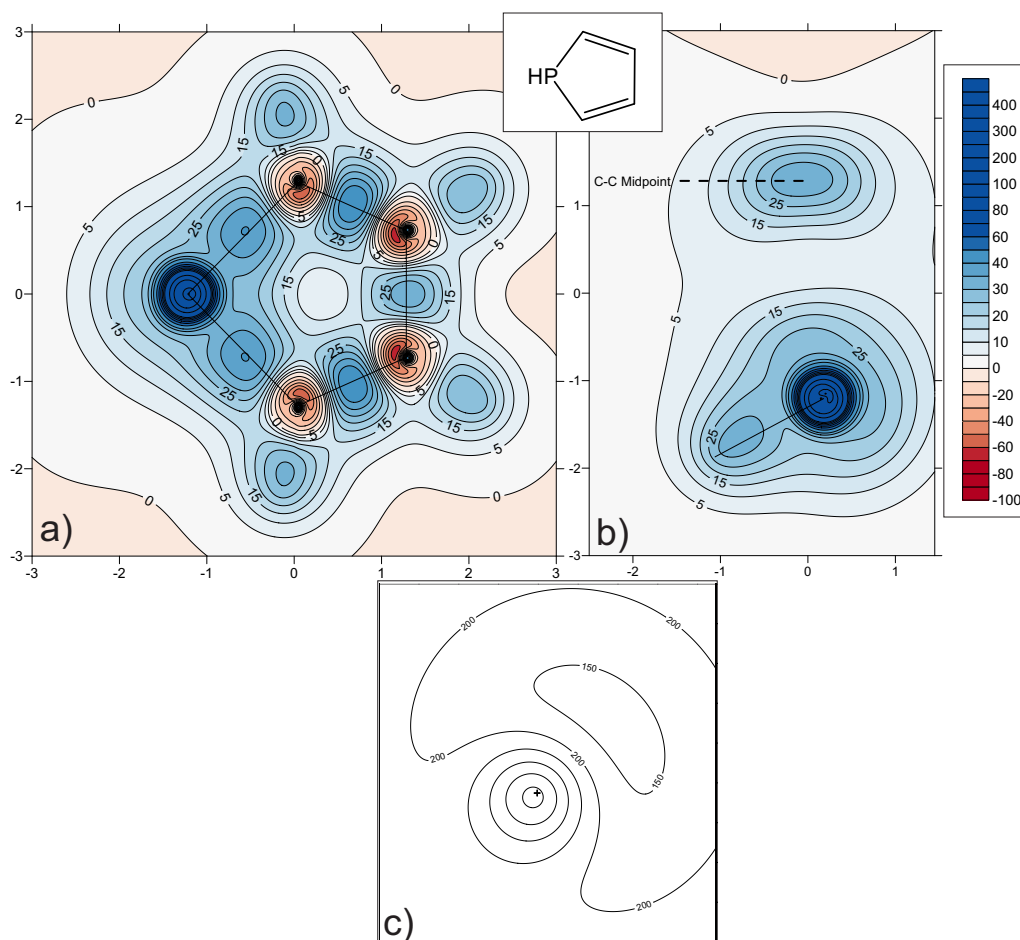
Figure 6.5: Contour plot of the isotropic chemical shieldings (ppm) for phosphole through a) molecular plane, b) a vertical plane bisecting the P atom and the C–C bond and c) an ultra-fine grid (with 0.001 Å spacing) over the phosphorus atom in the vertical plane calculated at the MP2/6-311++G(d,p) level of theory. Note that the molecular plane plot is a stitched plot and that the contour fill colour has been removed from figure c) for clarity.

The resemblance of the shielding contours surrounding the C=C formal double

bonds to those seen in ethene and benzene is clear. The formal single C–C bond in phosphole however, is unlike that seen in ethane, as the shielding maxima would suggest. Instead, the bonding region is reminiscent of the C=C double bonds but with a weaker magnitude. This implies that the comparison of bond lengths, like those found by Chesnut and co-workers, is not sufficient to fully describe the bonding in phosphole. Continuing with bond comparison, the two unique C–H bonds display quite different shielding regions along the bonds, something which was not seen as distinctly in any of the other five-membered heterocycles studied so far. Moreover, the C–C bond cross section seen in Figure 6.5b shows the distinctive oval shape of a double bond, with a very slight deformation on the inside of the ring indicating weak aromaticity.

Table 6.5: Isotropic shieldings for the symmetry-unique nuclei and bond maxima in pholpholide ion (in ppm), calculated at the HF-GIAO/6-311++G(d,p) and MP2-GIAO/6-311++G(d,p) levels of theory. C_1 refers to the carbon adjacent to the P.

	$\sigma_{iso}(P)$	$\sigma_{iso}(C_1)$	$\sigma_{iso}(C_2)$	$\sigma_{iso}(H_1)$	$\sigma_{iso}(H_2)$
HF	260.16	50.72	74.22	24.82	25.39
MP2	266.63	75.46	84.69	24.79	24.88

	$\sigma_{iso}(P–C_1)$	$\sigma_{iso}(C_1–C_2)$	$\sigma_{iso}(C_2–C'_2)$	$\sigma_{iso}(C_1–H_1)$	$\sigma_{iso}(C_2–H_2)$
HF	49.07	50.11	46.24	30.55	31.07
MP2	47.79	48.46	47.29	30.99	30.45

The deshielded regions surrounding the carbon nuclei highlight the inequivalence of the carbon environments, a trait which is evident in the less aromatic heterocycles. Furthermore, the space surrounding the phosphorus atom is well shielded, for similar reasons as seen for the sulphur in thiophene, although there is only very weak evidence of a lowered shielding region. This indicates poor conjugation with the rest of the ring. This, along with the C–H bond disparity, C–C bond cross-section and the carbon inequivalence suggests only weak aromaticity which is in accordance with literature findings.[42,125–128]

The phospholide anion displays bonding regions in Figure 6.6 which are all fairly consistent demonstrating the increased conjugation that is possible in this planar system. This is apparent both in the shielding maxima in Table 6.5, but also

the shielding surfaces around the bonds as seen in the contour plots. This high degree of π conjugation is further seen in the shielding present 1 Å above the ring.
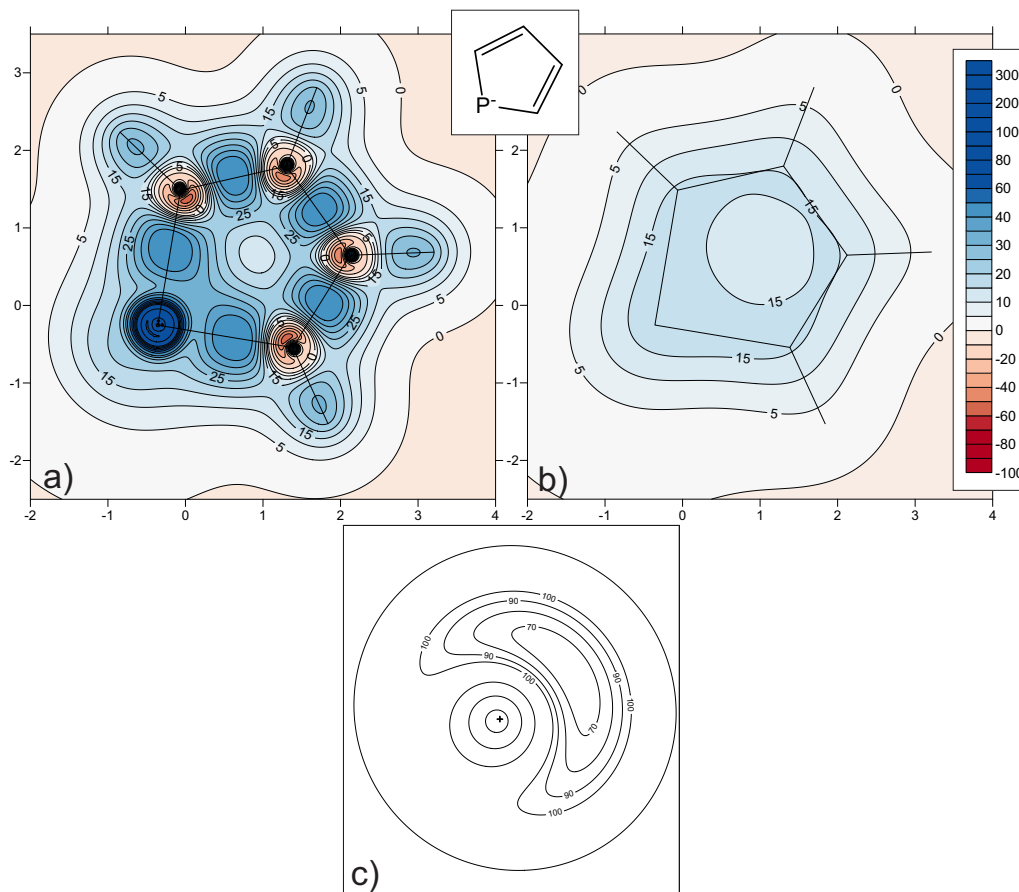
Figure 6.6: Contour plot of the isotropic chemical shieldings (ppm) for phospholide ion through a) molecular plane, b)1 Å above molecular plane and c) an ultra-fine grid (with 0.001 Å spacing) over the phosphorus atom calculated at the MP2/6-311++G(d,p) level of theory. Note that the contour fill colour has been removed from figure c) for clarity.

Interestingly, in the pholide ion, there is a greater inequivalence between the carbon nuclear shieldings than in phosphole, but with far more equivalent deshieldings around the carbon nuclei. These features can be explained by the effect of the phosphorus lying in the plane of the ring for the charged molecule which allows better conjugation, resulting in more equivalent deshielded regions, but which also has a greater impact on the adjacent carbon nuclei themselves. The space surrounding the phosphorus itself exhibits a region of lowered shielding towards the centre of the ring which is consistent with features seen previously around large heteroatoms in aromatic molecules. All of this confirms that

the phospholide anion is far more aromatic than its non-planar counterpart, phosphole.

6.3 Five-Membered Azoles

The atom numbering for the azoles in this section is as follows: C_1 refers to the carbon positioned between N and heteroatom X, C_2 is that adjacent to the N but not heteroatom X and finally, C_3 is adjacent to heteroatom X but not N. Analogous numbering is applicable to the hydrogens. The "first" heteroatom refers to X (O, S and NH) where the heteroatom donates two π electrons to the ring. The "second" heteroatom, in these systems, is the lone N.

Table 6.6: Isotropic shieldings for the nuclei and NICS(0), NICS(0.5) and NICS(1) values for imidazole, oxazole and thiazole (in ppm), calculated at the HF/6-311++G(d,p) and MP2/6-311++G(d,p) levels of theory.

| | Imidazole (X = NH) | | Oxazole (X = O) | | Thiazole (X = S) | |
	HF	MP2	HF	MP2	HF	MP2
$\sigma_{iso}(N)$	−44.25	1.10	−31.49	9.73	−106.32	−49.25
$\sigma_{iso}(X)$	101.66	109.40	39.20	36.89	298.12	280.73
$\sigma_{iso}(H_X)$	24.05	23.39	−	−	−	−
$\sigma_{iso}(C_1)$	46.57	67.39	28.98	48.09	23.18	52.46
$\sigma_{iso}(C_2)$	55.93	67.88	48.70	57.59	69.41	78.48
$\sigma_{iso}(C_3)$	73.84	84.53	58.99	70.73	44.59	56.34
$\sigma_{iso}(H_1)$	24.31	24.53	24.16	24.23	23.14	23.60
$\sigma_{iso}(H_2)$	24.66	24.59	24.35	24.12	24.96	24.58
$\sigma_{iso}(H_3)$	25.03	24.88	24.75	24.68	23.98	23.85
NICS(0)	−13.88	−13.87	−11.35	−12.44	−13.02	−13.06
NICS(1)	−10.86	−10.92	− 9.47	−10.15	−11.21	−11.76

It can be seen that the $\sigma_{iso}(N)$ values obtained at the HF and MP2 methods are considerably different, which is consistent with the findings of previous work, both in this thesis and published work.[124] In comparison, the isotropic shieldings of the first heteroatoms vary far less. Assuming the concept of Nyulàszi et al.[116]

that the "first" heteroatom is the major influence on ring aromaticity, this suggests that in all three molecules, the N is playing the least dominant role in affecting the aromaticity of the ring. Table 6.6 also shows little variation in the proton shieldings between methods, where all values are within 0.5 ppm of each other. This is all consistent with previous chapters.

Interestingly, the NICS(0) values, at both theory levels, and the HF NICS(0.5) values reported in Table 6.6 indicate that imidazole is the most aromatic, followed by thiazole and finally with oxazole as the least aromatic. In contrast, the NICS(1) and MP2 NICS(0.5) values propose the order thiazole $>$ imidazole $>$ oxazole. This reiterates the importance of excluding σ electron contributions to the isotropic shielding with respect to describing aromaticity as well as the dangers of reducing aromaticity to a single value.

The effect of the various heteroatoms on the carbon shieldings is also worth noting. In imidazole, it can be seen that the $\sigma_{iso}(C_1)$ and $\sigma_{iso}(C_2)$ values are fairly similar, while this is not the case in the other two azoles. This again suggests that the first heteroatom, X, has more impact on the aromaticity of the ring than the second heteroatom (N in each azole here). However, it can also be seen that the shielding of the carbon adjacent to both N and NH has a similar $\sigma_{iso}(C)$ value to that of the carbon adjacent to only the N. In oxazole, all three carbon shieldings are fairly distinct, with the carbon adjacent only to the O being the most shielded. In the case of thiazole, $\sigma_{iso}(C_1)$ and $\sigma_{iso}(C_3)$ are comparatively similar, with $\sigma_{iso}(C_2)$ being significantly more shielded.

However, it is the contour plots of the $\sigma_{iso}(\mathbf{r})$ values in the surrounding space that give the best overview of the properties of these three azoles. These can be seen in Figure 6.7. The regions of shielding enclosing the various chemical bonds clearly show the nature of the bonding in each molecule. The $\sigma_{iso}(\mathbf{r})$ maximum for each of these shielded regions can also illustrate the subtle variations in the bonding and can be seen in Table 6.7. Interestingly, all of the C–X bonds have similar $\sigma_{iso}(\mathbf{r})$ values at their maximum points. However, when these bonds are observed in Figure 6.7, it can be seen that there are slight differences in the shapes of the enclosed shielded regions.
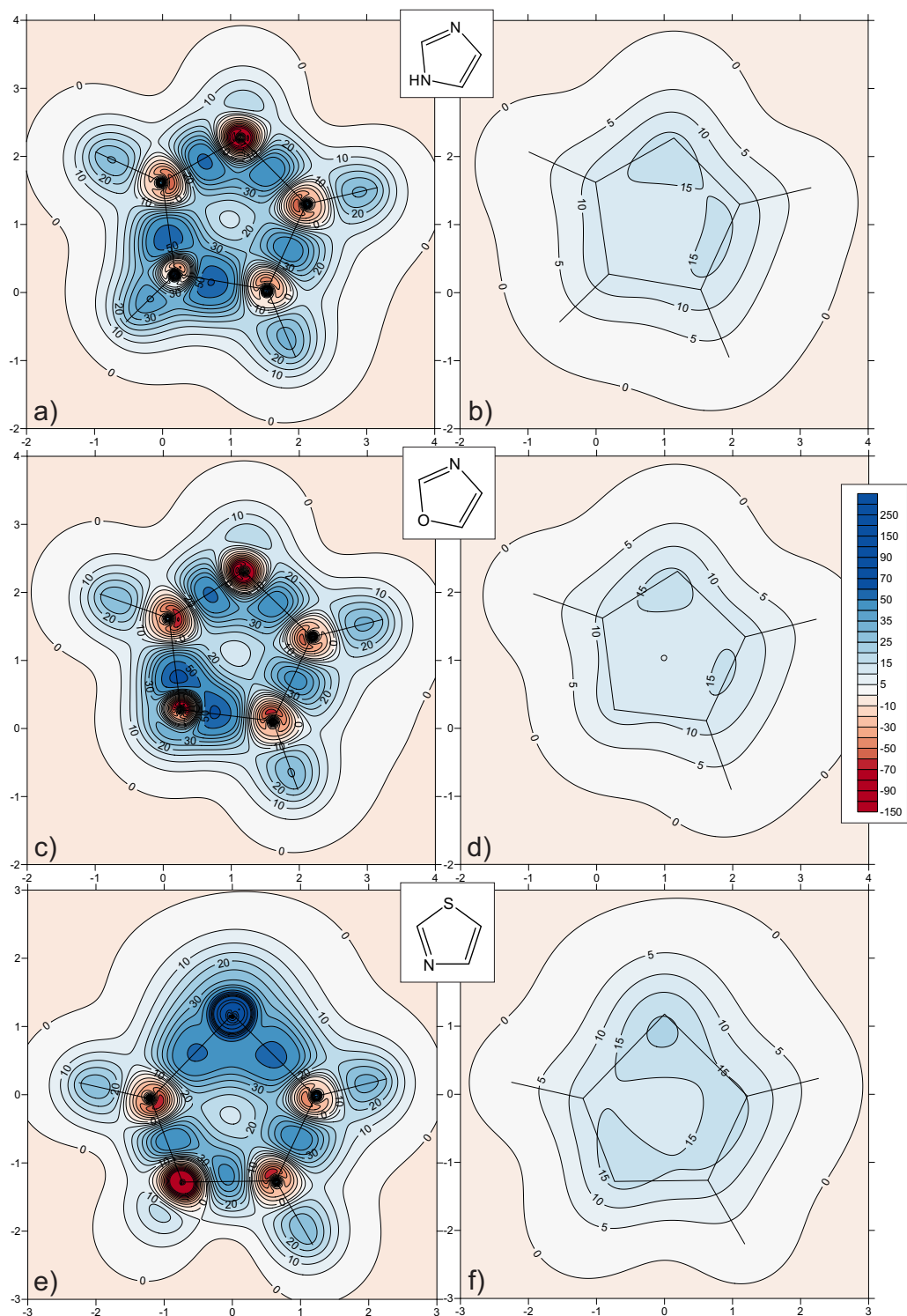
Figure 6.7: Contour plot of the isotropic chemical shieldings (ppm) for imidazole through a) molecular plane and b)1 Å above molecular plane, oxazole through c) molecular plane and d) 1 Å above the molecular plane and thiazole through e) molecular plane and f) 1 Å above molecular plane calculated at the MP2/6-311++G(d,p) level of theory.

Table 6.7: Highest isotropic shieldings within carbon-heteroatom and carbon-carbon bonding regions in imidazole, oxazole and thiazole (in ppm). Approximate values taken from the $\sigma_{iso}(\mathbf{r})$ grids in the respective molecular planes calculated at the MP2/6-311++G(d,p) level of theory.

| | Highest $\sigma_{iso}(\mathbf{r})$ value | | |
	Imidazole (X = NH)	Oxazole (X = O)	Thiazole (X = S)
C_1–X	59	64	52
C_1–N	53	53	48
C_2–N	49	46	43
C_2–C_3	47	44	47
C_3–X	61	62	54

The C–N bonds vary more than the C–X bonds, which perhaps reflects the difference in the degrees of single and double bond character exhibited in these molecules. Likewise, the double bond characters of the C_1–N and C_2–C_3 bonds can be compared. It can be noticed that these two bonds are most similar in $\sigma_{iso}(\mathbf{r})$ value in thiazole, and least so in oxazole. Furthermore, the total range of $\sigma_{iso}(\mathbf{r})$ values is smallest in thiazole and largest in oxazole. Since bond equalisation is often a property attributed to aromaticity, it can therefore be concluded that thiazole has a greater degree of bond equalisation and therefore, is more aromatic than imidazole, with oxazole being the least aromatic.

The σ_{iso} values on the nuclei, in combination with the contour plots in Figure 6.7, can give valuable comparisons of the various heteroatoms. It has been previously noted that sp and sp^2 hybridised atoms in the second row exhibit a region of deshielding surrounding their nuclei. It can be seen here that the regions surrounding the X nuclei are very similar to those seen in furan, pyrrole and thiophene earlier in this chapter, which is fairly intuitive. But the region surrounding the N is quite different, both from the results of previous work, and from the nitrogen in the NH of imidazole. Interestingly, whilst the magnitude of the deshielded surroundings varies between systems, the general features remain constant. The effect of the lone pairs on the N causes the region around the nucleus to become heavily deshielded in all three systems. However, despite this heavy deshielding, the nitrogens do not seem to perturb the shielding above the ring, hence their

relatively weak effect on the overall aromaticity.

Observation of the delocalisation, or lack thereof, of the isotropic shielding at 1 Å above the molecular planes can also be indicative of degrees of aromaticity. It can be seen that in the case of oxazole, the contour plot shows two significantly localised regions of shielding 1 Å above the molecular plane, similar to furan seen previously. In imidazole, the two shielded lobes are elongated and almost join in the middle. This suggests a greater degree of delocalisation, and therefore aromaticity. Furthermore, the regions above the two unique nitrogen environments can be distinguished easily at 1 Å above the ring. Finally, thiazole has a shielded region at 1 Å above the molecule which is almost complete around the circumference of the ring, reminiscent of the plots for thiophene. This implies that thiazole has a much more homogeneous delocalisation of the π density around the ring and therefore is the most aromatic of these three azoles.

In fact, these azoles can be compared to the contour plots generated previously for furan, pyrrole and thiophene for the purpose of putting all six in order of increasing aromaticity. Thiophene has the most complete ring of delocalised shielding at 1 Å above the molecular plane, therefore is the most aromatic. Thiazole is similar, but has a slight gap and so is less aromatic. Pyrrole displays one large shielding 'banana' around the carbons so is less aromatic than thiazole but more so than imidazole which has two separate lobes of shielding. Furan has slightly more localised shieldings but the least aromatic molecule is oxazole with the smallest localised regions of shielding at a distance of 1 Å above the molecular plane. So, the order of increasing aromaticity becomes thiophene > thiazole > pyrrole > imidazole > furan > oxazole.

6.4 Six-Membered Heterocycles

There are also many chemically important six-membered aromatic heterocycles. Nitrogen nuclei can be found in pyridine and pyrimidine, the latter of which forms the building block for several DNA/RNA bases, and phosphorus can be investigated further, this time in phosphabenzene.

Table 6.8: Isotropic shieldings for the symmetry-unique nuclei and bond maxima in pyridine (in ppm), calculated at the HF-GIAO/6-311++G(d,p) and MP2-GIAO/6-311++G(d,p) levels of theory. C_1 refers to the carbon adjacent to the N.

	$\sigma_{iso}(N)$	$\sigma_{iso}(C_1)$	$\sigma_{iso}(C_2)$	$\sigma_{iso}(C_3)$	$\sigma_{iso}(H_1)$	$\sigma_{iso}(H_2)$	$\sigma_{iso}(H_3)$
HF	−104.02	29.61	67.18	46.39	22.99	24.59	23.99
MP2	−56.65	47.66	71.24	65.59	22.98	24.16	24.05

	$\sigma_{iso}(N–C_1)$	$\sigma_{iso}(C_1–C_2)$	$\sigma_{iso}(C_2–C_3)$	$\sigma_{iso}(C_1–H_1)$
HF	41.66	39.87	43.48	26.95
MP2	40.08	38.32	42.47	26.86

	$\sigma_{iso}(C_2–H_2)$	$\sigma_{iso}(C_3–H_3)$
HF	30.99	29.30
MP2	29.97	29.44

Pyridine is the first of these systems to be investigated and the results can be seen in Table 6.8 and Figure 6.8. The inequivalence of the unique carbon environments can be clearly seen in Figure 6.8a and from the carbon nuclear shieldings. The carbon shieldings are around 48 ppm for the carbons adjacent to the nitrogen, denoted C_1, around 71 ppm for C_2 and a lower shielding of around 66 ppm for C_3 which lies furthest from the nitrogen. The same trend is true of the H nuclear shieldings. This trend is mirrored by the regions of deshielding around the same carbon nuclei. The C_1 nuclei are surrounded by a fairly intense red region of deshielding while the C_2 atoms are far less deshielded. In accordance with the values from Table 6.8, the C_3 environment has a deshielded area that is of an intermediate value between the other two environments, though fairly similar to that of C_2. This perturbation of the carbon environments by the nitrogen atom also affects the shielding visible in Figure 6.8b at 1 Å above the molecule and results in a lower aromaticity than benzene.
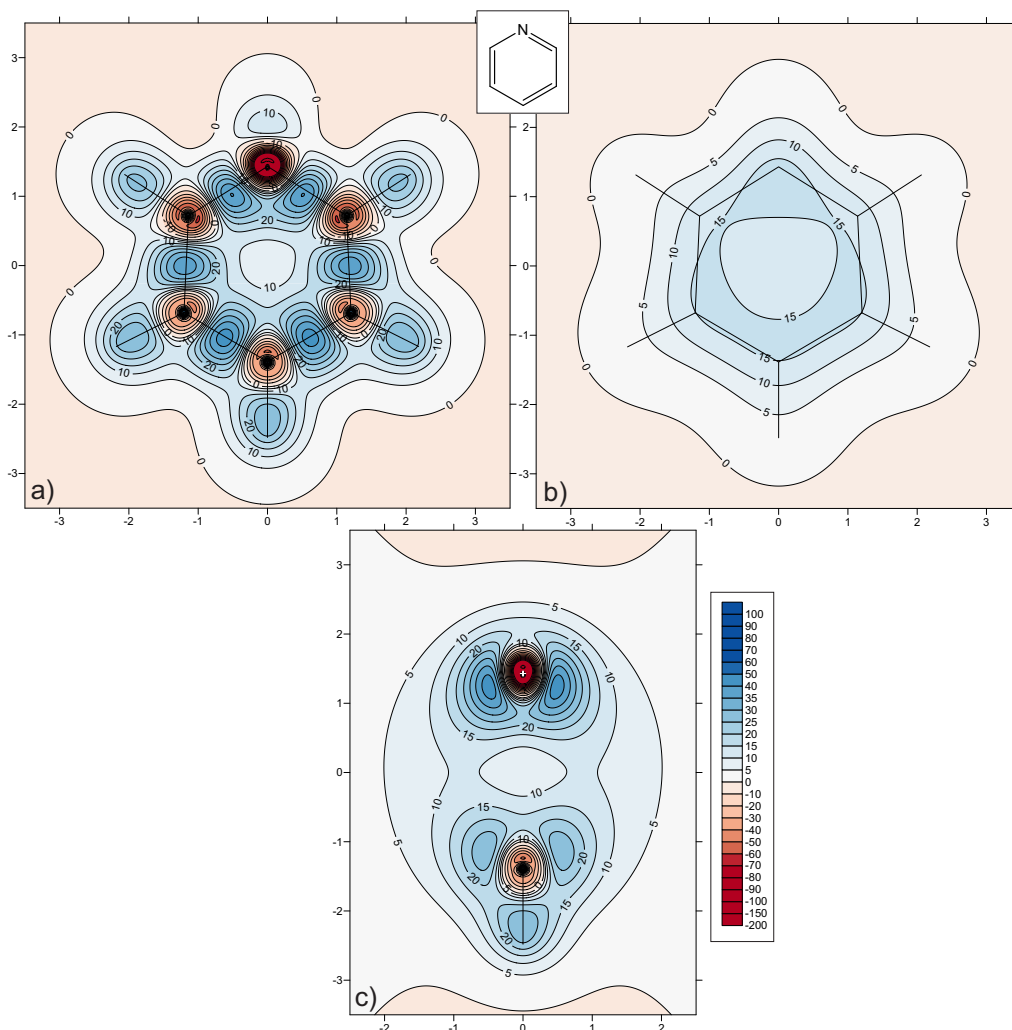
Figure 6.8: Contour plot of the isotropic chemical shieldings (ppm) for pyridine through a) molecular plane, b)1 Å above molecular plane and c) a vertical plane bisecting C–H and the N atom calculated at the MP2/6-311++G(d,p) level of theory.

On inspection of the bonding regions around the pyridine ring, it can be seen that the bonds all have similar maxima, though their shielding contours are subtly different. The C–N bonding regions display a shielding maximum that is pulled noticeably off-centre towards the middle of the ring, though this effect is less pronounced in the C–C bonds. The C_1–C_2 bonds exhibit the weakest shielding maximum, though only by about 2 ppm. The overall structure of the shielded bonding regions around the ring is consistent with than seen in bonds with an order of between 1.5 and 2, which is as expected. Finally, the vertical plane through pyridine, seen in Figure 6.8c, shows the π doughnuts above and below the molecule which are characteristic of aromatic systems. The inhomogeneity of this feature is also evident as the cross-section over the nitrogen atom is significantly more shielded

that that above the opposing carbon atom.

Table 6.9: Isotropic shieldings for the symmetry-unique nuclei and bond maxima in pyrimidine (in ppm), calculated at the HF-GIAO/6-311++G(d,p) and MP2-GIAO/6-311++G(d,p) levels of theory. C_1 refers to the carbon in between both N atoms and C_2 the carbon adjacent to only one N.

	$\sigma_{iso}(N)$	$\sigma_{iso}(C_1)$	$\sigma_{iso}(C_2)$	$\sigma_{iso}(C_3)$	$\sigma_{iso}(H_1)$	$\sigma_{iso}(H_2)$	$\sigma_{iso}(H_3)$
HF	-63.35	25.17	21.92	71.00	22.78	23.00	24.94
MP2	-41.85	42.13	43.96	70.58	22.58	23.12	24.34

	$\sigma_{iso}(N{-}C_1)$	$\sigma_{iso}(N{-}C_2)$	$\sigma_{iso}(C_2{-}C_3)$	$\sigma_{iso}(C_1{-}H_1)$
HF	39.18	42.94	39.50	26.07
MP2	36.64	40.67	37.96	25.81

	$\sigma_{iso}(C_2{-}H_2)$	$\sigma_{iso}(C_3{-}H_3)$
HF	26.87	31.61
MP2	27.09	30.20

Analogous results can be seen for pyrimidine, a six-membered heterocycle with two nitrogen atoms within the ring, in Table 6.9 and Figure 6.9. In this instance, the three carbon nuclei adjacent to a heteroatom all exhibit similar shielding values and deshielded surroundings whereas the lone carbon not adjacent to any heteroatoms (denoted C_3) is significantly different. The lack of additivity of the effect of multiple neighbouring nitrogens is also seen in imidazole. This results in further perturbation of the aromaticity compared to pyridine, which is highlighted by the plot 1 Å above the pyrimidine molecule. This means that pyrimidine displays less aromaticity than pyridine, which in turn is less aromatic than benzene. This is in agreement with other work.[129]
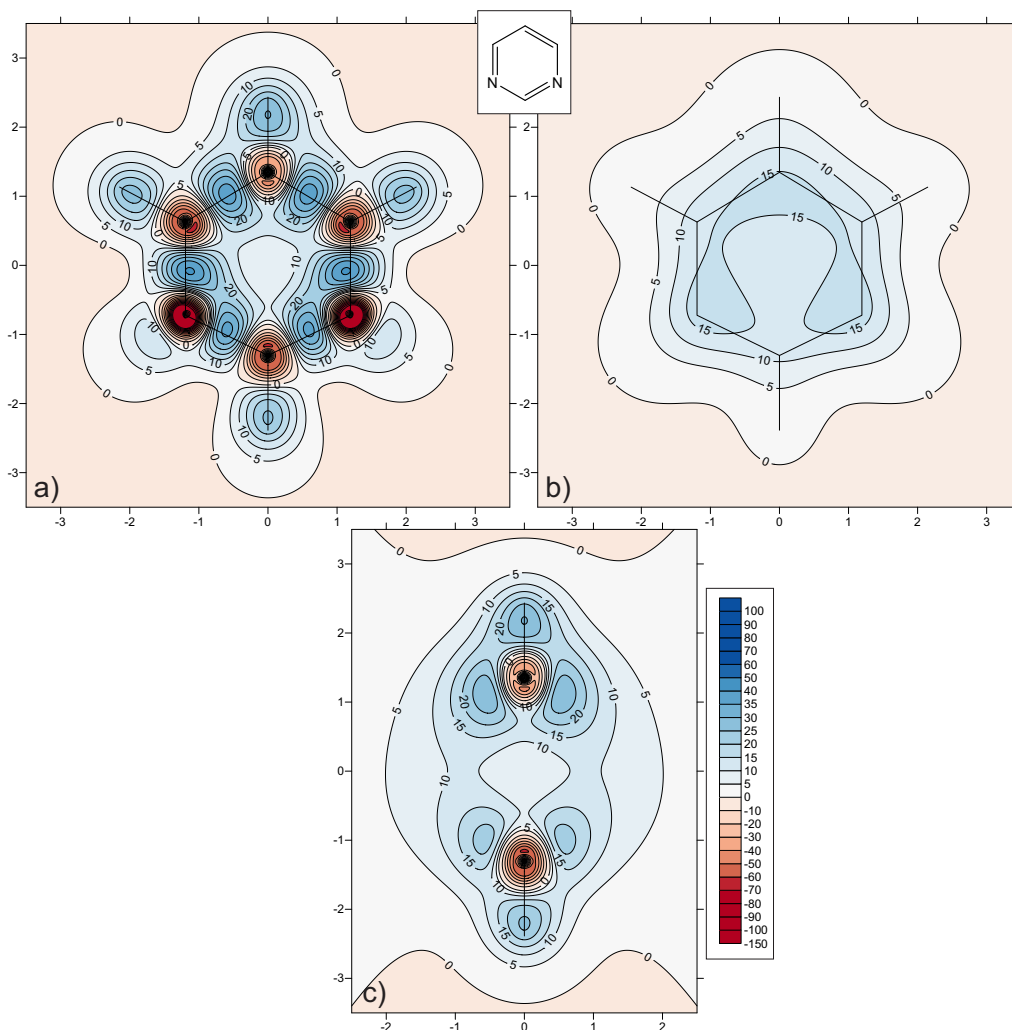
Figure 6.9: Contour plot of the isotropic chemical shieldings (ppm) for pyrimidine through a) molecular plane, b)1 Å above molecular plane and c) a vertical plane bisecting C–H and the C–H between the two N atoms calculated at the MP2/6-311++G(d,p) level of theory.

The disruption of the ring conjugation is also reflected by the ring bonding regions. As seen in pyridine, the C–N bonds are pulled towards the ring centre while the C–C are not, but here the two unique C–N bonds are also distinct from each other with different bond shielding maxima as well as different shielding contours. Interestingly, the bond maximum for the $N–C_1$ bond is quite close to that of the $C_2–C_3$ bond.

The vertical plane seen in Figure 6.9c shows the same distortion of the π doughnut above/below the ring as in pyridine, but to a lesser degree. This is mainly due to the vertical plane being positioned through a nitrogen atom in pyridine, but not

for the case of pyrimidine. Comparison between the two plots therefore requires caution.

The final six-membered heterocycle to consider is phosphabenzene (also called phosphinine). Unlike its five-membered relative, phosphole, the phosphorus in phosphabenzene does not exist in a pyramidal conformation. Instead it lies in a planar configuration maintaining the ring planarity and, therefore, its aromaticity. The shielding calculation results for this system can be found in Table 6.10 and Figure 6.10.

Table 6.10: Isotropic shieldings for the symmetry-unique nuclei and bond maxima in phosphabenzene (in ppm), calculated at the HF-GIAO/6-311++G(d,p) and MP2-GIAO/6-311++G(d,p) levels of theory. C_1 refers to the carbon adjacent to the P and C_3 the carbon opposite the P.

	$\sigma_{iso}(P)$	$\sigma_{iso}(C_1)$	$\sigma_{iso}(C_2)$	$\sigma_{iso}(C_3)$	$\sigma_{iso}(H_1)$	$\sigma_{iso}(H_2)$	$\sigma_{iso}(H_3)$
HF	104.39	22.66	51.58	56.79	22.91	23.85	24.31
MP2	134.49	45.21	64.20	70.06	22.88	23.66	24.13

	$\sigma_{iso}(P-C_1)$	$\sigma_{iso}(C_1-C_2)$	$\sigma_{iso}(C_2-C_3)$	$\sigma_{iso}(C_1-H_1)$
HF	41.16	40.10	41.70	27.49
MP2	38.78	39.37	41.09	27.46

	$\sigma_{iso}(C_2-H_2)$	$\sigma_{iso}(C_3-H_3)$
HF	28.90	29.86
MP2	28.47	29.56

Once again, the carbon environments possess significantly different shielding values, though the value range is intermediate between that for pyridine and that for pyrimidine. The shielding along the ring bonds are all quite different, with the C–P bonds being very broad and pulled slightly around the large phosphorus while the C–C bonds are typical for aromatic systems, though still distinct. The shielding 1 Å above the ring is quite continuous, however, the size of the phosphorus compared to the nitrogen heteroatoms in the previous systems must also be considered. The carbon inequivalence and bonding regions suggest that phosphabenzene is slightly less aromatic than pyridine (consistent with NICS(1) calculations

in other work[130]) though more so than pyrimidine. The vertical plane through the carbon atom opposite the phosphorus displays almost identical features to those seen in pyridine. The phosphorus, however, has distorted the so-called π doughnuts so that they merge at that end of the ring. This is due to to size of the phosphorus atom.
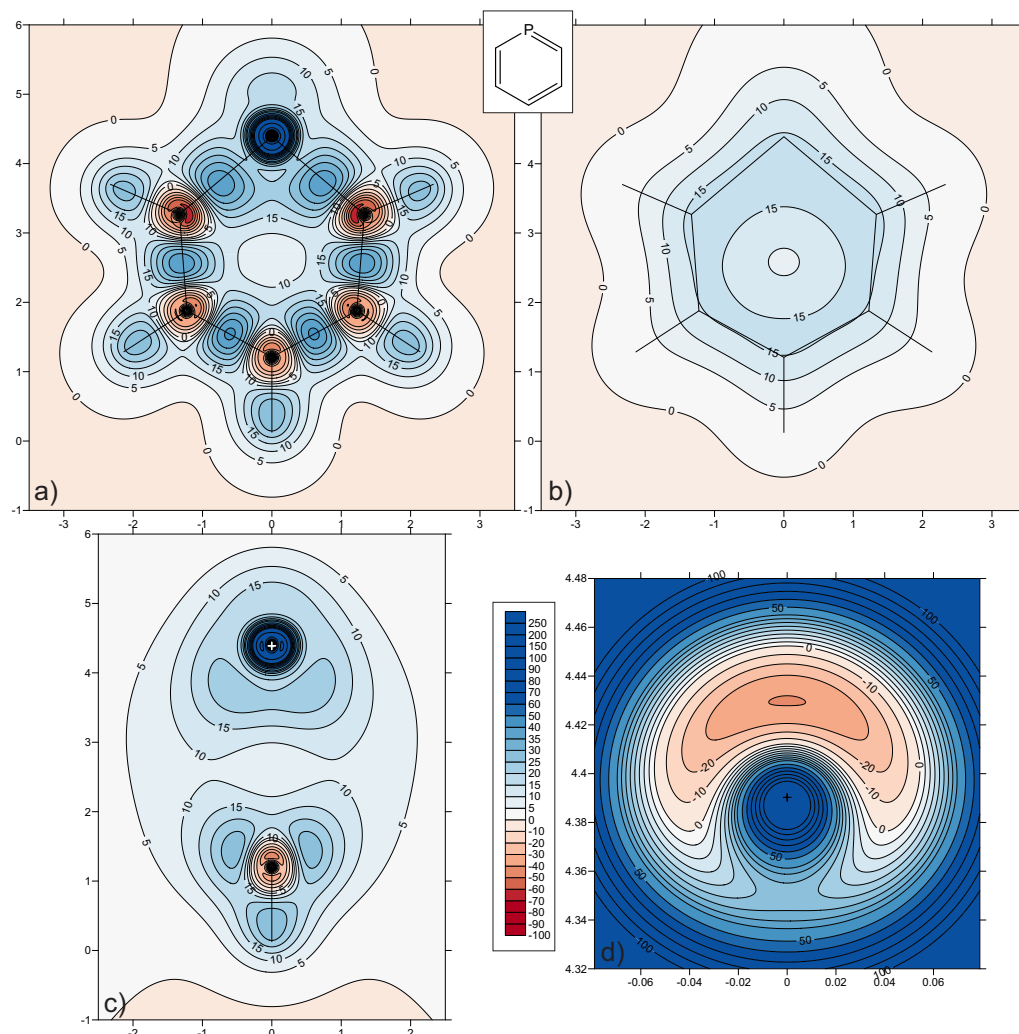
Figure 6.10: Contour plot of the isotropic chemical shieldings (ppm) for phosphabenzene through a) molecular plane, b)1 Å above molecular plane, c) a vertical plane bisecting C–H and the P atom and d) an ultra-fine grid (with 0.001 Å spacing) over the phosphorus atom calculated at the MP2/6-311++G(d,p) level of theory.

When the phosphorus is studied in more detail (see Figure 6.10d) with an ultra-fine grid, it is clear that, just like in the case of the sulphur in thiophene, the typical deshielded halo of conjugated atoms is hidden by the increased size and electron density of the element. This shows that despite the orbital size difference, there

is still effective overlap for efficient conjugation. This is compatible with the ring possessing aromatic properties.

6.5   Conclusions

It has been seen through the study of a wide variety of heterocycles that the relative degrees of system aromaticity can be successfully characterised by comparison of carbon environment equivalence, bonding regions and the shielding 1 Å above a molecule. It was shown that C–C bond cross-sections in rings become more distorted into a kidney-shape structure upon an increase in aromaticity. With the use of this information, the order of increasing aromaticity oxazole < furan < imidazole < pyrrole < thiazole < thiophene could be established.

Larger heteroatoms were also investigated, with similar results being used to show that selenophene possesses an aromaticity intermediate between that of furan and thiophene, lying somewhere slightly more aromatic than pyrrole. The pyramidal conformation of the phosphorus in phosphole was shown to significantly reduce its aromatic character in comparison with its planar, anionic counterpart. The weak aromatic properties exhibited by phosphole, despite its non-planarity, are most likely a result of the size of the phosphorus atom as well as conjugative and hyperconjugative interactions of the PH with the butadiene moiety.

The phosphorus atoms in both phosphole and the pholide anion exhibit small areas of lowered shielding around their nuclei and towards the ring centre. However, this region was more significant in the anion, showing the increased conjugation and therefore higher aromaticity. A more dramatic version of the feature, which actually reaches negative shielding values, is seen around the phosphorus in phosphabenzene. This confirms that the larger elements are not devoid of the deshielded surroundings attributed to participation in a conjugated system, but instead they are simply masked by the increased atom size and extra electron density.

Six-membered heterocycles were also probed and similar reasoning determined that pyrimidine was less aromatic than pyridine with phosphabenzene being similar, but also slightly less aromatic, than pyridine.

Overall it has been shown that magnetic shielding calculations through the space

surrounding heterocycles is highly effective at gaining insight into the aromaticity and bonding of molecules and can be used to compare and contrast these properties.

Substituent Effects

"The more I think about the physical portion of Schrödinger's theory, the more repulsive I find it...What Schrödinger writes about the visualizability of his theory 'is probably not quite right,' in other words it's crap."
Werner Heisenberg writing to Pauli, 1926

7.1   Introduction

Substituents are a common feature in all organic chemistry. The effects these substituents have on the molecule they are bonded to have long been studied and characterised by a variety of methods. For example, an investigation into substituent effects on the aromaticity of benzene was carried out in 2004 using multiple criteria, and it was concluded that substituents have very little impact on the aromaticity of benzene.[131] A study of substituents on H-bonding and aromaticity found that substituent effect stabilisation energies depended greatly on the H-bond distance, the same as the aromaticity.[132] This means there is a key relationship between substituents, H-bonding and aromaticity worth studying.

The investigation of intramolecular hydrogen bonding as well as keto-enol tautomerism can be carried out by studying diketone systems like malonaldehyde and acetylacetone. Work using crystal structure correlations on various diketones showed that the distance between the two oxygen atoms can be correlated with the degree of π delocalisation between the two oxygen-containing groups.[133] It was found that short distances between the two oxygens correspond to strong π bond delocalisation and can be used to infer the formation of a strong hydrogen-bond. *Ab initio* and semi-empirical calculations on acetylacetone also attempted to determine the strength of the intramolecular hydrogen bond and, in doing so, identified the most stable conformation as well as confirmed the presence of aromatic character in the 6 π electron cyclic transition state.[134] The impact of electron-withdrawing and electron-donating groups on the π delocalisation and hydrogen-bond character in malonaldehyde has been studied with energetic and geometric calculations[135] but not with magnetic shielding plots like those used here. These shielding calculations can be used to probe any aromatic character within the pseudo six membered ring as well as substituent effects and the intramolecular hydrogen bonding.

The structure of toluene was optimised at the MP2/cc-pVTZ level of theory and a ground state was confirmed by frequency analysis. The geometry of aniline was experimentally determined using microwave spectroscopy.[136] The structure of phenol was also experimentally determined by microwave spectra.[137] The structures of 2-nitrophenol and 4-nitrophenol were both optimised at the MP2/6-311G(d,p) level of theory. Monofluorobenzene's structure was experimentally determined using microwave spectroscopy[138] and hexafluorobenzene was deter-

mined by electron diffraction.[139] All of the substituted ethenes studied here were optimised at the MP2/6-311++G(d,p) level of theory. Finally, the various malonaldehyde structures were optimised at the B3LYP/DZP++ level of theory by Hargis and co-workers.[135]

Thanks should go to a fellow PhD student, Thomas Newby, who suggested the idea of comparing 2-nitrophenol and 4-nitrophenol and who shared his experimental work on the same systems.

7.2 Substituted Benzenes

Aniline is the first substituted benzene to be studied here and the results can be seen in Figure 7.1. The shielding observed through the molecular plane shows the expected aromatic features found for the case of benzene, but with several perturbations caused by the NH_2 substituent.
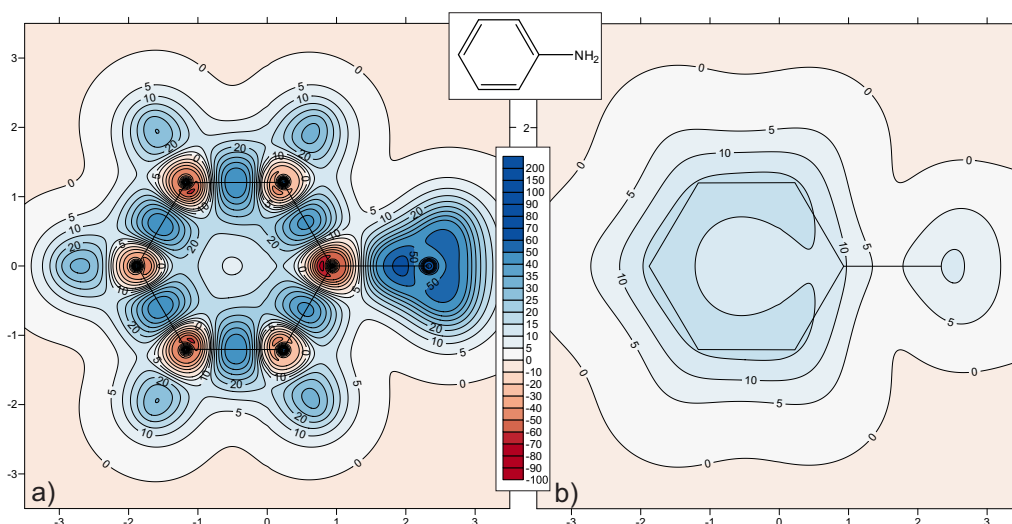
Figure 7.1: Contour plot of the isotropic chemical shielding (ppm) through aniline in a) the molecular plane and b) 1 Å above calculated at the HF/6-311++G(d,p) level of theory. Note that these are both stitched plots with the molecule overlay showing the atoms that lie in the plane of the calculation.

The regions of deshielding around the carbon nuclei display an alternation in the magnitude of the deshielding intensity. The carbons at the *meta* positions are slightly more deshielded than the *ortho* and *para* carbons. The carbon directly attached to the amino group, however, has the most deshielded halo. A similar alternation in trend can be seen for the C–H bonding regions. Perhaps most in-

teresting is the region surrounding the nitrogen. It can be seen that the N nucleus is devoid of a deshielded surrounding which would be present if there was π conjugation between the amino group and the ring. An NH_2 substituent possesses a nitrogen lone pair which is usually considered to be available for donation into a conjugated π system. However, the lack of deshielding around the nitrogen and the lack of shielding at 1 Å above the molecule over the C–N bond all imply no such π donation in this instance.

The bonding regions around the aniline ring all display typical shielding regions associated with C–C aromatic bonds. Those closest to the amino group are slightly weaker than the others and this is due to the electronegativity difference between carbon and nitrogen. The shielding above the molecule shows a homogeneous shielded region around the circumference of the ring with only a small discontinuity over the substituted carbon. This shows only a minimal disruption to the aromaticity of aniline by the amino group which will allow only slightly weaker overall aromaticity compared to benzene.
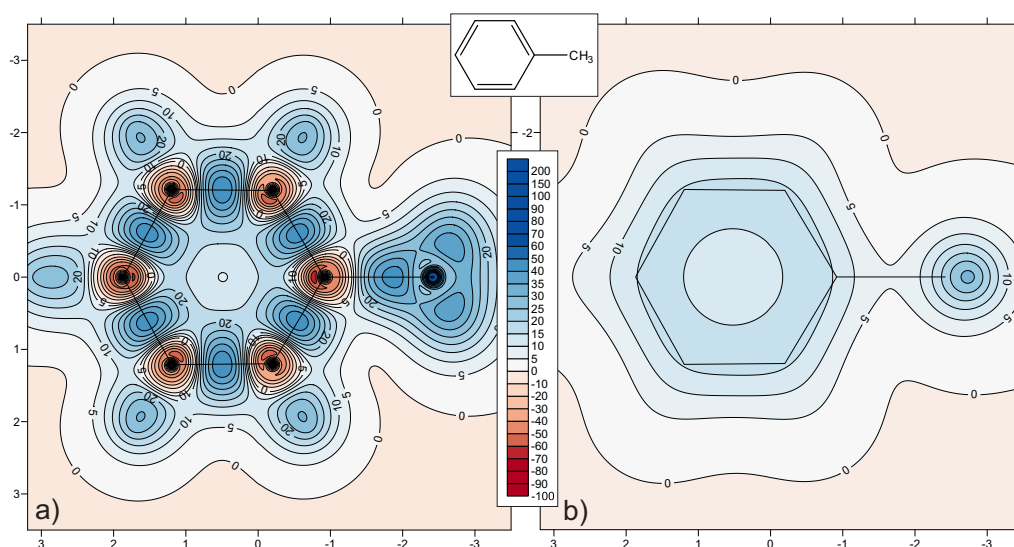
Figure 7.2: Contour plot of the isotropic chemical shielding (ppm) through toluene in a) the molecular plane and b) 1 Å above calculated at the HF/6-311++G(d,p) level of theory. Note that these are both stitched plots with the molecule overlay showing the atoms that lie in the plane of the calculation.

For toluene (see Figure 7.2), there are several subtle, but important, differences found in the isotropic shielding results. Firstly, while the substituted carbon in toluene still possesses the most deshielded halo of the molecule (like in aniline), there is no alternation of the other carbon environments. This shows that the

methyl group has far less impact on the ring than the amino group of aniline. Furthermore, the C–C bonding regions are almost identical in toluene. The shielding 1 Å above toluene appears completely unperturbed by the substituent which, along with the carbon equivalence seen in the molecular plane, will allow a higher aromaticity than for aniline.

The methyl group C–C bond is fairly well shielded, although the shielding is pulled away from the ring and towards the methyl carbon. This gives a slight appearance of a multiple bond but without any shielding feature directly above it. The weak shielding observed above this bond is simply the overlap of the ring shielding with the shielding of the methyl hydrogen which lies in the direction of the 1 Å above plane. Overall, toluene appears to have only a slightly weaker aromaticity than parent benzene.

The next substituent under investigation is the hydroxyl group of phenol. In this case (Figure 7.3), the shielding in the molecular plane shows an intense deshielding around the substituted carbon, fairly weak deshielding around the *ortho* carbons and only slightly more around the others. There is no alternation like there was in aniline, but there is less equivalence than for toluene. The C–C bonding regions show a similar trend to that seen in aniline, but in the case of phenol, there is obviously less symmetry due to the conformation of the substituent.
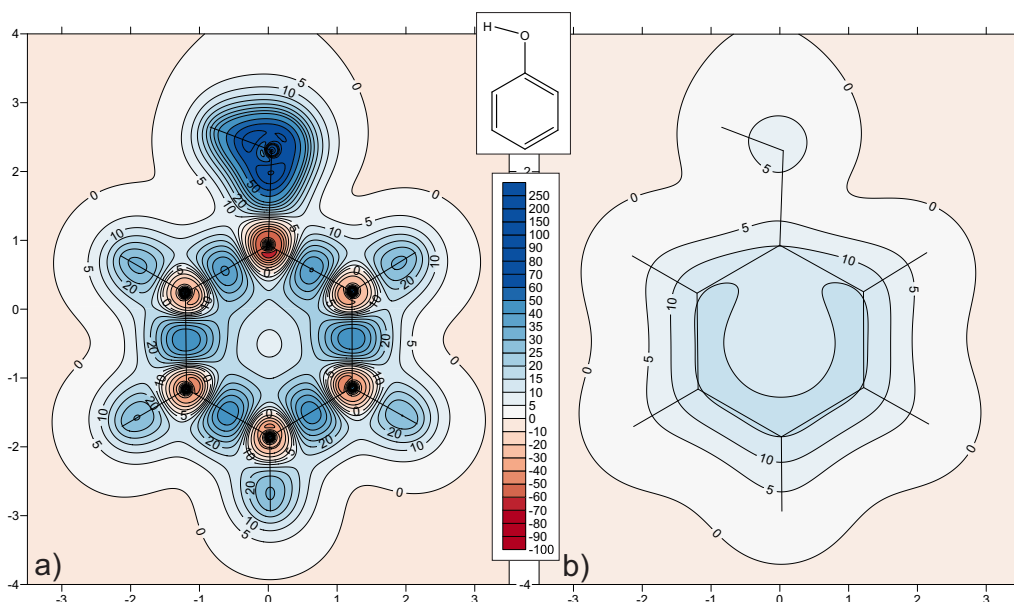
Figure 7.3: Contour plot of the isotropic chemical shielding (ppm) through phenol in a) the molecular plane and b) 1 Å above calculated at the MP2/6-311++G(d,p) level of theory.

The shielding 1 Å above phenol is very similar to that seen in aniline with a band of shielding around the majority of the ring but with a disruption over the substituted carbon. In the case of phenol, this disruption is larger than for aniline suggesting a lower aromaticity as a result. The shielding over the substituent is very localised and again, there is no deshielding around the substituent central atom, in this case, oxygen. This shows the lack of π conjugation between the hydroxyl group and the ring which allows for only limited effects on the ring aromaticity. A study of the relationship between aromaticity and substituent effects, which used several NICS calculations along with other aromaticity criteria, concluded that there is very little influence on the π structure and therefore only a limited effect on the benzene moiety caused by a substituent.[131] However, the method used in the present work shows that, while the effects seen so far are reasonably small, they are appreciable and, moreover, noticeable differences between the substituent effects are possible. Other work has also found differences between substituents and their effect on rings[140] but the present work allows the study of bonding and carbon environments alongside a study of relative aromaticities.
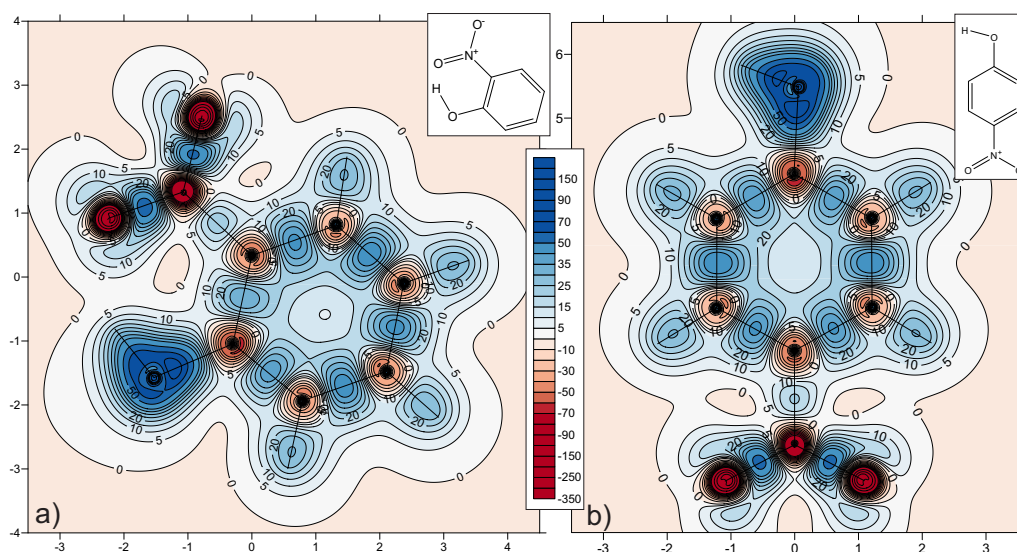
Figure 7.4: Contour plot of the isotropic chemical shielding (ppm) through molecular plane of a) 2-nitrophenol and b) 4-nitrophenol calculated at the MP2/6-311++G(d,p) level of theory.

The introduction of a nitro group to phenol lead to the calculation of the shielding in and around both 2- and 4-nitrophenol. This allows for the study of both substituent effects and intramolecular hydrogen bonding in the same system. Furthermore, as mentioned earlier in this chapter, some experimental work has been

carried out by a colleague at the University of York comparing the reactivities of these two molecules[141] and this can be considered alongside the calculations performed here.

The shielding through the molecular planes of both nitrophenols can be seen in Figure 7.4. The first feature to observe is the nitro group. The symmetry of this group is noticeably altered in 2-nitrophenol where there is a neighbouring hydroxyl group which allows intramolecular H-bond formation. The N–O bond involved with the H-bond has slightly more shielding along the bond than the other N–O in the same molecule. Moreover, the O–H bond of the hydroxyl group in 2-nitrophenol has less shielding along the bond than the analogous bond in 4-nitrophenol. Just as for the water dimer, while the H-bond itself is not clearly visible, the effects of this interaction on the molecule are apparent. There is also a notable difference in the C–N bond shielding between the two molecules. The C–N bond in 2-nitrophenol is slightly more shielded, and therefore stronger, than the same bond in 4-nitrophenol.

The C–C bonding region around the benzene moieties are also interesting. While all of the bonds have the typical shielding features of aromatic C–C bonds, there are small differences between the different bonds. In both molecules, the C–C bond one bond away from a substituent has the largest shielding region, though not necessarily the highest shielding maximum. The C–C bonds adjacent to the nitro group (not including that which is also adjacent to the hydroxyl group) are all fairly similar in shape and magnitude. The same is true of the bonds next to only the hydroxyl group. Subtle differences between the carbon deshieldings are also evident which shows the widespread impact of the substituents across the whole molecule. For example the deshielding around the nitro substituted carbon is 'c' shaped and positioned away from the hydroxyl group in 2-nitrophenol. However, in 4-nitrophenol, the highest deshielding, which is more intense than for 2-nitrophenol, is positioned in a small lobe facing the nitro group and only a tiny amount on the opposite side of the nucleus.

From the examination of the carbons, substituents and bonds, it is clear that there is a significant difference between these two systems. In the experimental work on polymerisation inhibition by Newby,[141] the asymmetry of 2-nitrophenol and, in particular, the nitro group, was responsible for a notable difference in the reactivity of this molecule over 4-nitrophenol. From this it is clear that detailed pictures of substituent effects can be used to explain, and perhaps predict, experimental

results.

The final substituted benzenes are mono- and hexafluorobenzene (see Figures 7.5 & 7.6). The isotropic shielding plots for monofluorobenzene are very similar, both in the molecular plane and above, to those obtained for phenol. This includes an intense deshielding around the substituted carbon, weak deshieldings around the other carbons with no alternation pattern and bonding regions which are all typical of benzene but weaker adjacent to the substituted carbon. The shielding at 1 Å above the molecule has an identical shaped shielding region around the majority of the ring with a disruption over the substituted carbon. This shows that the hydroxyl and fluorine substituents have similar impacts on the aromaticity and properties of the benzene ring to which they are attached.
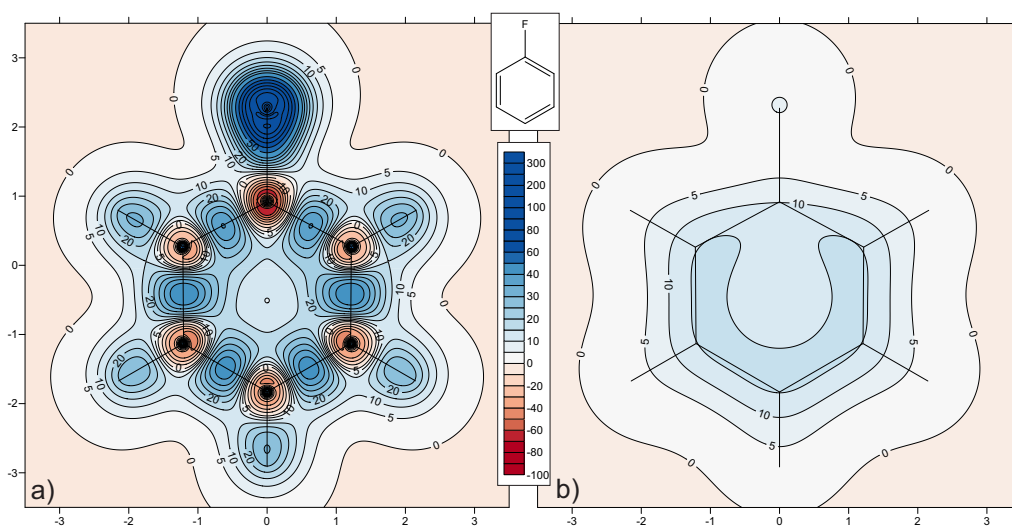
Figure 7.5: Contour plot of the isotropic chemical shielding (ppm) through monofluorobenzene in a) the molecular plane and b) 1 Å above calculated at the MP2/6-311++G(d,p) level of theory.

The isotropic shielding in and around hexafluorobenzene are quite different from any of the results seen in this chapter. The shielding around the fluorine atoms is identical to that seen for monofluorobenzene, but the benzene moiety is quite unusual. The carbons are all surrounded by a moderately deshielded region, as expected, but the C–C bonding regions are significantly distorted by the fluorine atoms. The regions of shielding along the C–C bonds are weaker than for benzene or monofluorobenzene and have been pulled noticeably inwards towards the ring centre. This suggests a change in the bonding character around the rings. Furthermore, the shielding at 1 Å above the ring lacks a doughnut of higher

shielding over the carbons and instead just displays a weakly shielded disc over the whole centre. This, along with the weakened C–C bonds, shows a lowering of the aromaticity of the ring. This is the result of the electron-withdrawing nature of the six fluorine substituents. It is even possible, considering the shielding plots, that the aromaticity could be considered to be destroyed, leaving the whole molecule as non-aromatic in character.
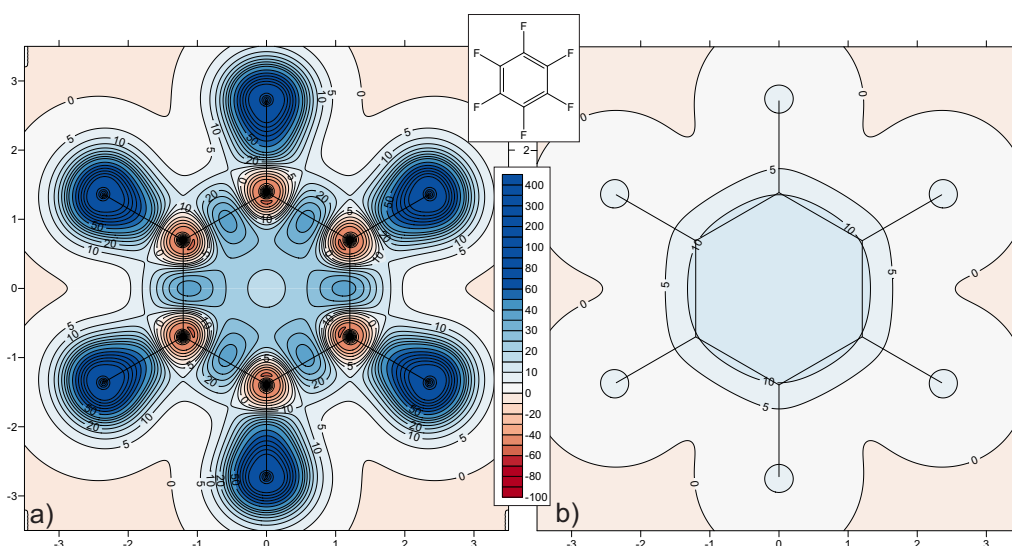
Figure 7.6: Contour plot of the isotropic chemical shielding (ppm) through hexafluorobenzene in a) the molecular plane and b) 1 Å above calculated at the MP2/6-311++G(d,p) level of theory.

Energy calculations performed on these fluorobenzenes also found the hexafluorobenzene was less aromatic than monofluorobenzene.[142] However, NICS(0) and NICS(1) calculations found that monofluorobenzene was slightly more aromatic than benzene and that hexafluorobenzene was far more aromatic than either.[143] Extra cyclic resonance energies and dissected NICS calculations found that C_6F_6 displayed similar aromaticity to benzene[144] while NICS(1)$_{zz}$ calculations by other authors showed that the ring current diminishes with increasing fluorination of a benzene ring.[145] It is clear that subtle differences in the implementation of the NICS technique on these fluorinated benzenes can dramatically alter the findings on the relative aromaticities.

7.3 Substituted Ethenes

In this section, four substituents on ethene will be investigated, two of which have been studied when attached to benzene in the previous section, and the other two involve triple bonds. It is these triply bonded substituents which will be studied first, namely but-1-en-3-yne (also called vinylacetylene) and acrylonitrile (Figures 7.7 & 7.8).
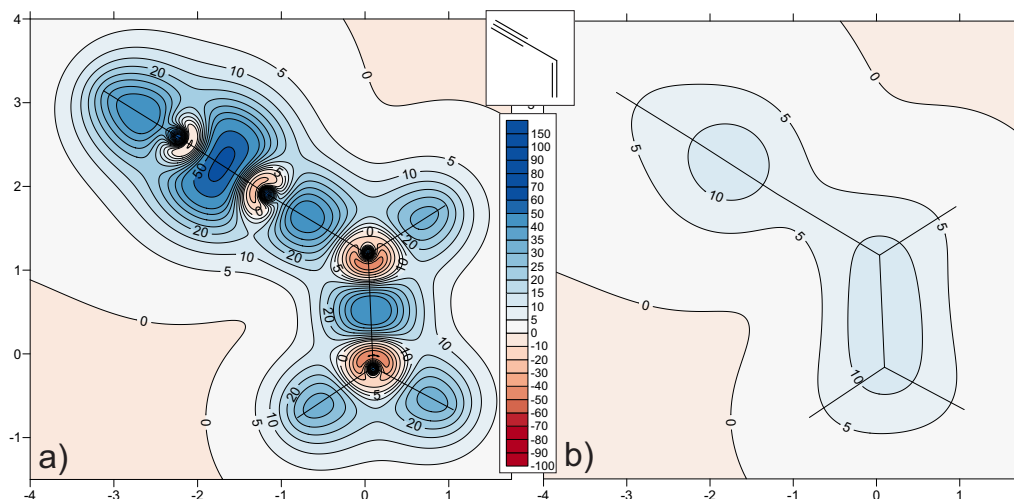
Figure 7.7: Contour plot of the isotropic chemical shielding (ppm) through but-1-en-3-yne in a) the molecular plane and b) 1 Å above calculated at the MP2/6-311++G(d,p) level of theory.

The isotropic shielding plot through the molecular plane of but-1-en-3-yne (Figure 7.7a) displays all the typical features of ethene and ethyne all in one molecule. The same is true of the 1 Å above plot. Small disturbances in the shielding can be seen in the features around the two central carbons where the ethene and ethyne moieties meet. However, these disturbances are relatively subtle with only a slight increase in the deshielding around the sp carbon and a slight decrease in the deshielding around the sp^2 carbon. Moreover, the C–C bond between the formal double and triple C–C bonds has a fairly wide, well shielded region in between the nuclei suggesting a strong bond which is closer to a double bond than a single bond in character. This is caused by the conjugation across the molecule.
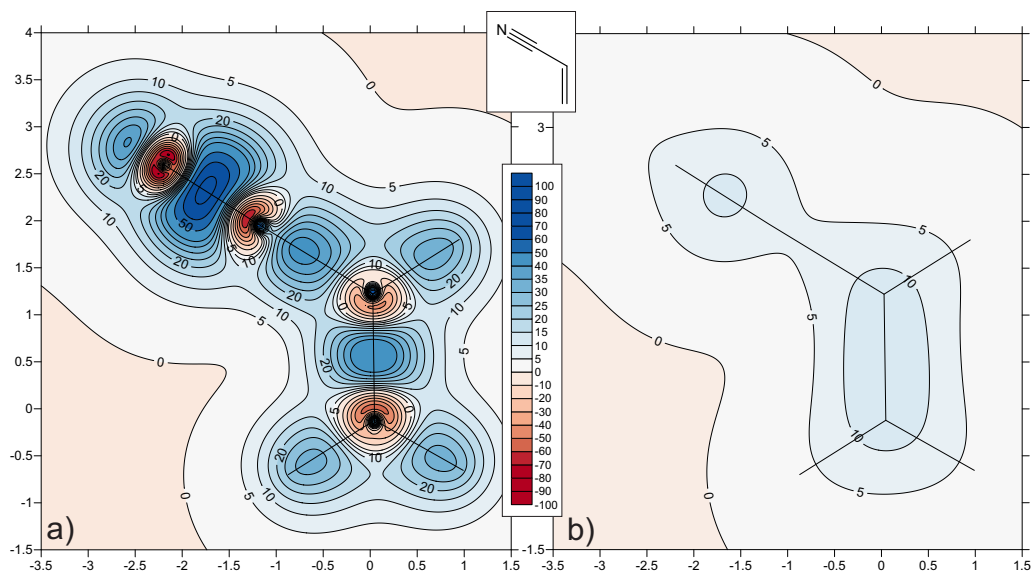
Figure 7.8: Contour plot of the isotropic chemical shielding (ppm) through acrylonitrile in a) the molecular plane and b) 1 Å above calculated at the MP2/6-311++G(d,p) level of theory.

Very similar features can be seen for the case of acrylonitrile but with some changes in shielding magnitude. For example, the C–C triple bond is much more shielded in the molecular plane but has less shielding at 1 Å directly above it. The C=C double bond is almost identical to that seen for but-1-en-3-yne though there are differences in the deshielding around the carbon nuclei. The two carbons in the C=C double bond of acrylonitrile are significantly less equivalent than those in but-1-en-yne. This suggests a less homogeneous shielding distribution caused by less homogeneous conjugation. This is mirrored by the more localised shielding above acrylonitrile than above but-1-en-3-yne. Furthermore, the deshielding around the cyano group carbon is far more intense than in the equivalent carbon in but-1-en-3-yne. The nitrogen of the cyano group has strongly deshielded lobes in a direction perpendicular to the C–C triple bond and displays a small shielded region around the lone pair.

This is the first cyano group to be studied with this method, but the features of but-1-en-3-yne are fully consistent with plots for ethene, ethyne and various conjugated systems. The next substituent to be studied is the nitro group of nitroethene (or nitroethylene) which has been seen earlier in this chapter as a substituent on a phenol ring.
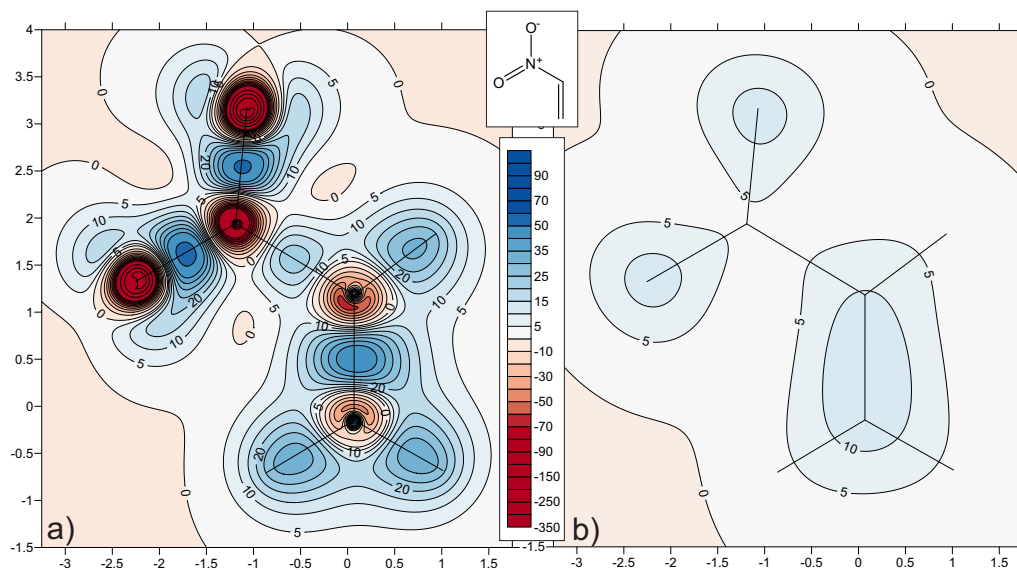
Figure 7.9: Contour plot of the isotropic chemical shielding (ppm) through nitroethene in a) the molecular plane and b) 1 Å above calculated at the MP2/6-311++G(d,p) level of theory.

The nitro group on nitroethene has shielding features that are intermediate between those seen for the nitro group in 2-nitrophenol and 4-nitrophenol. Nitroethene is more symmetrical than 2-nitrophenol but less so than 4-nitrophenol. This subtly alters the shielding along and above the N–O bonds and the deshielding around the oxygen atoms, but otherwise has little effect. The C–N bond is much weaker than the analogous bond in the two substituted ethenes seen already. This is also seen in the lack of shielding above this region in nitroethene compared with the same region in the other two ethenes. The deshielding around the substituted carbon is more intense than the terminal carbon, which is the opposite trend to that seen in acrylonitrile, and highlights the different impacts of the various substituents on the ethene moiety. The nitro group also causes the most distortion of the substituents seen so far to the shielding above the C=C double bond.
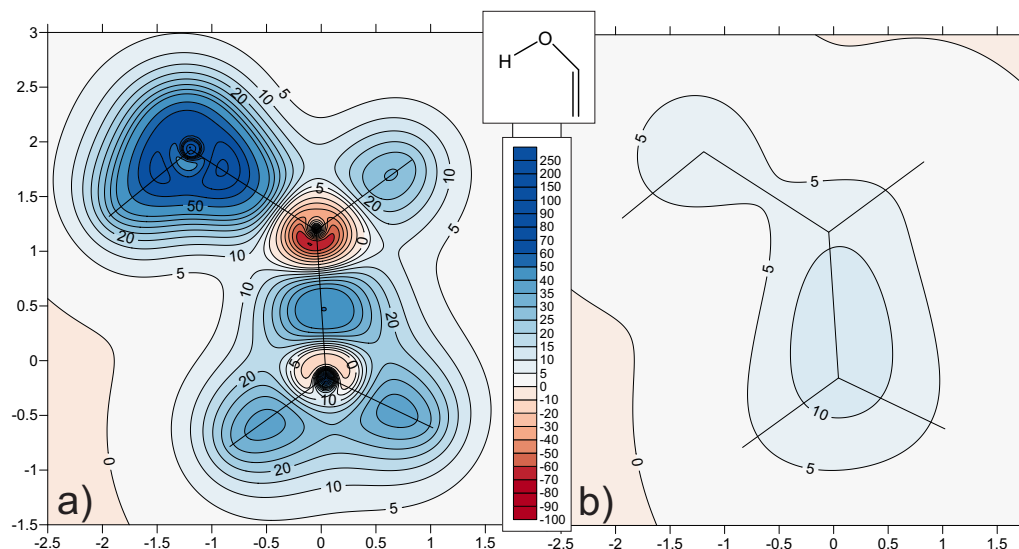
Figure 7.10: Contour plot of the isotropic chemical shielding (ppm) through ethenol in a) the molecular plane and b) 1 Å above calculated at the MP2/6-311++G(d,p) level of theory.

The final substituent in this section is the hydroxyl group, previously seen in the cases of phenol and nitrophenol. In the case of ethenol here (also called vinyl alcohol), the features in the ethene moiety are similar to those in nitroethene, but more pronounced. The terminal carbon only has a weakly deshielded surrounding and the substituted carbon region is quite strongly deshielded. The shielding directly above the C–C bond is also distorted, in the same way as above nitroethene, but far more exaggerated in the case of ethenol. It appears that the hydroxyl group has a greater impact on the properties of the ethene backbone than the nitro group. Furthermore, the oxygen itself has no region of deshielding around the nucleus, as it does in furan, for example. It does exhibit a small region of decreased shielding between the O–H and C–O bonds but shielding values do not become negative. The distinction between the oxygen in furan, for example, and the oxygen in ethenol or nitrophenol is clear. This is a reflection on the types of bonding the oxygen atom is involved in and the degree of conjugation/lone pair donation.

From this work on substituted ethenes it can be seen that different groups have significant effects on the isotropic shielding in and around the ethene moiety. It is also possible to observe subtle differences between one group attached to different systems, for example, the nitro group in the cases of nitroethene, 2-nitrophenol and 4-nitrophenol. The degree of conjugation and the type of inter-

action a substituent has with the attached molecule can be probed using this technique.

7.4   Malonaldehyde & Derivatives

Ground state malonaldehyde (also called 1,3-propanedialdehyde or 1,3-propanedione) in the mono-enol form is the first molecule to be studied in this section (Table 7.1 & Figure 7.11a), followed by the transition state that occurs during proton transfer between the two oxygens (Table 7.2 & Figure 7.11b).

Table 7.1: Isotropic shielding for the nuclei and bond maxima in ground state malonaldehyde (in ppm), calculated at the HF-GIAO/6-311++G(d,p) and MP2-GIAO/6-311++G(d,p) levels of theory.

	$\sigma_{\text{iso}}(C_{C=O})$	$\sigma_{\text{iso}}(C_{\text{centre}})$	$\sigma_{\text{iso}}(C_{C-O})$	$\sigma_{\text{iso}}(H_{C=O})$	$\sigma_{\text{iso}}(H_{\text{centre}})$	$\sigma_{\text{iso}}(H_{C-O})$
HF	−10.81	94.93	13.27	22.92	26.99	24.66
MP2	10.02	95.48	31.18	22.63	26.67	24.69

	$\sigma_{\text{iso}}(O_{C=O})$	$\sigma_{\text{iso}}(O_{O-H})$	$\sigma_{\text{iso}}(H_{O-H})$	$\sigma_{\text{iso}}(C-C)$	$\sigma_{\text{iso}}(C=C)$	$\sigma_{\text{iso}}(C=O)$
HF	−182.69	186.47	18.53	32.27	44.11	48.75
MP2	−159.02	194.26	18.66	31.69	42.07	39.94

	$\sigma_{\text{iso}}(C-O)$	$\sigma_{\text{iso}}(C-H_{C=O})$	$\sigma_{\text{iso}}(C-H_{\text{centre}})$	$\sigma_{\text{iso}}(C-H_{C-O})$
HF	77.07	24.45	35.22	28.69
MP2	74.36	23.91	34.53	28.67

The isotropic shielding values on the nuclei in both forms of malonaldehyde can be seen in Tables 7.1 & 7.2. One point to mention is the large disparity between theory levels for the values of the carbon shieldings on the carbons attached directly to an oxygen. In both cases, this causes a difference in sign between the two values. The disparity for the oxygen nuclei shieldings is smaller. It is also interesting to note that there are significant differences in the shielding maxima along the various C–H bonds showing that these bonds are easily distinguished, despite being often ignored in other work as being uninteresting or less important. The shielding on the H atom that is attached to an oxygen in the ground state and

transitions between the two oxygens in the transition state is also noteworthy. It can be seen that the shielding on this nucleus changes from around 19 ppm in the ground state to only 9 ppm in the transition state. There is an even more dramatic effect on the oxygen shieldings. In the ground state, the O–H oxygen has a shielding of approximately 194 ppm and the carbonyl oxygen around −159 ppm. However, in the transition state the oxygen shieldings reach an intermediate between the two at about 42 ppm which is a huge shielding change. In comparison with other oxygen nuclei, for example the oxygen in the carbonyl of acrolein (−272 ppm), the oxygen in furan (56 ppm) and the oxygen in water (344 ppm or slightly lower if part of a H-bond), it can be seen that the ground state oxygens are typical of carbonyl and hydroxyl groups, while the transition state oxygens are more consistent with an oxygen within an aromatic system. This would suggest aromaticity within the transition state as has been seen in other work.[134]

Table 7.2: Isotropic shielding for the nuclei and bond maxima in transition state malonaldehyde (in ppm), calculated at the HF-GIAO/6-311++G(d,p) and MP2-GIAO/6-311++G(d,p) levels of theory.

	$\sigma_{iso}(C_{C-O})$	$\sigma_{iso}(C_{centre})$	$\sigma_{iso}(H_{terminal})$	$\sigma_{iso}(H_{centre})$	$\sigma_{iso}(O)$	$\sigma_{iso}(H_{O-H})$
HF	− 9.18	98.39	23.34	26.91	36.21	7.02
MP2	12.92	96.31	23.28	26.47	41.59	8.56

	$\sigma_{iso}(C-O)$	$\sigma_{iso}(C-C)$	$\sigma_{iso}(C-H_{terminal})$	$\sigma_{iso}(C-H_{centre})$
HF	63.09	38.94	25.84	35.74
MP2	56.40	37.67	25.70	34.41

However, it has been established that aromaticity is a complex property and so the shielding surfaces around the molecules should also be considered. These can be seen in Figure 7.11 where there are many interesting features to notice. Firstly, the shielding features around the oxygens in both molecules mirror the conclusion drawn from the $\sigma_{iso}(O)$ values earlier. The carbonyl oxygen has a strongly deshielded aura with no visible shielding directly over the nucleus. The hydroxyl group oxygen environment is typical of previously seen hydroxyl groups, for example, in phenol, ethenol and water. This includes a shielded surrounding of the oxygen, though with a small region of slightly lower shielding, and strong

shielding along the bonds which also encompass the oxygen atom. Finally, the oxygens in the transition state have a strongly deshielded surrounding but with a region of shielding directly over the nucleus. They also display a well shielded C–O bond with the maximum pulled towards the oxygen though not encompassing it as for the hydroxyl group. There are also small areas of shielding in the area of the lone pairs. All of these features are consistent with the oxygen environment in furan and oxazole, both aromatic rings. The shielding around the oxygen bulges slightly towards the transitioning hydrogen too, showing a hint of bonding interaction. These distinctions between the three types of oxygen environment are perhaps the clearest of the elements studied so far.
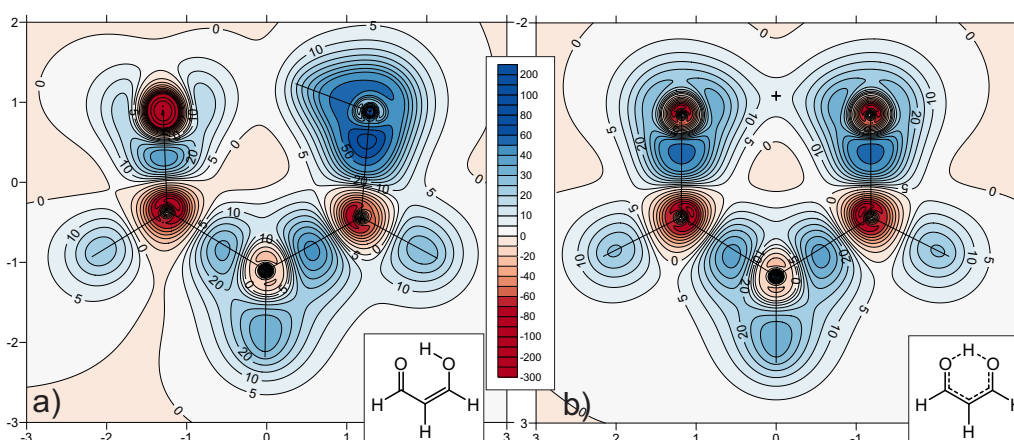
Figure 7.11: Contour plot of the isotropic chemical shielding (ppm) through the molecular plane of malonaldehyde a) at the C_s parent structure and b) at the C_{2v} transition state calculated at the MP2/6-311++G(d,p) level of theory. The black cross in b) denotes the position of the transitioning hydrogen.

The carbon surroundings are also interesting. The carbonyl carbon has many similarities with the terminal carbons in the transition state malonaldehyde. This is caused by the conjugation seen in both instances. The carbon in ground state malonaldehyde at the hydroxyl terminus also exhibits a strongly deshielded surrounding, though slightly less than for the carbons previously noted. This is due to the C=C double bond as well as the hydroxyl group. Notably, the central carbon only displays a weakly deshielded surrounding and this can be attributed to the effect of the hydroxyl substituent on a C=C double bond, as seen for the case of ethenol. The carbon environments seen here are very similar in nature to those seen in ethenol.

Finally, the bonding regions are worth consideration as well. The different C–

H bonding regions are all distinct, as illustrated previously by the bond shielding maxima. The C–O bonds of varying types are also quite distinctive and all are typical of the relevant groups which they belong to, just as the oxygen environments are. But perhaps the most interesting bonding regions are those between neighbouring carbon atoms. In ground state malonaldehyde, there is a clear difference between the two C–C bonds. The formal double bond is reasonably typical of a double bond though slightly weaker than an isolated C=C double bond. The C–C formal single bond is atypical of a single C–C bond and is reminiscent of a double bond. This, in combination with the weakened formal double bond, shows conjugation across the molecule which alters the C–C bonding character. In fact, both C–C bonds have very similar shielding features.

Having studied unsubstituted malonaldehyde as a benchmark, it is now possible to investigate the effects of various substituents on the same system. Three substituted malonaldehydes will be studied here. **Mal-1** is malonaldehyde with two terminal methyl groups, also called acetylacetone. **Mal-2** has two terminal amino groups and a nitro group on the central carbon (also called nitromalonamide). Finally, **Mal-3** also has two terminal amino groups, like in **Mal-2**, but has a BH_2 substituent on the central carbon instead. X-ray studies have revealed that **Mal-2** has the shortest H-bond.[146] Previous work[147,148] has found that electron-withdrawing groups on the central carbon atom of malonaldehyde shorten the intramolecular H-bond. When electron-withdrawing groups are substituted onto the terminal carbons, this H-bond is lengthened. Conversely, electron-donating groups on the terminal carbons result in H-bond shortening. These effects can be further studied here with magnetic shielding calculations.

The results from these three malonaldehyde derivatives can be seen in Table 7.3 and Figure 7.12. The first features of interest are the various carbonyl groups. It can be seen from both the values in the table and the isotropic shielding plots that the carbonyl in **Mal-1** is quite different from the other two. The shielding value of the oxygen in **Mal-1** is around -124 ppm whereas the other two malonaldehyde derivatives are closer to 80 ppm. From the previous work on parent malonaldehyde, it has been established that the carbonyl oxygen in **Mal-1** is typical of a carbonyl oxygen. However, the oxygens in **Mal-2** and **Mal-3** are closer in shielding value to the aromatic oxygens present in furan and oxazole. This shows the relative degrees of aromatic character between the three malonaldehyde derivatives and has implications for the nature and strength of the H-bond as a result.

Table 7.3:   Isotropic shieldings for the nuclei and bond maxima in derivatives of malonaldehyde (in ppm), calculated at the HF-GIAO/6-311++G(d,p) and MP2-GIAO/6-311++G(d,p) levels of theory. R is the first atom of the substituent attached to the terminal carbons i.e. R = C in **Mal-1** and N in **Mal-2** & **Mal-3**.

		Mal-1	**Mal-2**	**Mal-3**
$\sigma_{iso}(C_{C=O})$	HF	-24.27	9.08	1.08
	MP2	-1.85	23.93	16.60
$\sigma_{iso}(C_{centre})$	HF	97.28	77.73	104.56
	MP2	97.84	93.51	103.44
$\sigma_{iso}(C_{C-O})$	HF	-3.63	8.25	-0.31
	MP2	16.10	22.11	13.62
$\sigma_{iso}(O_{C=O})$	HF	-132.49	82.57	69.93
	MP2	-123.53	90.01	76.20
$\sigma_{iso}(O_{O-H})$	HF	161.53	144.63	144.05
	MP2	171.22	153.93	152.35
$\sigma_{iso}(R_{C=O})$	HF	165.63	155.72	170.37
	MP2	167.34	166.23	179.53
$\sigma_{iso}(R_{C-OH})$	HF	171.39	156.08	174.08
	MP2	174.09	168.33	183.98
$\sigma_{iso}(B)$	HF	–	–	67.99
	MP2	–	–	67.47
$\sigma_{iso}(N_{NO_2})$	HF	–	-250.27	–
	MP2	–	-51.43	–

Consideration of the hydroxyl group oxygen is also interesting. The shielding on the hydroxyl oxygen in **Mal-1** is around 172 ppm which is close to the 194 ppm seen in parent malonaldehyde. However, in the other two malonaldehydes, the shielding is around 153 ppm which is consistent with the stronger H-bonds in

these two systems suggested by the carbonyl oxygen shieldings. The carbons adjacent to the oxygens are also noteworthy. For example, the carbonyl carbon in **Mal-1** is slightly deshielded while the other two derivatives possess shielded carbons. This also shows the differences caused by the various substituents. In parent malonaldehyde, the carbonyl carbon had a shielding of 10 ppm, for comparison. It is most interesting that the addition of substituents to this molecule has such a dramatic impact on the system.

There are many features in the isotropic shielding contour plots worth discussion. Firstly, the H-bond region. There is a clear difference between **Mal-1** and the other two malonaldehyde derivatives which have shorter H-bond distances resulting in weak shielding across part of this area. In **Mal-1**, the carbonyl group is very typical of carbonyls not involved in H-bonding. However, the other two molecules have carbonyl groups that have similar features to the C–O groups seen in transition state malonaldehyde. This reflects the conclusions already drawn from the oxygen shielding values i.e. the greater aromatic character exhibited by **Mal-2** and **Mal-3** than **Mal-1**.

Just as for the parent malonaldehyde, the C–C bonding regions are also useful to study. In the case of **Mal-1** there is a distinct difference between the two unique C–C bonds. In the other 2 derivatives, there is only a little difference between the C–C bonding regions. This decrease in obvious bond alternation is consistent with the increase in aromaticity predicted previously.

The substituents themselves all display features that are typical of those seen in previous examples of the same groups. It can also be noted that in all cases of malonaldehyde derivatives, and the parent molecule, the central carbon possesses a significantly less deshielded surrounding that the terminal carbons. The regions of most intense deshielding around the central carbon in parent malonaldehyde and **Mal-1** is positioned pointing towards the intramolecular H-bond. However, in **Mal-2** and **Mal-3**, this region is located along the C–substituent bond.
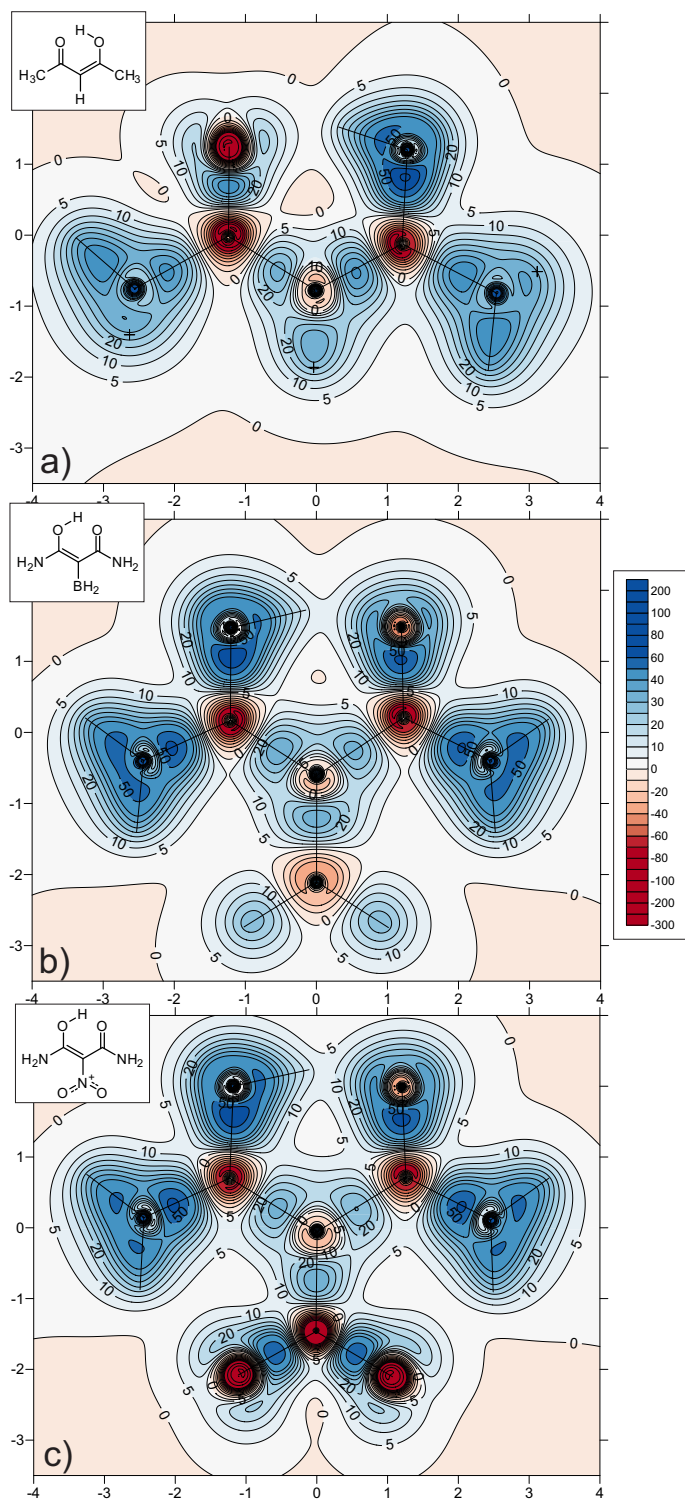
Figure 7.12: Contour plot of the isotropic chemical shielding (ppm) through the molecular plane of malonaldehyde derivatives a) malonaldehyde with terminal methyl groups (**Mal-1**), b) malonaldehyde with terminal amino groups and a central BH_2 group (**Mal-3**) and c) malonaldehyde with terminal amino groups and a central nitro group (**Mal-2**) all calculated at the MP2/6-311++G(d,p) level of theory. The black crosses denote the projections of the out-of-plane hydrogens.

Malonaldehyde, in both its ground and transition state, was compared to three derivatives of the same system. The oxygen shielding for **Mal-3**, with terminal amino substituents and a central BH_2 substituent, is the closest to those seen in oxazole and furan suggesting the greatest aromatic character and therefore the strongest H-bond. This is also consistent with the other features present in the isotropic shielding plots such as the lack of C–C bond alternation and the carbon shielding values. In contrast, **Mal-1** with terminal methyl groups is least aromatic and most similar to the parent malonaldehyde. The similarity of **Mal-2** and **Mal-3** was noted in other work on these systems as were the same H-bond findings.[135] It seems from this study that amino groups on terminal carbons significantly increase the aromaticity of the pseudo ring, though the central substituent seems to have limited effect.

7.5   Conclusions

The effects of various substituents on benzene, ethene and malonaldehyde were studied. Aniline was found to have slightly less aromaticity than parent benzene with the amino group displaying a slight disruption to the shielding 1 Å above the ring. The nitrogen in the amino group also displayed no deshielding around the nucleus showing no π conjugation with the ring. The methyl group of toluene perturbed the shielding above the ring less than the amino group of aniline and has more equivalent carbon environments than aniline. This makes toluene more aromatic than aniline and almost as aromatic as benzene. Phenol has more disruption to the shielding above the ring than for aniline which makes it less aromatic than aniline. However, like aniline, phenol displays no π conjugation between the substituent and the ring. The same findings were true of monofluorobenzene. Hexafluorobenzene, however, is quite different. It exhibits distorted C–C bonding regions and the absence of a shielding doughnut 1 Å above the ring suggesting a non-aromatic character. Overall, it was found that this shielding technique is more sensitive to substituent effects than NICS calculations.[131]

The study of *ortho-* and *para*-nitrophenol allowed the investigation of intramolecular H-bonding in these molecules as well as comparison with experimental work.[141] It was found that there are global effects across the whole system caused by the position of the two substituents in these nitrophenols. The detailed information obtained from this work was able to corroborate the altered reactivities of these

molecules obtained from polymerisation inhibition experiments.[141]

Next, substituted ethenes were examined and it was found that substituents have significant effects on the shielding in and around the ethene moiety. Furthermore, the nitro group in nitroethene is distinct from that in the nitrophenols earlier. The degree of conjugation between the ethene and the substituent can be determined by consideration of the shielding 1 Å above the molecules as well as the C=C bonding region and the deshielded regions around the carbon nuclei.

Finally, malonaldehyde and three derivatives were studied. It was discovered than the shielding of oxygen nuclei can clearly distinguish the type of environment that they are in. Furthermore, use of the oxygen shielding values as well as the shielding around the oxygen nuclei can be used to determine the relative amounts of aromaticity within the pseudo-ring formed by the intramolecular H-bond. This also, indirectly, gives relative H-bond strength information. It was found that nitromalonamide had the most aromatic character and therefore the strongest H-bond.

Conclusions

"Genius comes with insanity as a sidekick"

Benjamin Horner

8.1 Conclusions

In the work presented in this thesis, chemical bonding, aromaticity and antiaromaticity have been investigated using two- and three-dimensional applications of isotropic shielding calculations. These have been carried out with very finely spaced grids in the area surrounding a large range of molecules and then have been used to study their various properties, with great success.

Throughout this investigation, it has been found that HF and MP2 methods produce qualitatively identical results. The main difference between the methods is the magnitude of the shielding for the atoms and surrounding area of π bonded systems. It was also found that high quality geometries are vital in producing accurate shielding features, although general bonding features remain consistent between the methods. Furthermore, two DFT methods were used, B3LYP and M06, but both had significant problems. Any cost advantages of these methods over other *ab initio* calculations were negated by the incredibly fine integration grid that was required in order to recognise molecular symmetry. Moreover, the isotropic shielding plots exhibited an artificial rounding with shielding values that were significantly different from those obtained by HF and MP2. For these reasons, DFT was not considered as appropriate for the rest of this work.

This technique has proven highly sensitive when describing chemical bonding. Features typical of single, double and triple bonds have been identified and it was found that use of the maximum shielding along a bond is insufficient for fully describing the bonding character. Important features to consider are the magnitude and shape of the whole shielding region encompassing the internuclear space. Bond cross-sections also provide useful insight, with single and triple bonds having a circular cross-section and double bonds being more elliptical. Furthermore, any deformation of these bond cross-sections can give information on other molecular properties, for example, within an aromatic system, the greater the aromaticity, the more kidney-shaped the bond cross-section becomes. The shielding 1 Å above chemical bonds can provide details of the degrees of conjugation through a molecule as well as about the nature of the bond below.

All of these features of bonding can be used to determine approximate bond orders as well as to distinguish between single, double and triple bonds of different types. For example, C–H bonds are quite different depending on the environment that they are in and there is a clear difference between a C=C double bond and a

carbonyl double bond.

Detailed information on the bonding types is also available by studying the regions surrounding atoms. It has been found that fully saturated atoms have a shielded surrounding, but that any unsaturation leads to regions of deshielding around the nuclei involved. These regions of deshielding afford insight into the conjugation in a molecule as well as the relative degrees of unsaturation. For example, the deshielding around the carbons in ethene are fairly intense and spherical, but those in ethyne are far more distorted and less intense. This is typical of doubly and triply bonded systems, respectively.

H-bonding can also be studied, and this was done both inter- and intramolecularly. It was seen in these studies that, while there is little in the way of shielding features along the H-bond itself, the impact of the H-bond on the molecule(s) involved was important. In the case of malonaldehyde and three derivatives, the shielding values on the oxygen atoms directly involved in the H-bond clearly determined the type of oxygen environments, which lead to information on the relative H-bond strengths and pseudo ring aromaticities. From the oxygen shielding values, and the surrounding shielding contours, it is clear which derivatives have the most aromaticity and therefore the strongest H-bond. This, in turn, gives useful insight into the effect of the various substituents on the malonaldehyde structure.

A range of aromatic rings have been studied and key features of aromaticity have been identified. Along with the kidney-shaped bond cross-sections mentioned above, the deshielded areas around the nuclei in the ring are also very important. The more equivalent these regions are around the ring in question, the more aromatic the system. This is perhaps seen more clearly in the shielding present 1 Å above the molecule. In these plots, the more homogeneous the shielding halo is above the ring, the more aromatic the overall system is. These results can then be used to successfully compare relative aromaticities.

In the case of antiaromatic systems, the bonding regions display significant bond bending which, as seen in antiaromatic COT, is mainly caused by the antiaromaticity rather than ring strain. The bond cross-sections in antiaromatic systems are triangular rather than the kidney-shape of aromatic systems. Moreover, antiaromatic rings have a deshielded, dumbell-shaped/cylindrical feature at the ring centre protruding notably above and below the plane of the molecule. Interestingly, cyclobutene had a small deshielding feature at the ring centre so, while not

traditionally considered as antiaromatic, the degree of π delocalisation induces a small degree of antiaromaticity in the system.

Heavy-atom analogues of benzene were studied and an apparent lack of deshieldings around the heavier atoms was noted. However, later studies of heavy atoms in heterocycles concluded that these deshieldings are still present, but are harder to observe due to the increased size of the heavy atoms. These then require ultra-fine grids of isotropic shielding calculations in order to study these regions.

Polycyclic systems have also been investigated with many interesting findings. It was found that multiple ring systems should have their aromaticity considered as a whole rather than individual, local aromaticities. Benzocyclobutadiene and benzodicyclobutadiene were shown to exhibit both aromatic and antiaromatic properties. The two geometric isomers of benzodicyclobutadiene were significantly different, with one form displaying distinct aromatic and antiaromatic sections and the other only displaying aromatic characteristics. Moreover, the conjugation between rings in polycyclic systems, including three fulvalenes, were examined with some systems showing a more additive aromatic nature than others.

The effect of charge on cyclic molecules was explored and it was found that, in aromatic systems, an overall positive charge increases the magnitude of the deshielded regions around nuclei and weakens the bonding regions. Conversely, an overall negative charge on aromatic systems results in weaker deshieldings around nuclei and stronger bonds. The instance of disodiation on the COT dianion showed little impact on the shielding features with the exception of a slight strengthening of the C–C bonds.

Finally, an investigation into the effect of different substituents on benzene, ethene and malonaldehyde was carried out. For the examples of substituted benzenes, it was discovered that there was little π conjugation observed between the benzene moiety and the substituent but that there was still considerable effect on the bonding regions and carbon nuclei within the ring. Furthermore, there were significant differences observed between the different groups that were studied. The same is true of the substituted ethenes.

In conclusion, the application of magnetic shielding calculations across very finely spaced grids at appropriate positions through molecules has been seen to be a highly sensitive and effective technique for studying a wide range of systems and properties. It has proven far more insightful and sensitive than the popular NICS

technique, along with having a far wider scope. Detailed information has been obtained for a huge range of molecules, ranging from the archetypal aromatic and antiaromatic systems, to the more unusual, such as diborane and hexager-mabenzene. Throughout this work, the results have provided an analysis of π conjugation through molecules, the nature of chemical bonding of all types as well as comparison of relative aromaticities, all of which are key to a deeper understanding of important molecules. The prospects for such a simple yet effective and informative method are almost endless.

A

Example Fortran Code

The following is an example of the Fortran 95 code used to generate the GAUS-SIAN09 input files for a molecular plane grid:

```fortran
program grid

Writes a grid of ghost atoms in the xy plane

implicit real*8 (a-h, o-z)
character*200 runfp, runf
character*3 fileno
logical fexist, fopen
parameter (xmax=4.5d0,ymax=2.5d0,delta=0.05d0)

n = 0
m = 0
nf = 0
runfp = 'a-ace.mp2.6-311ppgss.xy.nmr.run'

x = -4.5d0
do while (x.le.xmax)
   y = -2.5d0
   do while (y.le.ymax)
      n = n + 1
      m = m + 1
      if ((n.eq.1).or.(m.gt.95)) then
        if (n.gt.1) then
           write (1, *)
           write (1, '(''!'')')
           close(1)
           fopen = .false.
           m = 1
        endif
        nf = nf + 1
        if (nf.gt.999) then
           write (6, '(''Cannot handle more than 999 files'')')
           go to 100
```

```fortran
          endif
          write (fileno, '(i3.3)') nf
          runf = trim(runfp) // '.' // fileno
          write (6, *) trim(runf)
          inquire (file = runf, exist = fexist)
          if (fexist) then
            open(1, file = runf, status = 'old')
            close(1, status = 'delete')
          endif
          open (1, file = runf, status = 'new')
          fopen = .true.
          write (1, '(''#!/bin/ksh'')')
          write (1, '(''export out=a-ace.mp2.6-311ppgss.xy.nmr.out.'',
.         a)') fileno
          write (1, '(''/usr/bin/time -ao $out '',
.         ''/usr/local/g09/g09 >$out 2>>$out <<!'')')
          write (1, '(''# MP2/6-311++G(d,p) SCF(Tight) '',
.         '' NMR CPHF(Separate) Test'')')
          write (1, *)
          write (1, '(''a-ace MP2/6-311++G** nmr xy grid atoms'')')
          write (1, *)
          write (1, '(''0 1'')')
          write (1, '(''C 0   -2.532328     0.755122     0.000000 '')')
          write (1, '(''C 0   -1.197059     0.068125     0.000000 '')')
          write (1, '(''O 0   -1.265450    -1.255684     0.000000 '')')
          write (1, '(''C 0    0.000000     0.737633     0.000000 '')')
          write (1, '(''C 0    1.244320    -0.002209     0.000000 '')')
          write (1, '(''O 0    1.269930    -1.247775     0.000000 '')')
          write (1, '(''C 0    2.537537     0.780397     0.000000 '')')
          write (1, '(''H 0    0.006343     1.820557     0.000000 '')')
          write (1, '(''H 0    3.382002     0.090826     0.000000 '')')
          write (1, '(''H 0    2.583065     1.424233     0.883743 '')')
          write (1, '(''H 0    2.583065     1.424233    -0.883743 '')')
          write (1, '(''H 0   -3.327056     0.008377     0.000000 '')')
          write (1, '(''H 0   -2.633691     1.389171    -0.884651 '')')
          write (1, '(''H 0   -2.633691     1.389171     0.884651 '')')
          write (1, '(''H 0   -0.310702    -1.553299     0.000000 '')')
        endif
        write (1, '(''Bq 0 '', 2F10.6, '' 0.0 '')') x, y
        y = y + delta
      end do
    x = x + delta
end do
```

```fortran
write (6, '(''Number of ghost atoms: '', I6)') n
if (fopen) then
   write (1, *)
   write (1, '(''!'')')
   close (1)
endif

stop
end
```

The following is an example of the Fortran 95 code used to generate the GAUS-
SIAN09 input files for a diagonal grid i.e. one which does not lie along any of the
Cartesian axes:

```fortran
      program grid
c
c——— Writes a grid of ghost atoms in the x(mid−yz) plane
c
      implicit real*8 (a–h, o–z)
      character*200 runfp, runf
      character*3 fileno
      character*2 atomno
      logical fexist, fopen
      parameter (rmax=3.50d0,xmax=3.50d0,delta=0.05d0)
c
      n = 0
      m = 0
      nf = 0
      theta = datan(0.781000d0/0.674500d0)
      runfp = 'c4h4rect.hf.6−311ppgss.diag.nmr.run'
c
      r = 0d0
      do while (r.lt.rmax)
        x = −3.5d0
        do while (x.lt.xmax)
          n = n + 1
          m = m + 1
          if ((n.eq.1).or.(m.gt.95)) then
            if (n.gt.1) then
              write (1, *)
              write (1, '(''!'')')
              close (1)
```

```fortran
         fopen = .false.
         m = 1
       endif
       nf = nf + 1
       if (nf.gt.999) then
         write (6, '(''Cannot handle more than 999 files.'')')
         go to 100
       endif
       write (fileno, '(i3.3)') nf
       runf = trim(runfp) // '.' // fileno
       write (6, *) trim(runf)
       inquire (file = runf, exist = fexist)
       if (fexist) then
         open(1, file = runf, status = 'old')
         close(1, status = 'delete')
       endif
       open (1, file = runf, status = 'new')
       fopen = .true.
       write (1, '(''#!/bin/ksh'')')
       write (1, '(''export out=c4h4rec.hf.6-311ppgss.di.nmr.out.'
     .       ',
     .        a)') fileno
       write (1, '(''/usr/bin/time -ao $out '',
     .      ''/usr/local/g09/g09 >$out 2>>$out <<!'')')
       write (1, '(''%NProc=4'')')
       write (1, '(''%Mem=4Gb'')')
       write (1, '(''# HF/6-311++G(d,p) SCF(Tight) '',
     .      '' NMR CPHF(Separate) Test'')')
       write (1, *)
       write (1, '(''C4H4 rect HF/6-311++G** nmr N-grid atoms'')')
       write (1, *)
       write (1, '(''0 1'')')
       write (1, '(''C 0     0.000000     0.674500     0.781000 '')')
       write (1, '(''C 0     0.000000     0.674500    -0.781000 '')')
       write (1, '(''C 0     0.000000    -0.674500    -0.781000 '')')
       write (1, '(''C 0     0.000000    -0.674500     0.781000 '')')
       write (1, '(''H 0     0.000000     1.437382     1.541224 '')')
       write (1, '(''H 0     0.000000     1.437382    -1.541224 '')')
       write (1, '(''H 0     0.000000    -1.437382    -1.541224 '')')
       write (1, '(''H 0     0.000000    -1.437382     1.541224 '')')
     endif
     y = r*cos(theta)
     z = r*sin(theta)
```

```
         write (1, '(''Bq 0 '', 3F10.6)') x, y, z
         x = x + delta
       end do
       r = r + delta
     end do
100  write (6, '(''Number of ghost atoms: '', I6)') n
     if (fopen) then
       write (1, *)
       write (1, '(''!'')')
       close(1)
     endif
c
     stop
     end
```

Finally, the following is an example of the code used to generate (x,y) coordinates from (x,y,z) coordinates for the diagonal grids plotted by the previous code. This was required to obtain the two-dimensional contour plots.

```
     program daxy
c
c——— Writes the xz coordinates of the C4H4 diag grid
c
     implicit real*8 (a–h, o–z)
     parameter (rmax=3.50d0, xmax=3.50d0, delta=0.05d0)
c
     theta = datan(0.781000d0/0.674500d0)
c
     r = 0d0
     do while (r.lt.rmax)
       x = −3.5d0
       do while (x.lt.xmax)
         y = r*cos(theta)
         z = r*sin(theta)
         ynew = dsqrt(y**2 + z**2)
         if (y.lt.0d0) ynew = −ynew
         write (6, '(''yz'' 2F10.6, '' xy'', 2F10.6)') y, z, x, ynew
         x = x + delta
       end do
       r = r + delta
     end do
c
```

```
    stop
    end
```

Abbreviations

B3LYP	Becke 3-Parameter Lee-Yang-Parr density functional
CASSCF	Complete Active Space Self-Consistent Field
DFT	Density Functional Theory
GIAO	Gauge Including Atomic Orbital
H-Bond	Hydrogen Bond
HF	Hartree-Fock
ICSS	Isochemical Shielding Surface
M06	Minnesota 06 functional
MBPT	Many-Body Perturbation Theory
MCSCF	Multiconfiguration Self-Consistent Field
MP2	Møller-Plesset second-order perturbation theory
NICS	Nucleus Independent Chemical Shift
NMR	Nuclear Magnetic Resonance

References

[1] L. Pauling, *The nature of the chemical bond*, Cornell University, 3rd edn., 1960, vol. 53.

[2] J. C. Slater, *Phys. Rev.*, 1931, **37**, 481–489.

[3] R. S. Mulliken, *J. Am. Chem. Soc.*, 1950, **72**, 4493–4503.

[4] Z. Konkoli and D. Cremer, *Int. J. Quant. Chem.*, 1998, **67**, 1–9.

[5] S. J. Blanksby and G. B. Ellison, *Acc. Chem. Res.*, 2003, **36**, 255–263.

[6] R. Kalescky, E. Kraka and D. Cremer, *J. Phys. Chem. A*, 2013, **117**, 8981–8995.

[7] D. G. de Oteyza, P. Gorman, Y.-C. Chen, S. Wickenburg, A. Riss, D. J. Mowbray, G. Etkin, Z. Pedramrazi, H.-Z. Tsai, A. Rubio, M. F. Crommie and F. R. Fischer, *Science*, 2013, **340**, 1434–1437.

[8] E. Arunan, G. R. Desiraju, R. a. Klein, J. Sadlej, S. Scheiner, I. Alkorta, D. C. Clary, R. H. Crabtree, J. J. Dannenberg, P. Hobza, H. G. Kjaergaard, A. C. Legon, B. Mennucci and D. J. Nesbitt, *Pure Appl. Chem.*, 2011, **83**, 1619–1636.

[9] S. J. Grabowski, *Chem. Rev.*, 2011, **111**, 2597–625.

[10] A. J. Dingley and S. Grzesiek, *J. Am. Chem. Soc.*, 1998, **120**, 8293–8297.

[11] E. D. Isaacs, A. Shukla, P. M. Platzman, D. R. Hamann, B. Barbiellini and C. A. Tulk, *Phys. Rev. Lett.*, 1999, **82**, 600–603.

[12] X.-Z. Li, B. Walker and A. Michaelides, *Proc. Natl. Acad. Sci.*, 2011, **108**, 6369–6373.

[13] B. Silvi, *J. Mol. Struct.*, 2002, **614**, 3–10.

[14] R. Bochicchio, R. Ponec, A. Torre and L. Lain, *Theor. Chem. Acc.*, 2001, **105**, 292–298.

[15] R. Ponec, G. Yuzhakov and D. L. Cooper, *Theor. Chem. Acc.*, 2004, **112**, 419–430.

[16] M. Faraday, *Phil.Trans. R. Soc.*, 1825, **115**, 440–466.

[17] E. Hückel, *Z. Phys.*, 1931, **70**, 204–286.

[18] E. Hückel, *Z. Phys.*, 1931, **72**, 310–337.

[19] J. W. Armit and R. Robinson, *J. Chem. Soc. Trans.*, 1925, **127**, 1604–1618.

[20] M. Calvin and K. W. Wilson, *J. Am. Chem. Soc.*, 1945, **67**, 2003–2007.

[21] S. Winstein, *J. Am. Chem. Soc.*, 1959, **81**, 6524–6525.

[22] R. V. Williams, *Chem. Rev.*, 2001, **101**, 1185–1204.

[23] E. Heilbronner, *Tetrahedron Lett.*, 1964, **5**, 1923–1928.

[24] D. M. Lemal, *Nature*, 2003, **426**, 776–777.

[25] D. Ajami, O. Oeckler, A. Simon and R. Herges, *Nature*, 2003, **426**, 819–821.

[26] J. Aihara, *J. Am. Chem. Soc.*, 1978, **100**, 3339–3342.

[27] M. J. S. Dewar, *Bull. Soc. Chim. Belg.*, 1979, **88**, 957–967.

[28] M. Dewar and M. McKee, *Pure Appl. Chem.*, 1980, **52**, 1431–1441.

[29] M. J. S. Dewar, *J. Am. Chem. Soc.*, 1984, **106**, 669–682.

[30] E. Osawa, H. W. Kroto, P. W. Fowler and E. Wasserman, *Phil. Trans. R. Soc. Lond. A*, 1993, **343**, 1–8.

[31] R. F. Curl, R. E. Smalley, H. W. Kroto, S. O'Brien and J. R. Heath, *J. Mol. Graph. Model.*, 2001, **19**, 185–186.

[32] R. Breslow, J. Brown and J. Gajewski, *J. Am. Chem. Soc.*, 1967, **89**, 4383–4390.

[33] R. Breslow, *Acc. Chem. Res.*, 1973, **6**, 393–398.

[34] J. A. Pople and K. G. Untch, *J. Am. Chem. Soc.*, 1966, **88**, 4811–4815.

[35] D. Moran, M. Manoharan, T. Heine and P. V. R. Schleyer, *Org. Lett.*, 2003, **5**, 23–26.

[36] A. E. Kuznetsov, K. A. Birch, A. I. Boldyrev, X. Li, H.-J. Zhai and L.-S. Wang, *Science (80-.)*., 2003, **300**, 622–625.

[37] A. I. Boldyrev and L.-S. Wang, *Chem. Rev.*, 2005, **105**, 3716–3757.

[38] A. T. Balaban, D. C. Oniciu and A. R. Katritzky, *Chem. Rev.*, 2004, **104**, 2777–2812.

[39] M. K. Cyrañski, P. v. R. Schleyer, T. M. Krygowski, H. Jiao and G. Hohlne-icher, *Tetrahedron*, 2003, **59**, 1657–1665.

[40] Z. Chen, J. I. Wu, C. Corminboeuf, J. Bohmann, X. Lu, A. Hirsch and P. V. R. Schleyer, *Phys. Chem. Chem. Phys.*, 2012, **14**, 14886–14891.

[41] Z. Chen, C. S. Wannere, C. Corminboeuf, R. Puchta and P. v. R. Schleyer, *Chem. Rev.*, 2005, **105**, 3842–3888.

[42] P. v. R. Schleyer, C. Maerker, A. Dransfeld, H. Jiao and N. J. R. van Eikema Hommes, *J. Am. Chem. Soc.*, 1996, **118**, 6317–6318.

[43] C. S. Wannere and P. v. R. Schleyer, *Org. Lett.*, 2003, **5**, 605–608.

[44] R. G. Viglione, R. Zanasi and P. Lazzeretti, *Org. Lett.*, 2004, **6**, 2265–2267.

[45] C. E. Johnson and F. A. Bovey, *J. Chem. Phys.*, 1958, **29**, 1012–1014.

[46] N. H. Martin, D. M. Loveless, K. L. Main and D. C. Wade, *J. Mol. Graph. Model.*, 2006, **25**, 389–395.

[47] N. H. Martin, J. E. Rowe and E. L. Pittman, *J. Mol. Graph. Model.*, 2009, **27**, 853–859.

[48] N. H. Martin, M. R. Teague and K. H. Mills, *Symmetry (Basel).*, 2010, **2**, 418–436.

[49] N. H. Martin, J. D. Brown, K. H. Nance, H. F. Schaefer III, P. v. R. Schleyer, Z. X. Wang and H. L. Woodcock, *Org. Lett.*, 2001, **3**, 3823–3826.

[50] P. Lazzeretti, *Phys. Chem. Chem. Phys.*, 2004, **6**, 217–223.

[51] P. Lazzeretti, *Prog. Nucl. Magn. Reson. Spectrosc.*, 2000, **36**, 1–88.

[52] P. v. R. Schleyer, H. Jiao, N. J. R. van Eikema Hommes, V. G. Malkin and O. L. Malkina, *J. Am. Chem. Soc.*, 1997, **119**, 12669–12670.

[53] P. v. R. Schleyer, M. Manoharan, Z. X. Wang, B. Kiran, H. Jiao, R. Puchta and N. J. R. van Eikema Hommes, *Org. Lett.*, 2001, **3**, 2465–2468.

[54] H. Fallah-Bagher-Shaidaei, C. S. Wannere, C. Corminboeuf, R. Puchta and P. v. R. Schleyer, *Org. Lett.*, 2006, **8**, 863–866.

[55] A. Stanger, *J. Org. Chem.*, 2006, **71**, 883–893.

[56] S. Klod and E. Kleinpeter, *J. Chem. Soc., Perkin Trans. 2*, 2001, 1893–1898.

[57] E. Kleinpeter, S. Klod and A. Koch, *J. Mol. Struct. THEOCHEM*, 2007, **811**, 45–60.

[58] E. Kleinpeter, A. Holzberger and P. Wacker, *J. Org. Chem.*, 2008, **73**, 56–65.

[59] M. Baranac-Stojanović, A. Koch and E. Kleinpeter, *Chem. Eur. J.*, 2012, **18**, 370–376.

[60] C. Møller and M. Plesset, *Phys. Rev.*, 1934, **46**, 618.

[61] B. O. Roos, in *The complete active space self-consistent field method and its applications in electronic structure calculations*, ed. K. P. Lawley, John Wiley & Sons, Ltd., 1987, pp. 399–445.

[62] P. Hohenberg and W. Kohn, *Phys. Rev.*, 1964, **136**, B864–B871.

[63] W. Kohn and L. Sham, *Phys. Rev.*, 1965, **140**, A1133–A1138.

[64] A. D. Becke, *J. Chem. Phys.*, 1993, **98**, 1372–1377.

[65] Y. Zhao and D. G. Truhlar, *Theor. Chem. Acc.*, 2008, **120**, 215–241.

[66] M. J. Frisch, G. W. Trucks, H. B. Schlegel, G. E. Scuseria, M. A. Robb, J. R. Cheeseman, G. Scalmani, V. Barone, B. Mennucci, G. A. Petersson, H. Nakatsuji, M. Caricato, X. Li, H. P. Hratchian, A. F. Izmaylov, J. Bloino, G. Zheng, J. L. Sonnenberg, M. Hada, M. Ehara, K. Toyota, R. Fukuda, J. Hasegawa, M. Ishida, T. Nakajima, Y. Honda, O. Kitao, H. Nakai, T. Vreven, J. A. Montgomery, Jr., J. E. Peralta, F. Ogliaro, M. Bearpark,

J. J. Heyd, E. Brothers, K. N. Kudin, V. N. Staroverov, R. Kobayashi, J. Normand, K. Raghavachari, A. Rendell, J. C. Burant, S. S. Iyengar, J. Tomasi, M. Cossi, N. Rega, J. M. Millam, M. Klene, J. E. Knox, J. B. Cross, V. Bakken, C. Adamo, J. Jaramillo, R. Gomperts, R. E. Stratmann, O. Yazyev, A. J. Austin, R. Cammi, C. Pomelli, J. W. Ochterski, R. L. Martin, K. Morokuma, V. G. Zakrzewski, G. A. Voth, P. Salvador, J. J. Dannenberg, S. Dapprich, A. D. Daniels, . Farkas, J. B. Foresman, J. V. Ortiz, J. Cioslowski and D. J. Fox, *Gaussian 09 Revision B.1*, Gaussian Inc. Wallingford CT 2009.

[67] DALTON, a molecular electronic structure program, Release Dalton 2.0 (2005), see http://daltonprogram.org/.

[68] S. Bauer, *Chem. Rev.*, 1942, **31**, 43–75.

[69] M. E. Alikhani, F. Fuster and B. Silvi, *Struct. Chem.*, 2005, **16**, 203–210.

[70] E. Steiner and P. W. Fowler, *Int. J. Quant. Chem.*, 1996, **60**, 609–616.

[71] J. A. N. F. Gomes and R. B. Mallion, *Chem. Rev.*, 2001, **101**, 1349–83.

[72] A. Soncini, P. W. Fowler, P. Lazzeretti and R. Zanasi, *Chem. Phys. Lett.*, 2005, **401**, 164–169.

[73] S. Pelloni and P. Lazzeretti, *Chem. Phys.*, 2009, **356**, 153–163.

[74] S. Pelloni, G. Monaco, P. Della Porta, R. Zanasi and P. Lazzeretti, *J. Phys. Chem. A*, 2014, **118**, 3367–3375.

[75] Hehre, Radom, Pople and Schleyer, *Ab Initio Molecular Orbital Theory*, Wiley Interscience, 1986.

[76] E. A. Cherniak, *J. Chem. Phys.*, 1966, **45**, 104–110.

[77] K. Kveseth, R. Seip and D. A. Kohl, *Acta Chem. Scand. A*, 1980, **34**, 31–42.

[78] K. Tanabe and S. Saeki, *Bull. Chem. Soc. Jpn*, 1974, **47**, 1847–1851.

[79] N. V. Sidgwick, *The Electronic Theory of Valency*, Oxford University Press, 1929.

[80] L. Pauling, *J. Am. Chem. Soc.*, 1931, **53**, 3225–3237.

[81] G. N. Lewis, *J. Chem. Phys.*, 1933, **1**, 17–28.

[82] R. S. Mulliken, *J. Chem. Phys.*, 1935, **3**, 635–645.

[83] V. M. Dembitsky, *J. Nat. Med.*, 2008, **62**, 1–33.

[84] A. Sergeiko, V. V. Poroikov, L. O. Hanus and V. M. Dembitsky, *Open Med. Chem. J.*, 2008, **2**, 26–37.

[85] E. Lee-Ruff and G. Mladenova, *Chem. Rev.*, 2003, **103**, 1449–1484.

[86] J. C. Namyslo and D. E. Kaufmann, *Chem. Rev.*, 2003, **103**, 1485–1538.

[87] A. Mailyan, I. Krylov, C. Bruneau, P. Dixneuf and S. Osipov, *Synlett*, 2011, 2321–2324.

[88] J. Shimada, K. Hashimoto, B. H. Kim, E. Nakamura and I. Kuwajima, *J. Am. Chem. Soc.*, 1984, **106**, 1759–1773.

[89] M. J. Bassindale, P. Hamley and J. P. A. Harrity, *Tetrahedron Lett.*, 2001, **42**, 9055–9057.

[90] Y.-C. Shen, P. I. Tsai, W. Fenical and M. E. Hay, *Phytochemistry*, 1992, **32**, 71–75.

[91] J. L. Weiner, A. V. Buhler, V. J. Whatley, R. A. Harris and T. V. Dunwiddie, *J. Pharmacol. Exp. Ther.*, 1998, **284**, 95–102.

[92] J. E. Dahl, T. r. Stene, H. S. m. Koppang, R. Koppang and T. Stokke, *Acta Odontol. Scand.*, 1981, **39**, 195–200.

[93] D. B. McKay, M. J. Cobianchi and A. S. Schneider, *Pharmacology*, 1987, **35**, 155–162.

[94] A. Cabana, J. Bachand and J. Giguère, *Can. J. Phys.*, 1974, **52**, 1949–1955.

[95] M. Eckert-Maksić, M. Vazdar, M. Barbatti, H. Lischka and Z. B. Maksić, *J. Chem. Phys.*, 2006, **125**, 064310.

[96] G. J. Hill, D. L. Cooper and P. B. Karadakov, *J. Phys. Chem. A*, 2006, **110**, 7913–7917.

[97] P. B. Karadakov and K. E. Horner, *J Phys Chem A*, 2013, **117**, 518–523.

REFERENCES

[98] M. Baba, Y. Kowaka, U. Nagashima, T. Ishimoto, H. Goto and N. Nakayama, *J. Chem. Phys.*, 2011, **135**, 054305.

[99] D. L. Cooper and P. B. Karadakov, *Mol. Phys.*, 2014, **DOI:10.108**, year.

[100] A. Stanger, *J. Org. Chem.*, 2013, **78**, 12374–12380.

[101] R. Kalescky, E. Kraka and D. Cremer, *J. Phys. Chem. A*, 2014, **118**, 223–237.

[102] R. Brown, *Trans. Faraday Soc.*, 1948, **44**, 984–987.

[103] J.-i. Aihara and S. Oe, *Bull. Chem. Soc. Jpn*, 2003, **76**, 1363–1364.

[104] D. Baric and Z. B. Maksić, *J. Phys. Org. Chem.*, 2003, **16**, 753–763.

[105] D. Cremer and E. Kraka, *J. Am. Chem. Soc.*, 1985, **107**, 3800–3810.

[106] D. Cremer and J. Gauss, *J. Am. Chem. Soc.*, 1986, **108**, 7467–7477.

[107] D. Cremer, *Tetrahedron*, 1988, **44**, 7427–7454.

[108] J. I.-C. Wu, Y. Mo, F. A. Evangelista and P. v. R. Schleyer, *Chem. Commun.*, 2012, **48**, 8437–8439.

[109] Y. Endo, M. C. Chang and E. Hirota, *J. Mol. Spec.*, 1987, **126**, 63–71.

[110] A. Y. Sokolov, D. B. Magers, J. I. Wu, W. D. Allen, P. v. R. Schleyer and H. F. Schaefer III, *J. Chem. Theory Comput.*, 2013, **9**, 4436–4443.

[111] P. B. Karadakov, J. Gerratt, D. L. Cooper and M. Raimondi, *J. Mol. Struct. THEOCHEM*, 1995, **341**, 13–24.

[112] H. Fliegl, D. Sundholm, S. Taubert, J. Jusélius and W. Klopper, *J. Phys. Chem. A*, 2009, **113**, 8668–8676.

[113] R. H. Mitchell, P. Zhang, D. J. Berg and R. Vaughan Williams, *Chem. Commun.*, 2012, **48**, 8144–8146.

[114] F. R. Cordell and J. E. Boggs, *J. Mol. Struct. THEOCHEM*, 1981, **85**, 163–178.

[115] F. Fringuelli, G. Marino, A. Taticchi and G. Grandolini, *J. Chem. Soc., Perkin Trans. 2*, 1974, 332–337.

[116] L. Nyulászi, P. Varnai and T. Veszpremi, *J. Mol. Struct. THEOCHEM*, 1995, **358**, 55–61.

[117] F. Mata, M. C. Martin and G. O. Sø rensen, *J. Mol. Struct.*, 1978, **48**, 157–163.

[118] L. Nyulászi, J. T. Nielsen, J. Kirchheiner, G. Maltesen, J. Rastrup-Andersen and G. O. Sø rensen, *J. Mol. Struct.*, 1969, **3**, 491–506.

[119] B. Bak, D. Christensen, L. Hansen-Nygaard and J. Rastrup-Andersen, *J. Mol. Spec.*, 1961, **7**, 58–63.

[120] R. Brown, F. Burden and P. Godfrey, *J. Mol. Spec.*, 1968, **25**, 415–421.

[121] L. Nyulászi, E. Asmussen, J. Hø g, R. Maheshwari, C. Nielsen, I. Petersen, J. Rastrup-Andersen and G. O. Sø rensen, *J. Mol. Struct.*, 1971, **8**, 225–233.

[122] W. Pyckhout, N. Horemans, C. Van Alsenoy, H. Geise and D. W. H. Rankin, *J. Mol. Struct.*, 1987, **156**, 315–329.

[123] S. Cradock, P. B. Liescheski, D. W. H. Rankin and H. E. Robertson, *J. Am. Chem. Soc.*, 1988, **110**, 2758–2763.

[124] K. E. Horner and P. B. Karadakov, *J. Org. Chem.*, 2013, **78**, 8037–8043.

[125] W. Schaefer, A. Schweig and F. Mathey, *J. Am. Chem. Soc.*, 1976, **98**, 407–414.

[126] D. B. Chesnut and L. D. Quin, *Heteroat. Chem.*, 2007, **18**, 754–758.

[127] P. v. R. Schleyer, P. K. Freeman, H. Jiao and B. Goldfuss, *Angew. Chem. Int. Ed. Engl.*, 1995, **34**, 337–340.

[128] D. Chesnut and L. Quin, *J. Am. Chem. Soc.*, 1994, **116**, 9638–9643.

[129] W. Dong, H. Wang, Q. Ge and L. Wang, *Struct. Chem.*, 2007, **18**, 593–597.

[130] I. Alkorta and J. Elguero, *Magn. Reson. Chem.*, 2010, **48**, S32–37.

[131] T. M. Krygowski, K. Ejsmont, B. T. Stepien, M. K. Cyrañski, J. Poater and M. Solà, *J. Org. Chem.*, 2004, **69**, 6634–6640.

[132] T. M. Krygowski, J. E. Zachara and H. Szatylowicz, *J. Org. Chem.*, 2004, **69**, 7038–7043.

[133] G. Gilli, F. Bellucci, V. Ferretti and V. Bertolasi, *J. Am. Chem. Soc.*, 1989, **111**, 1023–1028.

[134] J. Dannenberg and R. Rios, *J. Phys. Chem.*, 1994, **98**, 6714–6718.

[135] J. Hargis, F. Evangelista, J. Ingels and H. F. Schaefer III, *J. Am. Chem. Soc.*, 2008, **130**, 17471–17478.

[136] D. Lister, J. Tyler, J. Hø g and N. Wessel Larsen, *J. Mol. Struct.*, 1974, **23**, 253–264.

[137] N. W. Larsen, *J. Mol. Struct.*, 1979, **51**, 175–190.

[138] L. Nygaard, T. Bojesen, T. Pedersen and J. Rastrup-Andersen, *J. Mol. Struct.*, 1968, **2**, 209–215.

[139] A. Almenningen, O. Bastiansen, R. Seip and H. Seip, *Acta Chem. Scand.*, 1964, **18**, 2115–2124.

[140] O. V. Shishkin, I. V. Omelchenko, M. V. Krasovska, R. I. Zubatyuk, L. Gorb and J. Leszczynski, *J. Mol. Struct.*, 2006, **791**, 158–164.

[141] T. E. Newby, *Ph.D. thesis*, University of York, 2014.

[142] A. Ebrahimi, N. Mostafavi and P. Karimi, *Int. J. Quant. Chem.*, 2014, **114**, 154–161.

[143] A. Heydar Pakiari and N. Bagheri, *J. Mol. Model.*, 2011, **17**, 2017–2027.

[144] J. I. Wu, F. G. Pühlhofer, P. v. R. Schleyer, R. Puchta, B. Kiran, M. Mauksch, N. J. R. V. E. Hommes, I. Alkorta and J. Elguero, *J. Phys. Chem. A*, 2009, **113**, 6789–6794.

[145] T. Okazaki and K. K. Laali, *Org. Biomol. Chem.*, 2006, **4**, 3085–3095.

[146] O. Simonsen and N. Thorup, *Acta Cryst. B*, 1979, **35**, 432–435.

[147] G. Buemi, *Chem. Phys.*, 2002, **277**, 241–256.

[148] G. Buemi and F. Zuccarello, *Chem. Phys.*, 2004, **306**, 115–129.